2010-05-28

Inhomogeneity-Induced Spin Current in Atomic and Condensed Matter Systems

Bailey Hsu
Brigham Young University - Provo

INHOMOGENEITY-INDUCED SPIN CURRENT IN ATOMIC AND CONDENSED MATTER SYSTEMS

by

Bailey C. Hsu

A dissertation submitted to the faculty of

Brigham Young University

in partial fulfillment of the requirements for the degree of

Doctor of Philosophy

Department of Physics and Astronomy

Brigham Young University

April 2010

BRIGHAM YOUNG UNIVERSITY

GRADUATE COMMITTEE APPROVAL

of a dissertation submitted by

Bailey C. Hsu

This dissertation has been read by each member of the following graduate committee and by majority vote has been found to be satisfactory.

Date	Jean-François S. Van Huele, Chair
Date	Manuel Berrondo
Date	Eric Hirschmann
Date	Branton J. Campbell
Date	Robert C. Davis

BRIGHAM YOUNG UNIVERSITY

As chair of the candidate's graduate committee, I have read the dissertation of Bailey C. Hsu in its final form and have found that (1) its format, citations, and bibliographical style are consistent and acceptable and fulfill university and department style requirements; (2) its illustrative materials including figures, tables, and charts are in place; and (3) the final manuscript is satisfactory to the graduate committee and is ready for submission to the university library.

Date

Jean-François S. Van Huele
Chair, Graduate Committee

Accepted for the Department

Ross L. Spencer, Chair
Department of Physics and Astronomy

Accepted for the College

Thomas W. Sederberg, Associate Dean
College of Mathematics and Physical Sciences

ABSTRACT

INHOMOGENEITY-INDUCED SPIN CURRENT IN ATOMIC AND CONDENSED MATTER SYSTEMS

Bailey C. Hsu

Department of Physics and Astronomy

Doctor of Philosophy

I derive and apply quantum propagator techniques to atomic and condensed matter systems. I observe many interesting features by following the evolution of a wavepacket. In atomic systems, I revisit the Stern-Gerlach effect and study the spin dynamics inside an inhomogeneous magnetic field. The results I obtained are not exactly the same as the *textbook* description of the effect which is usually a manifestation of a perfect space and spin entanglement. This discovery can provide insight on more reliable quantum computation device designs. In condensed matter systems, the doping concentration inhomogeneity leads to the Rashba spin-orbit interaction. This makes it possible to control the spin without the external magnetic field. By propagating the wave packet in systems exhibiting Rashba spin-orbit interactions, I discover several features such as spin separation, spin accumulation, persistent spin-helix, and ripple formation.

ACKNOWLEDGMENTS

I would like to acknowledge and thank my advisor Dr. Jean-François S. Van Huele for his commitment to helping me learn and succeed and for the many productive discussions related to this and other research projects which helped me to master concepts and ideas. Many thanks go to Dr. Manuel Berrondo for his idea on the numerical propagation method and never-ceasing inspirations. I would also like to express my gratitude to Dr. Branton Campbell for his guidance on Mathematica programming and academic-career planning. Last but not least, I would like to acknowledge Dr. Eric Hirschmann and affiliated members of Theoretical physics in BYU for their help with my presentation skills and manuscripts.

I would also like to thank the members of my committee for letters of recommendation and for introducing me to other professionals.

Contents

List of Figures

Chapter 1

Introduction and Motivation

My research is focused on understanding spin current in spin-dependent systems. This work has been driven by two elements. The first is the importance of the field of spintronics. The second is the desire to provide a comprehensive collection of propagators in physical systems in particular spin-dependent systems. The importance of spintronics can be argued as follows: The minimization of electrical circuits leads to unavoidable higher power dissipation. This minimization is necessary to ensure higher packing density. However, the power dissipation has motivated extensive research on finding an alternative solution to the current electronics technology. Since the circuit dimension has been minimized to such an extent that we can observe quantum phenomena in electric circuits, the technology based on the spin of the electron, which is a quantum manifestation of an electron, has emerged. This technology is often times coined as "spin-electronics" or "spintronics".

The spin, unlike the position and the momentum, provides an extra non-classical dimension. It is two-valued for spin-1/2 particles. Therefore it is a good candidate for logic devices (1/0 refers to up/down). In electronics, one is interested in the charge current. The flow can be pumped by an inhomogeneity in the electrical potential or

a constant electric field. Can one generate spin currents using a similar concept as in conventional electronics? Intuitively one would explore the interaction between a spin and a magnetic field. One familiar example is the Zeeman effect where one sees splitting of different spectral lines when a homogeneous magnetic field is present. But does this lead to spin currents? What is meant by spin current? When talking about charge current, one envisions motion in opposite directions for opposite charges, leading to a constant flow of charge. However, the story has a twist when it comes to spin. Charge is a scalar while spin is not. Unlike the charge, spin (usually characterized as spin-up or spin-down), is not a **permanent** physical identity. Spin-up can evolve or flip to spin-down, and back again. Therefore, for an initial random distribution of pure spin-ups and spin-downs in space, such as in Fig.1.1, one can create a spin current by either pushing spin-up and spin-down in opposite directions or by flipping spin-down to spin-up on one side and spin-up to spin-down on the other side. The result in Fig.1.2 can be obtained by either mechanisms. But there is a difference between the two mechanisms. A spin-dependent force is needed to generate the "push" in the first case while a position-dependent transition from spin-up to spin-down is required in the second case.

In this thesis, I focus on systems involving inhomogeneities which lead to spin-dependent forces: the Stern-Gerlach effect (SGE) (inhomogeneity in the field) and the Rashba effect (caused by an inhomogeneity in the material). SGE demonstrates the deflection of two spin components for silver atoms going through an *inhomogeneous* magnetic field. Based on a semiclassical argument, an inhomogeneous magnetic field generates a spin-dependent force which is proportional to the gradient of the field. In the Rashba effect one uses the spin-orbit coupling in the atoms of the material to create an internal magnetic field $\sim v \times E$ from an external electric field E. This electric field in the Rashba effect arises from an *inhomogeneous* doping concentration

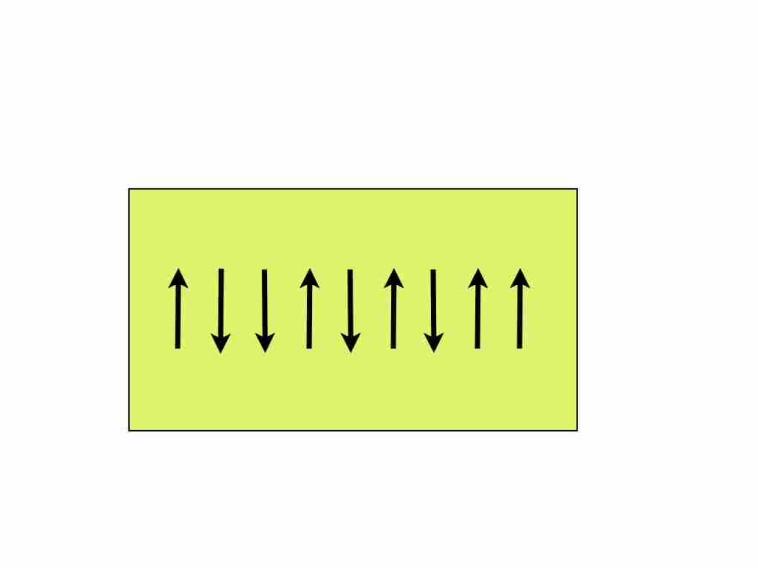

Figure 1.1 Spin Distribution at $t = 0$.

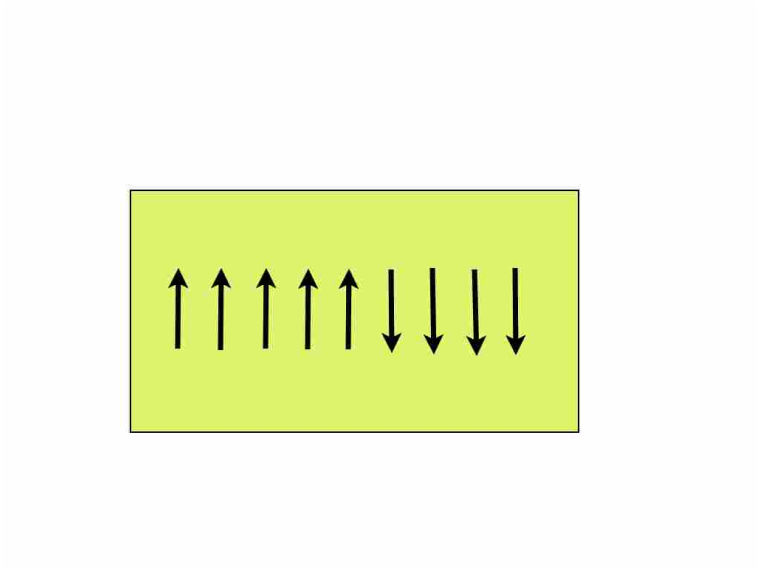

Figure 1.2 Spin Distribution at $t = \tau$.

across quantum wells. This inhomogeneity creates the internal electric field and, as a result, a magnetic field appears from spin-orbit couplings. Note that there are higher orders of inhomogeneities in the literature [1], for example the cubic Rashba and the cubic Dresselhaus effects.

To analyze the dynamics of the system, I use a quantum propagator approach. By considering so many different systems, I am able to add to the collection of existing propagators for Hamiltonians involving position, momentum, and spin variables. This approach relies on the construction of propagators, application of the propagation on the initial wave packets, and evaluating the evolution of (spin) densities by capturing them at successive time frames.

Propagator theory is a powerful tool in quantum mechanics. Propagators give conditional probabilities between two different points in space and time. There are several methods in the literature regarding the construction of the spinless quantum propagator. I give several methods for propagator construction in 1D in Chapter 2, and apply them to different purely spatial potentials $V(x)$ as examples. In Chapter 3 and 4, I extend the method to spin-dependent potentials.

Constructing the propagators in systems involving spin-orbit interactions (SOI) can be challenging due to the noncommutative properties of the spin operators. The spin operators for spin-1/2 particles can be represented by 2×2 matrices. These operators form a SU(2) group, generated by the Pauli matrices obeying $[\sigma_j, \sigma_k] = 2i\epsilon_{jkl}\sigma_l$. When applying a time-evolution operator which has noncommuting operators in the exponent, one needs Baker-Campbell-Hausdorff-like formulas to separate the exponentials. I find the Zassenhaus formula particularly useful because the final output can be applied to a wave function in a straightforward way.

Since I am interested in understanding the spin dynamics for wave packets in three separate situations: (1) free spins in a magnetic field (Stern-Gerlach), (2) spins

in condensed matter systems (Rashba), and (3) spins in atomic systems (atomic spin-orbit coupling), I have used the propagator approach to evaluate spin evolution in all three systems. There are several methods to construct propagators for the systems of interest. In Chapter 2, I describe them in full detail. I also extend them to spin-dependent systems. In Chapter 3, I highlight the condensed matter results which are covered in Appendix C. I provide a complete analysis of the Stern-Gerlach effect in Chapter 4. In Chapter 5, I conclude by summarizing features found in Rashba and Stern-Gerlach systems. I also discuss possible applications using this propagator method. I have also applied propagator methods in the area of econophysics and two corresponding papers are attached in the Appendix E.

Since most of my results on condensed matter and atomic systems are published, I have chosen to include the publications in the appendices. The Stern-Gerlach work, which is not published yet, appears in Chapter 4. Propagators have an applicability beyond spin and quantum mechanics, namely in systems described by partial differential equations with respect to time. In particular I am intrigued by similarities between the Schrödinger equation and equations in mathematical finance. As an illustration I rederive the Black-Scholes propagator in the second paper which appears in Appendix E. This work on spin propagators has led me to speculate on what the equivalent of the physical spin might look like in financial equations. This work is presented in the first paper in Appendix E. These two papers have been included of course, for completeness.

This work does not cover all aspects of spintronics, spin currents, or propagators. I refer the reader to the following general references on these topics. Spintronics is a very vast field. For spintronics, one can find more information on giant magneto-resistance (GMR) in Grünberg [2], on Rashba and Dresselhaus effects in [3, 4], on spin currents in [5]. For propagators, see Kleinert [6] and Schulman [7]. For the

Stern-Gerlach effect, see Manukian [8].

Chapter 2

Propagator Construction Method

Propagator theory is a powerful tool in quantum mechanics to display the evolution of states in position space. A propagator $K(x, x_0; t_f, t_i)$ gives the conditional probability amplitude between two position eigenstates at times separated by an interval $t = t_f - t_i$. Propagators are defined as

$$K(x, x_0; t_f, t_i) =< x|T(t_f, t_i)|x_0 > \tag{2.1}$$

where $T(t_f, t_i)$ is the time-evolution operator and obeys the time-dependent Schrödinger equation. If the Hamiltonian is time-independent, the time evolution operator can simply be written as

$$T(t) = \exp\left(\frac{Ht}{i\hbar}\right), \tag{2.2}$$

which also means that the time-evolution operator only depends on the time-interval and so does the propagator.[1] For the limit $t \to 0$, the propagator satisfies the initial

[1]The time-interval here can be $t_f - t_i$. For the sake of simplicity, I use t to represent the time-interval in the remainder of this thesis. This does not make any difference since the propagator only depends on the time-interval.

condition

$$\lim_{t\to 0} K(x, x_0; t) = \delta(x - x_0). \tag{2.3}$$

Note that once the propagators have been found, they can be applied to any initial distribution $\psi(x_0, 0)$ using the integral formula

$$\psi(x, t) = \int_{-\infty}^{\infty} K(x, x_0; t)\psi(x_0, 0)dx_0 \tag{2.4}$$

to obtain the evolved wave packet $\psi(x, t)$.

So an interesting question is whether there is a counterpart to the quantum propagator in the classical world! The answer is yes. The equivalent classical propagator is a Dirac delta function between 2 points x_f and x_i on the trajectory. The integral formula for the classical propagator can be expressed as

$$\psi(x(t)) = \int_{-\infty}^{\infty} \delta(x(t) - x_0)\psi(x_0)dx_0, \tag{2.5}$$

since a trajectory $x(t)$ has been defined in the classical world.

There are several methods in the literature regarding the construction of the spinless quantum propagator [9–19]. I derive five methods in this chapter and apply them to different potentials as examples. In Chapters 3 and 4, I extend the propagator method to spin-dependent systems where the propagators include 2×2 matrix representations of spin-1/2 particles and for which the integral formula in Eq.(2.4) will be modified.

2.1 Eigenfunction Expansion Method

Applying the definition of the propagator from Eq.(2.1), and using the completeness of the eigenfunctions of the Hamiltonian H, I obtain

$$K(x, x_0; t) = \sum_n < x| \exp\left(\frac{Ht}{i\hbar}\right) |E_n >< E_n|x_0 > . \tag{2.6}$$

Since

$$H|E_n\rangle = E_n|E_n\rangle, \quad \langle x_0|E_n\rangle = \psi_n(x_0), \tag{2.7}$$

the propagator can be written as

$$K(x, x_0; t) = \sum_n \psi_n(x_0)^* \psi_n(x) \exp\left(\frac{E_n t}{i\hbar}\right). \tag{2.8}$$

The sum is over all stationary states including degenerate ones [16]. I will now apply this method to the case of the free particle and that of the simple harmonic oscillator.

2.1.1 Free particle

The free particle in 1D case is the most straightforward case and serves for checking more complex cases by taking appropriate limits. The time-evolution operator is

$$T(t) = \exp\left(\frac{p_x^2 t}{2i\hbar m}\right). \tag{2.9}$$

By applying the eigenfunction expansion method, I integrate over all momentum values

$$K(x, x_0; t) = \int_{-\infty}^{\infty} \exp\left(\frac{p_x^2 t}{2i\hbar m}\right) \exp\left(\frac{p_x(x - x_0)}{i\hbar}\right) dp_x. \tag{2.10}$$

Performing the Fourier transform integral, I then obtain the propagator

$$K(x, x_0; t) = \sqrt{\frac{m}{2\pi i\hbar t}} \exp\left(-\frac{m(x - x_0)^2}{2i\hbar t}\right). \tag{2.11}$$

2.1.2 Simple Harmonic Oscillator

For the simple harmonic oscillator (SHO) with Hamiltonian $\frac{p_x^2}{2m} + \frac{1}{2}m\omega^2 x^2$, the eigenfunctions for the SHO contain Hermite polynomials H_n

$$\psi(x) = \frac{1}{2^{\frac{n}{2}}(n!)^{\frac{1}{2}}} \left(\frac{m\omega}{\hbar\pi}\right)^{\frac{1}{4}} \exp\left(-\frac{m\omega x^2}{2\hbar}\right) H_n\left(\sqrt{\frac{m\omega}{\hbar}} x\right). \tag{2.12}$$

One needs Mehler's formula [16]

$$\sum_{n=0}^{\infty} H_n(\xi)H_n(\eta)\frac{\nu^n}{2^n n!} = \frac{1}{\sqrt{1-\nu^2}}\exp\left(\frac{2\xi\eta-\nu^2(\xi^2+\eta^2)}{1-\nu^2}\right) \tag{2.13}$$

to use the eigenfunction expansion method. By substituting the Hermite polynomial into Mehler's formula and using $E_n = \hbar w(n+1/2)$, one can rewrite the propagator as

$$\begin{aligned} K(x,x_0;t) &= \sum_{n=0}^{\infty}\sqrt{\frac{m\omega}{\hbar\pi}}\frac{1}{2^n n!}\exp\left(-\frac{m\omega(x^2+x_0^2)}{2\hbar}\right)H_n(\sqrt{\frac{m\omega}{\hbar}}x)H_n(\sqrt{\frac{m\omega}{\hbar}}x_0) \\ &\quad\cdot\exp\left(-i\omega(n+\frac{1}{2})t\right). \end{aligned} \tag{2.14}$$

In order to use Mehler's formula, one sets $\exp(-i\omega tn)$ equal to ν^n and applies a change of variables $\xi = \sqrt{\frac{m\omega}{\hbar}}x, \eta = \sqrt{\frac{m\omega}{\hbar}}x_0$ to obtain

$$K(x,x_0;t) = \sum_{n=0}^{\infty}\sqrt{\frac{m\omega}{\hbar\pi}}\exp\left(-\frac{m\omega(x^2+x_0^2)}{2\hbar}-\frac{i\omega t}{2}\right)\frac{\nu^n}{2^n n!}H_n(\xi)H_n(\eta). \tag{2.15}$$

By use of the relation

$$\frac{1}{\sqrt{1-e^{-2i\omega t}}} = \frac{1}{\sqrt{2i\sin(\omega t)\exp\left(-i\omega t\right)}} \tag{2.16}$$

and some trivial algebraic operations, I obtain the propagator for the simple harmonic oscillator

$$K(x,x_0;t) = \sqrt{\frac{m\omega}{2\pi i\hbar\sin(\omega t)}}\exp\left(-\frac{m\omega(x^2\cos(\omega t)-2xx_0+x_0^2\cos(\omega t))}{2i\hbar\sin(\omega t)}\right). \tag{2.17}$$

2.2 Schwinger's Operator Method

An alternative method to construct the propagator is due to Schwinger. The basic idea of this method is to convert all momentum operators to position operators in order to act upon the position vector space [17]. I give some examples below.

2.2.1 Free Particle

For the free particle case, the Hamiltonian is

$$H = \frac{p_x^2}{2m}. \tag{2.18}$$

First, one solves for $x(t)$ and $p_x(t)$ using Heisenberg equations of motions for a general operator $\hat{A}$

$$\frac{d\hat{A}}{dt} = \frac{i}{\hbar}[H, \hat{A}] + \frac{\partial \hat{A}}{\partial t} \tag{2.19}$$

and obtain

$$\dot{\hat{x}} = \frac{\hat{p}_x(t)}{m}, \qquad \dot{\hat{p}_x} = 0. \tag{2.20}$$

The solutions to these equations are

$$\begin{aligned} \hat{p}(t) &= \hat{p}(0), \\ \hat{x}(t) &= \hat{x}(0) + \frac{\hat{p}_x(0)t}{m}. \end{aligned} \tag{2.21}$$

Then by writing $\hat{p}_x(t) = \hat{p}_x(0)$ in terms of $\hat{x}(t)$ and $\hat{x}(0)$, one obtains

$$\hat{p}_x(0) = \frac{m\Big(\hat{x}(t) - \hat{x}(0)\Big)}{t}. \tag{2.22}$$

Since the Hamiltonian is time-independent, $\hat{H}(0) = \hat{H}(t) = \hat{H}$

$$\hat{H} = \frac{m}{2t^2}\Big(\hat{x}(t) - \hat{x}(0)\Big)^2. \tag{2.23}$$

Since in the propagator the eigenstates $|x(t)\rangle$ appear as bras and $|x(0)\rangle$ as kets, I perform normal-ordering in order to apply the operators directly on the position vector,

$$[\hat{x}(0), \hat{x}(t)] \;=\; \frac{i\hbar t}{m} \tag{2.24}$$

$$\hat{H}(0) = \frac{m}{2t^2}\left(\hat{x}(t)^2 + \hat{x}(0)^2 - 2\hat{x}(t)\hat{x}(0) - \frac{i\hbar t}{m}\right) \tag{2.25}$$

$$\tilde{H}(t) = \frac{< x_i(t)|\hat{H}(0)|x_i(0) >}{< x_i(t)|x_i(0) >} \tag{2.26}$$

$$K(x, x_0; t) = C \cdot \exp\left(-\frac{i}{\hbar}\int^t \tilde{H}(\tau')d\tau'\right). \tag{2.27}$$

Note that the above integral is an indefinite integral. I retrieve the free particle propagator

$$K(x, x_0; t) = \sqrt{\frac{m}{2i\hbar\pi t}}\exp\left(\frac{i}{\hbar}\frac{m(x-x_0)^2}{2t}\right) \tag{2.28}$$

where $\hat{x}(0)|x(0)\rangle = x_0|x(0)\rangle$ and $\hat{x}(t)|x(t)\rangle = x|x(t)\rangle$ was applied.

2.2.2 Linear Potential

The Hamiltonian for a particle in a linear potential is

$$H = \frac{p_x^2}{2m} - fx, \tag{2.29}$$

where f is a constant. Applying Heisenberg's equations of motions

$$\dot{\hat{x}} = \frac{\hat{p}_x(t)}{m}, \qquad \dot{\hat{p}_x} = f \tag{2.30}$$

we find $x(t)$, where

$$\hat{x}(t) = \hat{x}(0) + \frac{\hat{p}_x(0)t}{m} + \frac{ft^2}{2m}. \tag{2.31}$$

Writing $\hat{p}_x(0)$ in terms of $\hat{x}(t)$ and $\hat{x}(0)$ gives

$$\hat{p}_x(0) = \frac{m\left(\hat{x}(t) - \hat{x}(0) - \frac{ft^2}{2m}\right)}{t}. \tag{2.32}$$

Because the Hamiltonian is time-independent, I have

$$\hat{H} = \frac{m}{2t^2}\left(\hat{x}(t) - \hat{x}(0) - \frac{ft^2}{2m}\right)^2 - f\hat{x}(0). \tag{2.33}$$

In analogy to the free particle case, normal-ordering is needed before operating on the position vector,

$$[\hat{x}(0), \hat{x}(t)] = \frac{i\hbar t}{m} \tag{2.34}$$

$$\hat{H}(0) = \frac{m}{2t^2}\left(\hat{x}(t)^2 + \hat{x}(0)^2 - 2\hat{x}(t)\hat{x}(0) - \frac{i\hbar t}{m} - \frac{\hat{x}(t)+\hat{x}(0)}{m} f t^2 + \frac{f^2 t^4}{4m^2}\right) \tag{2.35}$$

$$\tilde{H} = \frac{< x_i(t)|\hat{H}(0)|x_i(0) >}{< x_i(t)|x_i(0) >} \tag{2.36}$$

$$K(x_i{}'', t_1|x_i{}', t_0) = C \cdot \exp\left(-\frac{i}{\hbar}\int^{\tau} \tilde{H} d\tau'\right). \tag{2.37}$$

Finally, the propagator for the linear potential becomes

$$K(x, x_0; t) = \sqrt{\frac{m}{2i\hbar\pi t}} \exp\left(\frac{i}{\hbar}\left(\frac{m(x-x_0)^2}{2t} + \frac{f(x+x_0)t}{2} - \frac{f^2 t^3}{24m}\right)\right). \tag{2.38}$$

2.2.3 Simple Harmonic Oscillator

The Hamiltonian for a particle in a simple harmonic oscillator potential is

$$H = \frac{p_x^2}{2m} + \frac{m\omega^2 x^2}{2}, \tag{2.39}$$

where ω is the oscillation frequency and time-independent. Applying Heisenberg's equations of motions, I obtain

$$\dot{\hat{p}}_x = -m\omega^2 \hat{x}, \qquad \dot{\hat{x}} = \frac{\hat{p}_x}{m}. \tag{2.40}$$

By solving for $\hat{x}(t)$ and $\hat{p}(t)$, and by imposing the initial conditions for the operators, I get

$$\hat{x}(t) = \frac{\hat{p}_x(0)\sin(\omega t)}{m\omega} + \cos(\omega t)\hat{x}(0). \tag{2.41}$$

By writing $\hat{p}_x(0)$ in terms of $\hat{x}(t)$ and $\hat{x}(0)$, and also by using the commutation relation between $\hat{x}(t)$ and $\hat{x}(0)$, namely $[\hat{x}(0), \hat{x}(t)] = \frac{i\hbar\sin(\omega t)}{m\omega}$, the Hamiltonian can be written

as

$$\hat{H}(0) = \frac{m\omega^2}{2\sin(\omega t)^2}\left(\hat{x}(t) - \hat{x}(0)\cos(\omega t)\right)^2 + \frac{m\omega^2\hat{x}(0)^2}{2} \tag{2.42}$$

and the rest of the derivation is the same as in the case of the linear potential.

2.3 Classical Action Method

If the potential doesn't vary rapidly from one point to the other, the classical action method gives a good approximation. Actually, this method gives the exact result for a lot of cases. [2]

2.3.1 Free Particle

Starting off with the Lagrangian for the free particle

$$L = \frac{1}{2}m\dot{x}^2 \tag{2.43}$$

and solving the Euler-Lagrange equations of motion to obtain

$$\begin{aligned} \frac{d}{dt}\frac{\partial L}{\partial \dot{x}} - \frac{\partial L}{\partial x} &= 0 \\ m\ddot{x} &= 0 \end{aligned} \tag{2.44}$$

Therefore the general solution for $x(t)$ is the usual trajectory without any acceleration, namely

$$x(t) = x_0 + bt, \tag{2.45}$$

[2] This method is also referred to as the stationary phase method. A first (semiclassical) approximation of the propagator is given by considering the neighboring paths added constructively and this approximation does give exact results for a large class of problems. For more details, see Merzbacher *Quantum Mechanics* page 357 [16].

where b can be determined by from setting up another boundary condition. Choosing $x(\tau) = x$ in this case, b is obtained from

$$\begin{aligned} x &= x(0) + b\tau \\ b &= \frac{x - x_0}{\tau}. \end{aligned} \tag{2.46}$$

To calculate the classical action, I integrate the Lagrangian from time 0 to τ, $S = \int_0^\tau L dt$. Therefore using integration by parts and using the equation of motion in Eq.(2.44) I obtain

$$\begin{aligned} S &= \int_0^\tau \frac{1}{2} m\dot{x}^2 dt \\ &= \int_0^\tau \frac{1}{2} m\dot{x}\dot{x} dt \\ &= \frac{1}{2} mx\dot{x}|_0^\tau - \int_0^\tau \frac{1}{2} m\ddot{x}x dt \\ &= \frac{1}{2} mx(\tau)\dot{x}(\tau) - \frac{1}{2} mx(0)\dot{x}(0) - 0, \end{aligned} \tag{2.47}$$

and because $\dot{x} = b = \frac{x - x_0}{\tau}$,

$$\begin{aligned} S &= \frac{1}{2} mx\frac{x - x_0}{\tau} - \frac{1}{2} mx_0\frac{x - x_0}{\tau} \\ &= \frac{m(x - x_0)^2}{2\tau}. \end{aligned} \tag{2.48}$$

Thus the classical action method gives the propagator in the following form:

$$\begin{aligned} K(x, x_0; \tau) &= A \exp\left(\frac{i}{\hbar} S(x, x_0; \tau\right) \\ &= A \exp\left(\frac{i}{\hbar} \frac{m(x - x_0)^2}{2\tau}\right). \end{aligned} \tag{2.49}$$

A can be obtained by taking the limit $t \to 0$, in which it can be shown that $A = \frac{m}{2\pi i\hbar t}$. As a result, the final result is again

$$K(x, x_0; \tau) = \sqrt{\frac{m}{2\pi i\hbar t}} \exp\left(\frac{i}{\hbar} \frac{m(x - x_0)^2}{2\tau}\right). \tag{2.50}$$

2.3.2 Linear Potential

The Lagrangian for the linear potential $V(x) = kx$ is

$$L = \frac{1}{2}m\dot{x}^2 - kx. \tag{2.51}$$

Working out the Euler-Lagrange equation of motion

$$\ddot{x}(t) = -\frac{k}{m}, \tag{2.52}$$

and the general solution for $x(t)$ is given by

$$x(t) = x_0 + bt - \frac{k}{2m}t^2. \tag{2.53}$$

Similar to the free particle case, I set a boundary condition at the end point $x(\tau) = x$

$$x = x_0 + b\tau - \frac{k}{2m}\tau^2, \tag{2.54}$$

to obtain

$$b = \frac{x - x_0 + \frac{k}{2m}\tau^2}{\tau}, \tag{2.55}$$

and

$$\begin{aligned} x(t) &= x_0 + \frac{x - x_0 + \frac{k}{2m}\tau^2}{\tau}t - \frac{k}{2m}t^2, \\ \dot{x}(t) &= \frac{x - x_0 + \frac{k}{2m}\tau^2}{\tau} - \frac{k}{m}t. \end{aligned} \tag{2.56}$$

Using $\ddot{x}(t) = -\frac{k}{m}$, I calculate the action

$$\begin{aligned} S &= \int_0^\tau L dt \\ &= \int_0^\tau (\frac{1}{2}m\dot{x}^2 - kx)dt \\ &= \frac{1}{2}mx\dot{x}|_0^\tau - \int_0^\tau (\frac{1}{2}mx\ddot{x} + kx)dt \\ &= \frac{1}{2}mx\dot{x}|_0^\tau - \int_0^\tau \frac{1}{2}kxdt \end{aligned}$$

$$\begin{aligned} &= \frac{1}{2}mx\dot{x}|_0^\tau - \int_0^\tau \frac{1}{2}k(x_0 + bt - \frac{k}{2m}t^2)dt \\ &= \frac{1}{2}mx\dot{x}|_0^\tau - \frac{1}{2}kx_0\tau - \frac{1}{4}kb\tau^2 + \frac{k^2}{12m}\tau^3 \\ &= \frac{1}{2}mx\dot{x}|_0^\tau - \frac{1}{2}kx_0\tau - \frac{1}{4}k\frac{x - x_0 + \frac{k}{2m}\tau^2}{\tau}\tau^2 + \frac{k^2}{12m}\tau^3 \end{aligned} \tag{2.57}$$

and use the result of $\dot{x}(t)$

$$\dot{x}(0) = \frac{x - x_0 + \frac{k}{2m}\tau^2}{\tau}, \qquad \dot{x}(\tau) = \frac{x - x_0 - \frac{k}{2m}\tau^2}{\tau}. \tag{2.58}$$

I finally obtain the action for the linear potential

$$S(x, x_0; \tau) = \frac{m(x - x_0)^2}{2\tau} - \frac{k(x + x_0)\tau}{2} - \frac{k^2\tau^3}{24m}. \tag{2.59}$$

Again

$$K(x, x_0; \tau) = A\exp\left(\frac{i}{\hbar}S(x, x_0; \tau)\right), \tag{2.60}$$

where $A = \sqrt{\frac{m}{2\pi i\hbar t}}$. Finally, I obtain the propagator for the linear potential

$$K(x, x_0; \tau) = \sqrt{\frac{m}{2\pi i\hbar t}}\exp\left(\frac{i}{\hbar}(\frac{m(x - x_0)^2}{2\tau} - \frac{k(x + x_0)\tau}{2} - \frac{k^2\tau^3}{24m})\right). \tag{2.61}$$

2.4 Lie Algebra Method or Algebraic Method

There also exists a Lie Algebra method which uses the symmetry of the group to simplify the calculation of propagators. It is described in Wang [18]. From the definition of the time-evolution operator, I know that

$$\psi(x, t) = T(t, 0)\psi(x, 0) = \exp\left(-\frac{itH}{\hbar}\right)\psi(x, 0), \tag{2.62}$$

where H is the time-independent Hamiltonian.

I first work out the free-particle case, where Eq.(2.62) can be rewritten as,

$$\psi(x,t) = \exp\left(\frac{it\hbar\partial_{xx}^2}{2m}\right)\psi(x,0). \tag{2.63}$$

The Suzuki formula [3]

$$\exp(\alpha\partial_{xx})f(x) = \frac{1}{\sqrt{4\pi\alpha}}\int_{-\infty}^{\infty}\exp\left(-\frac{(x-y)^2}{4\alpha}\right)f(y)dy \tag{2.64}$$

is useful. By matching up coefficients and using the defining equation for the propagator

$$\psi(x,t) = \int_{-\infty}^{\infty}K(x,x_0;t)\psi(x_0,0)dx_0, \tag{2.65}$$

I can derive the free propagator in Eq.(2.11).

The free-particle propagator can be successfully obtained when the Suzuki formula is repeatedly used in different cases since the main goal of this method is to completely separate the kinetic energy term from the potential term where they don't usually commute. In the paper by Wang [18], the following cases are considered: linear, harmonic oscillator, and a combination of linear and harmonic oscillator potential. Here the linear potential problem suffices to illustrate the method.

The linear potential Hamiltonian, for example the electric potential energy for a charge e from a constant electric field, is given by

$$H = -\frac{\hbar^2\partial_{xx}}{2m} + ex. \tag{2.66}$$

First, I relate $[\partial_x^2, x] = 2\partial_x$ to $[a^2, a^\dagger] = 2a$, where a and $a^\dagger$ are annihilation and creation operators respectively, and I use Katriel's formula

$$\exp\left(\alpha a^+ + \beta a^r\right) = e^{\alpha a^+}\exp\left(\sum_{i=0}^{r}\beta\alpha^i\binom{r}{i}\frac{1}{1+i}a^{r-i}\right). \tag{2.67}$$

[3] See derivation in Suzuki's paper [20].

After substitution, the kinetic term and the potential term are separated in the following expression

$$\exp\left(-\frac{it}{\hbar}(-\frac{\hbar}{2m}\partial_{xx}+ex)\right)=\exp\left(-\frac{ietx}{\hbar}\right)\exp\left(\frac{i\hbar t}{2m}\partial_{xx}+\frac{et^2}{2m}\partial_x-\frac{it^3e^3}{6m\hbar}\right). \quad (2.68)$$

Using the displacement formula

$$e^{\alpha\partial_x}f(x)=f(x+\alpha) \quad (2.69)$$

and shifting the corresponding function, again I obtain the linear propagator as in Eq.(2.38).

For the harmonic oscillator case, $H=-\frac{\hbar^2}{2m}\partial_{xx}+\frac{1}{2}m\omega^2x^2$, three operators can be defined to create an su(2) algebra [4]. These are $L_-=\frac{1}{2}\partial_{xx}, L_+=\frac{1}{2}x^2$, and $L_3=\frac{1}{2}x\partial_x+\frac{1}{4}$ [5]. For the harmonic oscillator plus a linear potential case, it is straightforward to perform a translation in x such that the linear term is absorbed in a perfect square in x.

This method could be quite useful if schemes are available to create operators which generate a Lie algebra. Also, in the original paper, all the Hamiltonians discussed are spin-independent. Therefore it is interesting to see how this method can be applied in spin-dependent systems.

2.5 Merzbacher's Guessing Method

In Eugene Merzbacher's *Quantum Mechanics*, the author introduces a guessing method which will be worked out here for the free particle. The simple harmonic oscillator has been worked out in the book [16].

[4] su(2) satisfies $[L_+,L_-]=2L_3, [L_3,L_\pm]=\pm L_\pm$.

[5] In order to separate kinetic and potential energy terms, [21] and [22] is needed.

2.5.1 Free particle

First I assume an action function $S(x, x_0, t)$ of the form

$$S(x, x_0, t) = a(t)x^2 + b(t)xx_0 + a(t)x_0^2 + c(t). \tag{2.70}$$

Substituting this into the Hamilton-Jacobi equation,

$$\frac{\partial S}{\partial t} + \frac{1}{2m}(\frac{\partial S}{\partial x})^2 - \frac{i\hbar}{2m}\frac{\partial^2 S}{\partial x^2} + V(x) = 0, \tag{2.71}$$

where $V(x) = 0$ in this case, one obtains

$$\begin{aligned} &\dot{a}(t)x^2 + \dot{b}(t)xx_0 + \dot{a}(t)x_0^2 + \dot{c}(t) \\ &+\frac{1}{2m}\bigg(4a(t)^2x^2 + 4a(t)b(t)xx_0 + b(t)^2x_0^2\bigg) - \frac{i\hbar a(t)}{m} = 0. \end{aligned} \tag{2.72}$$

After rearranging, I obtain

$$\begin{aligned} &x^2\bigg(\dot{a}(t) + \frac{2a(t)^2}{m}\bigg) + xx_0\bigg(\dot{b}(t) + \frac{2a(t)b(t)}{m}\bigg) + x_0^2\bigg(\dot{a}(t)^2 + \frac{b^2}{2m}\bigg) \\ &+\dot{c}(t) - \frac{i\hbar a(t)}{m} = 0. \end{aligned} \tag{2.73}$$

By setting the four coefficients of the function that can be varied independently (x^2, xx_0, x_0^2, and 1) to zero, I get

$$\begin{aligned} \dot{a}(t) + \frac{2a(t)^2}{m} &= 0 \\ \dot{b}(t) + \frac{2a(t)b(t)}{m} &= 0 \\ \dot{a}(t)^2 + \frac{b^2}{2m} &= 0 \\ \dot{c}(t) - \frac{i\hbar a(t)}{m} &= 0. \end{aligned} \tag{2.74}$$

I now can check that

$$a(t) = \frac{m}{2t}, \quad b(t) = \frac{1}{t}, \quad c(t) = \frac{i\hbar}{2}ln(t) \tag{2.75}$$

satisfy Eq.(2.74). Once $a(t)$, $b(t)$, and $c(t)$ are found, I can write the propagator in terms of the function $S(x, x_0, t)$ to obtain

$$K(x, x_0; t) = e^{iS(x,x_0,t)/\hbar}. \tag{2.76}$$

As a result, the free particle propagator in Eq.(2.11) is obtained.

2.6 Elementary Transformation Method

An elementary transformation method is introduced by Tsaur [19] to simplify the Hamiltonian in order to obtain the propagator [6].

In the paper, three types of elementary transformations are presented: interchange, similarity, and point transformations defined as

- **I**nterchange:$(p, x) = (X, -P)$
- **S**imilarity: $(p, x) = (P + f'(x), X)$
- **P**oint:$(p, x) = (\frac{1}{g'(X)}P, g(X))$,

while each transformation function on the wavefunction is

$$\begin{aligned} \Psi(X,t) &= C_I\psi = \int_{-\infty}^{\infty} e^{-iX\xi}\psi(\xi,t)d\xi \\ \Psi(X,t) &= C_S\psi = e^{-if(X)}\psi(X,t) \\ \Psi(X,t) &= C_P\psi = \psi(g(X),t) \end{aligned} \tag{2.77}$$

and the inverse wavefunction transformations are

$$\begin{aligned} \psi(x,t) &= C_I^{-1}\Psi = \frac{1}{2\pi}\int_{-\infty}^{\infty} e^{ix\xi}\Psi(\xi,t)d\xi \\ \psi(x,t) &= C_S^{-1}\Psi = e^{-if(x)}\Psi(x,t) \\ \psi(x,t) &= C_P^{-1}\Psi = \Psi(g^{-1}(x),t). \end{aligned} \tag{2.78}$$

[6]The title of the paper is on the Green function, however, it is actually the propagator according to the definition explained in the paper.

It is also mentioned in the paper, that in some cases, the Hamiltonian can be transformed into one dependent variable. Therefore a x-linear transformation L_x : $F(p) + G(p)x = P$ is introduced

$$\begin{aligned} \Psi &= C_{L_x}\psi = (e^{-if(\xi)} \int_{-\infty}^{\infty} e^{-i\xi\eta}\psi(\eta,t)d\eta)_{\xi=g^{-1}(X)} \\ \psi &= C_{L_x}^{-1}\Psi = \frac{1}{2\pi}\int_{-\infty}^{\infty} e^{ix\xi}e^{if(\xi)}\Psi(g(\xi),t)d\xi, \end{aligned} \tag{2.79}$$

while $f'(x) = F(x)/G(x), g'(x) = -1/G(x)$. In order to illustrate the idea, the example of the linear potential propagator is given here.

2.6.1 Linear Potential

The Hamiltonian for a linear potential in one dimension is

$$H = \frac{p^2}{2m} - Ux. \tag{2.80}$$

This Hamiltonian can be successfully reduced to one variable in the new coordinate by using the x-linear transformation. By matching up the coefficient of $F(p) = \frac{p^2}{2m}$ and $G(p) = -U$ and work out $f(x)$ and $g(x)$, I obtain

$$f(x) = -\frac{x^3}{6mU}, \qquad g(x) = \frac{x}{U}, \qquad g^{-1}(X) = UX. \tag{2.81}$$

Starting from the initial condition for the propagator $K(x,x';0) = \delta(x-x')$ and by applying the transformation

$$\begin{aligned} \tilde{K}(X,x';0) &= C_{L_x}\delta(x-x') \\ &= (e^{i\frac{\xi^3}{6Um}} \int_{-\infty}^{\infty} e^{-i\xi\eta}\delta(\eta-x')d\eta)_{\xi=UX} \\ &= e^{i\frac{U^2X^3}{6m} - iUXx'}. \end{aligned} \tag{2.82}$$

Since the transformed Hamiltonian only depends on P in this case, the solution to the time-dependent Schrödinger equation $i\hbar\frac{\partial K}{\partial t} = H(P)K$ with the initial condition

$K(X, x; 0)$ is

$$K(X, x'; t) = e^{-iH(P)t} K(X, x'; 0). \tag{2.83}$$

Applying the interchange transformation $P = C_I^{-1} X C_I$ leads to $e^{-iH(P)t}$ $= C_I^{-1} e^{-iH(X)t} C_I$. After straightforward algebraic manipulations, I obtain

$$K(X, x'; t) = \int_{-\infty}^{\infty} [\frac{1}{2\pi} \int_{-\infty}^{\infty} e^{-iH(\xi)t + i\xi(X-\eta)} d\xi] K(\eta, x'; 0) d\eta. \tag{2.84}$$

As a result

$$\begin{aligned} \tilde{K}(X, x'; t) &= \int_{-\infty}^{\infty} [\frac{1}{2\pi} \int_{-\infty}^{\infty} e^{i\xi(X-t-\eta)}] \tilde{K}(\eta, x'; 0) d\eta d\xi \\ &= \tilde{K}(X - t, x'; 0) = e^{\frac{iU^2(X-t)^3}{6m} - iU(X-t)x'}. \end{aligned} \tag{2.85}$$

The integral is trivial due to the delta function. Next the inverse transformation gives the propagator

$$\begin{aligned} K(x, x'; t) &= C_{L_x}^{-1} \tilde{K}(X, x'; t) \\ &= \frac{1}{2\pi} \int_{-\infty}^{\infty} e^{ix\xi} e^{-i\frac{\xi^3}{6Um}} \tilde{K}(\frac{\xi}{U}, x'; t) d\xi. \end{aligned} \tag{2.86}$$

After integration, I obtain the linear potential propagator in Eq.(2.38).

There are a few other examples of this method, including the free particle, harmonic oscillator, centrifugal potential, and centripetal barrier potential cases. However, only one-dimensional case have been considered. It would be useful to extend this method to two-dimensional cases. The easiest case would be two independent coordinates since each dimension can be solved separately. For cases with coupled dimensions, dimensions have to be uncoupled in order to perform the one-dimensional elementary transformations. Otherwise, a similar transformation involving two dimensions has to be introduced. For example, a similar point transformation

$\mathbf{P} : (p, x) = (\frac{P}{g'(X)}, g(X))$ in one dimension can be extended to two coupled dimensions.

I provide a summary of the analytic methods (based on section numbers) in Table 2.1.

Section Number	Free Particle	Linear Potential	Simple Harmonic Oscillator
2.1	√	♡	√
2.2	√	√	√
2.3	√	√	♣
2.4	√	√	♣
2.5	√	♣	♣
2.6	♣	√	√

Table 2.1 Symbol explanation. √ indicates that the method has been used and has been shown in this thesis, ♣ indicates that the method can be used but has not been shown in this thesis, and ♡ indicates that it is difficult to apply this method.

2.7 Numerical Propagation Methods

In the previous six subsections, I have derived propagators without considering the spin degree of freedom. To achieve propagation in spin systems, I will need one more method in which the wave function evolves one step at a time. The difficulty to derive analytic spin propagators lies in the noncommutative property of spin operators. In systems without spin, there are also noncommutative operators such as position x and momentum p. However in these cases the noncommutativity is less difficult to handle.

To apply the eigenfunction expansion method from section 2.1, the exact eigen-

functions and their summation formula need to be known. In section 2.2 and section 2.3, one needs to be able to solve $x(t)$ and $p(t)$ exactly in order to substitute them in the expression for the Hamiltonian. This turns out to be a problem for the Pauli matrices $\sigma_x(t), \sigma_y(t)$, and $\sigma_z(t)$ in 2D inhomogeneous Stern-Gerlach systems. To apply the classical action method of section 2.4, one needs a noncommutative operation whose commutator is constant to truncate the series. Also Merzbacher's guessing method becomes intractable for Pauli matrices. As far as the elementary transformation method in section 2.6, it is developed for 1D only and the extension to higher dimensions is not straightforward.

In what follows, I use the Trotter product formula [57] to find spin evolution when noncommutativity between Pauli matrices arises. By using the Trotter product formula on the time-evolution operator and by projecting the result onto the initial and the final position eigenstates, I can construct analytic propagators for systems involving noncommuting Pauli matrices. However, it is still challenging to perform an analytic integration of the non-Gaussian integrand due to the presence of Pauli matrices. Therefore I perform a Monte-Carlo integration to evaluate the spin local density $\langle \mathbf{S} \rangle(x, y)$, namely a projection over spin space only. This method is more reliable when more sample points are used. This method is used for 2D Rashba systems. I provide a sample Matlab code in Appendix F.2 to illustrate the Monte-Carlo method.

Note that even with approximated analytic propagators, the application of the integral formula can still be a daunting task. In order to evaluate the evolution of wave packets in a more efficient way without any numerical integration, I use the Trotter product formula for noncommuting operators a_1 and a_2

$$\exp\Big(-\tau(a_1+a_2)\Big)\psi(x,0) \approx \lim_{n\to\infty}\left(\exp(-\frac{\tau}{2n}a_1)\exp(-\frac{\tau}{n}a_2)\exp(-\frac{\tau}{2n}a_1)\right)^n \psi(x,0). \tag{2.87}$$

In particular, I can set a_1 to be the potential energy term and a_2 to be the kinetic energy term. Instead of using the propagator integral formula, I apply the time-evolution operator directly to the wave packet. The Trotter product formula in Eq.(2.87) allows ones to operate on the wave packet repeatedly. Since both the wave packet and the potential are in the coordinate representation, the operation is purely multiplicative. Before applying the kinetic operator, I need to perform a Fourier transform on all grid points. After applying the kinetic operator, an inverse Fourier transform on all (momentum) grid points is needed. Once I recover the evolved wave packet in a coordinate representation for a time interval τ/n, I can generate spin density plots by projecting wave packets in specific spin directions. As for the limitations of this method, note that in order for Eq.(2.87) to hold, the τ/n needs to be set small enough (n large enough). This can be verified through the stability of the results as n increases. One also needs to specify regions large enough, so that effects from the artificial periodic boundary do not appear. The numerical propagation method described in this section is used for obtaining Stern-Gerlach results involving 2D inhomogeneities. I provide a sample Matlab code in Appendix F.3.

I use both Mathematica and Matlab to simulate spin evolution in both Rashba and Stern-Gerlach systems. I use Mathematica when working with 1D Rashba and 1D Stern-Gerlach where analytic propagators are available. I provide a sample code written in Mathematica for the 1D Rashba system in Appendix F.1.

I use Matlab when I work with the numerical propagation method. The reason is that, in my experience, Matlab runs faster regarding the process of generating animations based on frames.

There are no stability issues in the Mathematica evaluation. Everything is analytic, including the evolved wave packets after an analytic Gaussian integration. What is shown in Mathematica is exact and the plots are numerical evaluation of an-

Section	AP		CM (R=RASHBA)			SG	
	confined	unconfined	ESRD	R 1D	R 2D	1D	2D
2.1							
2.2							
2.3		p.113	p.117				
2.4	p.116		p.118	p.129		p.41	
2.5							
2.6							
2.7					p.129		p.44

Table 2.2 A list of spin propagators for atomic physics (both confined and confined), condensed matter (ESRD, Rashba 1D, and Rashba 2D), and Stern-Gerlach (both 1D and 2D) systems extended from the methods (1st column) targeted at spinless propagators.

alytic expressions. However in the Matlab evaluation, where I use successive Fourier transforms in the numerical propagation method, the boundary has to be carefully chosen. If a longer animation is preferred, a larger boundary is needed due to the motion of the wave packet. However, a larger boundary would also lead to more grid points for precision purposes. One has to choose an optimum time to avoid the appearance of boundary effects.

I provide a summary of the propagators for three spin-dependent systems: atomic physics (AP), condensed matter physics (CM), Stern-Gerlach systems (SG) in Table 2.2. The first column refers to the section number where a specific method is extended to these spin-dependent systems. There is no reason in principle to prevent all methods to be extended to spin systems.

Chapter 3

Spin-Orbit Coupling effects

3.1 Introduction

Spin-Orbit Coupling (SOC) is an interaction between a particle's spin and its motion. It occurs in many areas of physics. Discovered in the fine structure of atomic spectra [23], later introduced to explain the nuclear structure, it is now also of great interest in condensed matter systems, such as graphene [24] and semiconducting materials with promising spintronics applications [1,4]. It is also found in the physics of optical lattices mimicking condensed matter systems [25]. The SOC is characterized by interaction terms that contain position $\overrightarrow{r}$, momentum $\overrightarrow{p}$ and spin operators $\overrightarrow{S}$.

In "atomic" physics, the SOC term is $H_{SOC}^{atomic} = \gamma(r)\mathbf{S}\cdot\mathbf{L}$, where $\mathbf{L} = \mathbf{r}\times\mathbf{p}$. The coupling strength $\gamma(r)$ is determined by the Coulomb potential $V(r)$

$$\gamma(r) \sim \frac{\partial V(r)}{\partial r}. \tag{3.1}$$

I consider a special "atomic" SOC case where $V(r) = r$, subject to a parabolic confinement which corresponds to a Hamiltonian

$$H = \frac{p_x^2 + p_y^2}{2m} + \gamma\overrightarrow{\sigma}\cdot\mathbf{L} + \frac{1}{2}m\eta^2(x^2+y^2), \tag{3.2}$$

so that the highest order in the Hamiltonian is quadratic.

In condensed matter physics, the Structure Inversion Asymmetry (SIA) leads to the Rashba SOC term $H_{SOC}^{Rashba} = \frac{\alpha}{\hbar}(p_y\sigma_x - p_x\sigma_y)$ where α is the Rashba interaction strength [26, 27]. SIA originates from the inhomogeneity in the doping concentration in the quantum well, which induces an internal electric field, and thus leads to spin-orbit coupling as $v \times E$. It is also to be noted that a different asymmetry, namely Bulk Inversion Asymmetry (BIA) , leads to the Dresselhaus SOC term $H_{SOC}^{Dresselhaus} = \frac{\beta}{\hbar}(p_x\sigma_x - p_y\sigma_y)$ where β is the Dresselhaus interaction strength [28]. BIA originates from the lack of an inversion center in the crystal structure, such as the zinc-blende structure. What is significant about the Rashba and Dresselhaus effects is the ability to manipulate the spin degrees of freedom of an electron without applying an external magnetic field. In the semiconductor industry, the bulkiness of the magnet is a drawback when designing electrical circuits. Spin-orbit coupling provides one possible solution to this problem. It has been proposed that a Hamiltonian involving equal strength ($\alpha = \beta$) Rashba and Dresselhaus effects (ESRD) could be

$$H_{ESRD} = \frac{p_x^2 + p_y^2}{2m} + \frac{\alpha}{\hbar}(p_x + p_y)(\sigma_x - \sigma_y). \tag{3.3}$$

Likewise for opposite strength ($\alpha = -\beta$) Rashba and Dresselhaus effects (OSRD), a possible Hamiltonian is

$$H_{OSRD} = \frac{p_x^2 + p_y^2}{2m} + \frac{\alpha}{\hbar}(p_x - p_y)(\sigma_x + \sigma_y). \tag{3.4}$$

This leads to helicoidal motion and to the so-called Persistent Spin Helix [29], which is relevant to the development of the non-ballistic spin field-effect transistor [30].

Most current literature focuses on the stationary states (fixed energy) in the Rashba or Dresselhaus systems. The Hamiltonians involving either the Rashba or the Dresselhaus SOC resemble the free particle Hamiltonian. Therefore, a plane-wave solution with a phase modulated by the spin is often used. The issues around

the localization and the normalization of the solution are typically not discussed. A plane-wave solution is not and can not be normalized. Therefore it would not make sense to plot the spin density from a wave function which is not normalized in space. Also, the spreading of the wave packet can not be observed and calculated using a plane-wave solution. This motivates a study of a spin wave packet, namely functions with spin degree of freedom that are localized (Gaussian) in space in Rashba/Dresselhaus systems. The evolution of the spin wave packet will be addressed by using the propagator approach.

3.2 Propagator Construction

I have constructed analytic propagators in systems exhibiting spin-orbit interactions in the paper attached in Appendix C. I first construct the propagators for the system involving "atomic" spin-orbit coupling with and without confinement in Eq.(C.34) and Eq.(C.20). I then construct propagators for Equal-Strength-Rashba-Dresselhaus (ESRD) with and without confinement in Eq.(C.62) and Eq.(C.53) and Opposite-Strength-Rashba-Dresselhaus (OSRD) with and without confinement in Eq.(C.63) and Eq.(C.53). Later I apply the analytic propagators for the confined atomic spin-orbit coupled system and the confined ESRD to localized wave packets with an arbitrary initial spin states in Eq.(C.78) and in Eq.(C.79) respectively.

The ESRD (OSRD) is a special case where we can decouple spin and momentum operators by setting $\alpha = +(-)\beta$. Systems involving either Rashba or Dresselhaus SOC alone are more complicated than ESRD. I have looked at the case where only Rashba SOC is present with parabolic confinement in Appendix D. I have constructed analytic propagators for 1D Rashba wire with and without confinement in Eq.(D.2) and Eq.(D.3). I also derive analytic propagators for 2D Rashba systems with and

without confinement in Eq.(D.7) and Eq.(D.8). The construction of propagators in the 1D case requires successive operations of the time-evolution on the wave function. This approach is described in detail in Appendix C. The construction of propagators in the 2D case is based on the Trotter formula in Eq.(2.87) and Eq.(D.5) extended to Eq.(D.6).

It is noteworthy that the Rashba Hamiltonian can be reduced to the form $\overrightarrow{\sigma} \cdot \overrightarrow{L}$ by a semiclassical "effective" potential method [31]: a repeated application of the Heisenberg prescription for time-dependence of the position gives the acceleration of the particle, therefore the force and, by space integration, also the potential acting on the particle. For time-independent (or frozen) spin operators this potential yields precisely a spin-orbit coupling term

$$H_{eff} = \frac{p_x^2 + p_y^2}{2m} + C\overrightarrow{\sigma} \cdot \overrightarrow{L}, \tag{3.5}$$

where C depends on the Rashba strength α. Starting with a Rashba system which mixes $\mathbf{p}$ and $\overrightarrow{\sigma}$, the effective method produces a familiar spin-orbit term $\overrightarrow{\sigma} \cdot \overrightarrow{L}$. I have considered such systems in Appendix B.

3.3 Results

I have generated local spin density plots $\langle S_z \rangle$ for the system involving Rashba effective potential in Appendix B. It can be seen in Fig.(B.4) that the spin-up and spin-down components perform clockwise and counterclockwise motion respectively. It should also be noted that this effective potential is similar to the system proposed by Bernevig *et al* to generate the quantum spin Hall effect [32].

I also obtain the evolved wave packets in both systems in Eq.(C.78)(atomic) and in Eq.(C.79)(ESRD) with arbitrary spin components. I select an initial spin state and generate spin density plots in Fig.(C.1) and Fig.(C.2). I notice a counterclockwise

spin rotation for the spin-up component while I observe that the spin wave packet oscillates along the diagonal axis.

The localized wave packet used in Appendix B, C, and D is of the form

$$\psi(x_0, y_0, 0) = \frac{1}{\pi w_x w_y} \exp\left(-\frac{x_0^2}{2w_x^2} - \frac{y_0^2}{2w_y^2}\right)\Big(\chi|\uparrow\rangle + \xi|\uparrow\rangle\Big), \tag{3.6}$$

where $|\uparrow\rangle$ and $|\downarrow\rangle$ are up-in-z and down-in-z spin states with constant coefficients χ and ξ chosen to satisfy $|\chi|^2 + |\xi|^2 = 1$. Note that this wave packet is not normalized.[1] The choice of normalization constants does not affect dynamics but it does affect the arbitrary (color) scale in all 2D contour plots.

I generate plots of local spin density $\langle \mathbf{S} \rangle(x, y)$ for all cases in the Rashba systems. I highlight four features in both 1D and 2D Rashba systems. The reason why these four features were chosen is because most of them have been discussed in the literature and they provide a basis for me to understand more complex cases. In the 1D Rashba system, they are Spin Separation (SS), Bamboo-shooting structure (BSS), Persistent Spin Helix (PSH), and Spin Accumulation (SA) and I display them in Fig.(D.2), Fig.(D.3), Fig.(D.4), and Fig.(D.5). In these plots, I generate results for different choices of the Rashba strength α and the wave packet width w. I observe the decay of spin polarization at the origin in the 1D Rashba system and calculate the decay time which is provided in Eq.(D.12). The decay mechanism is different at different locations. For example, if I measure the spin polarization at the origin, the curve would be an exponentially decaying curve while if I measure points away from the origin, I would measure an increase in the spin polarization followed by an exponential decay. This can be explained from the fact that the wave packet is spreading out while

[1] The normalized wave packet would be

$$\psi(x_0, y_0, 0) = \frac{1}{\sqrt{\pi w_x w_y}} \exp\left(-\frac{x_0^2}{2w_x^2} - \frac{y_0^2}{2w_y^2}\right)\Big(\chi|\uparrow\rangle + \xi|\uparrow\rangle\Big). \tag{3.7}$$

the overall normalization has to be conserved. To illustrate SA, I generate plots at three different times to show the effects in Fig.(D.5). It is interesting to note that same spin components accumulate at the boundary after a time interval $\Delta t = \pi$.

In the 2D Rashba system, the four features I discover are Ripple Formation Structure (RFS), Triangular Oscillation (TO), and Asymmetric Spin Rotation (ASR), and Diagonal Symmetry Structure (DSS) and I display them in Fig.(D.6), Fig.(D.7), Fig.(D.8), and Fig.(D.9). In these plots, I compare results for different choices of the Rashba strength α and the wave packet widths in two dimensions w_x and w_y. In RFS with asymmetric width, I observe an interesting distortion, which I attribute to a spin Coriolis force.

In the paper presented in Appendix C, I take natural units $m = 1, \hbar = 1$ whereas the confinement strength η, the spin-orbit interaction strength γ, and the width of the wave packet w are given in absolute values. Compared with the paper presented in Appendix D, all figures in the work are presented in scaled units, namely $m = 1, \hbar = 1$, the Rashba strength $\alpha = f(d)$, and the width of the wave packet $w = f(d)$, where I have created a virtual length unit d. All of these values can be converted to realistic values that can be used to compare with experimental data. For example, in order to fit the minimum experimentally accessible α which is currently about 6×10^{-12} eV.m to the scaled choice of $\alpha = 0.5$ (low end), one selects the absolute length unit $d = 127.43$ nm and the unit time $t = 7$ ps. Similarly, one can fit $\alpha = 1$ (high end) to the maximum experimentally accessible α which is currently about 4×10^{-11} eV.m and again one can calculate the absolute unit length $d = 38.23$ nm and the time unit $t = 0.63$ ps.

3.4 Discussion

I have generated analytic propagators for several systems involving spin-orbit couplings. The constructions of these propagators have relied on an algebraic method [18], a classical action method, [16] and the Trotter formula in Eq.(2.87). I consider all cases with a parabolic confinement. This confinement can be attributed to the finiteness in the crystal structure or the sample.

After obtaining the analytic propagators, I apply them to localized wave packets by using either analytic integration (Gaussian) techniques or Monte-Carlo numerical integration techniques. The Monte-Carlo numerical integration is needed since the presence of two Pauli matrices leads to non-Gaussian forms of the exponent.

I have presented some selected results from all possible calculations. These results do not exhaust all possible features. I have also shown the effect of Rashba strength α and of the wave packet widths w on the spin dynamics in 1D and 2D cases. This could provide a good background check for future spin control devices. For example, if a faster spin separation is needed, it can be achieved by selecting a material with higher Rashba strength. The spin precession inside Rashba systems can be controlled by the gate voltage and the channel length. This means that the output spin state can be controlled by these two parameters.

Chapter 4

Stern-Gerlach effect

4.1 Introduction

The Stern-Gerlach effect (SGE) [62] is a natural laboratory for the measurement problem in quantum mechanics. It also provides evidence of spin quantization. In the experiment, a beam of silver atoms is split in two parts and deflected due to interaction of the spin with an inhomogeneous magnetic field. The magnetic moment observed is the intrinsic spin angular momentum since the ground state of the silver atoms has zero orbital angular momentum.

Theoretical descriptions of the SGE were originally framed in semi-classical terms [63–65]. Purely quantum mechanical treatments have been given by Bohm [66], Griffith [67] and others [8,68,69]. Scully and Shea [70] approached SGE with the *U-matrix* method, originally developed by Kennard [14] and applied to linear magnetic fields. Scully, Lamb and Barut revisited the issue for a "physical" SGE [71], namely a SGE in an inhomogeneous magnetic field that obeys Maxwell's equation $\nabla \cdot \mathbf{B} = 0$. In doing so they introduce a quantum mechanical propagator in spin space, a representation of

the time evolution operator both in coordinate and spin space. The results presented in [70] and [71] are incomplete however. The inconsistencies of the initial beam description in the SGE is also noteworthy to discuss. Several authors approached SGE with an initial coherent state, in contrast to the historical Stern-Gerlach experiment, where a beam of unpolarized silver atoms enters the field [72]. We show that this choice leads to different features in the SGE.

As part of this thesis, I have generalized the quantum mechanical propagator approach to spin-dependent Hamiltonians applicable to Stern-Gerlach (SG) configurations. The propagator $K(x, x_0; t - t')$ gives the conditional transition amplitude between two position eigenstate vectors $|x\rangle$ and $|x_0\rangle$ over a time interval $t-t'$ such that $K(x, x_0; t - t') = \langle x|U(t - t')|x_0\rangle$, where $U(t - t')$ is the time-evolution operator [16]. Without loss of generality, I set $t' = 0$ in this paper. Because the Hamiltonians involve spin operators, the propagators have a 2×2 matrix representation for spin-1/2 particles. Several methods are available in the literature [9, 13–15, 17, 19] but none of them addresses the spin-dependent terms in the potential energy. My goal has been to extend some of these methods to spin-dependent potentials of the SG type, that is, potentials combining spin under the form of Pauli matrices and coordinates through magnetic fields that are linear in the coordinates. Some spin-orbit potentials have become very important in the area of spintronics [1, 26, 28, 73].

4.2 Propagator Construction

4.2.1 1D Propagator Construction

In this thesis I focus on the propagation in the xz-plane perpendicular to the beam. This followS the convention of the traditional Stern-Gerlach theoretical setup shown

in Fig.4.1 where the $\hat{y}$ is both the beam direction and the dimension where no inhomogeneity of the magnetic field is present. I provide both analytical and numerical construction of propagators for 1D and 2D inhomogeneity cases respectively in what follows.

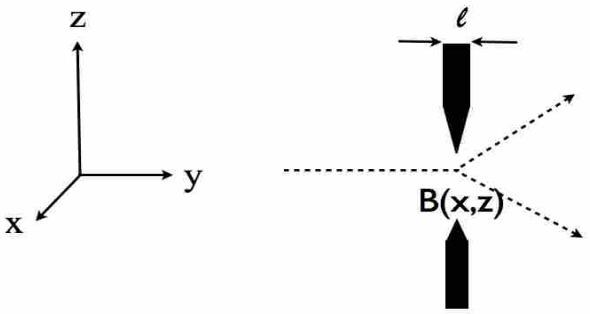

Figure 4.1 Plot of the traditional Stern-Gerlach geometry where l is the length of the magnet in the beam direction (y).

In the 1D inhomogeneity case, I consider two fields: an unphysical field $\mathbf{B}^u_{1D} = (0, 0, B_1 z)$ which does not satisfy $\nabla \cdot B = 0$ and a physical field $\mathbf{B}^p_{1D} = (0, 0, B_1 x)$ which satisfies $\nabla \cdot B = 0$, shown in Fig.4.3, where B_1 indicates the inhomogeneity strength. Both fields point in the z direction with the inhomogeneity in z and in x, respectively.

The Hamiltonians for these two fields are

$$H^u_{1D} = \frac{p_x^2 + p_z^2}{2m} - \mu B_1 z \sigma_z, \quad H^p_{1D} = \frac{p_x^2 + p_z^2}{2m} - \mu B_1 x \sigma_z. \tag{4.1}$$

I can construct the spin-1/2 propagators $K(\mathbf{x}, \mathbf{x}_0; t)$ from the propagator for spin-

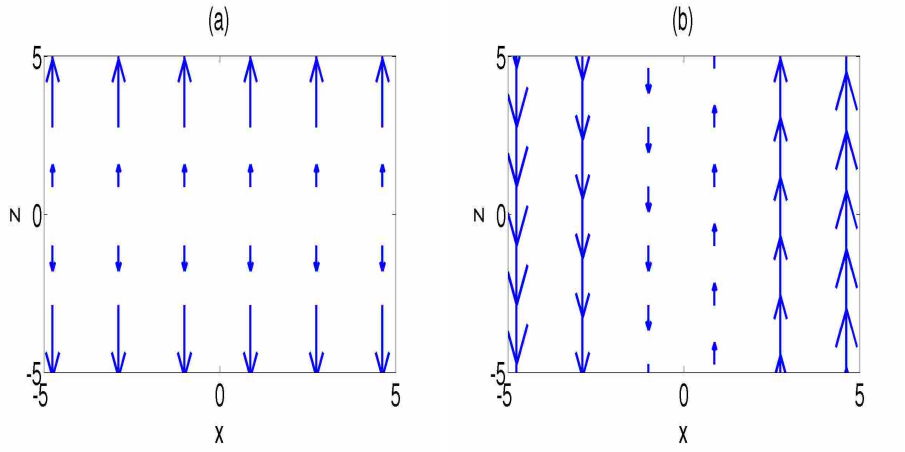

Figure 4.2 Plots of the magnetic field **B**. $(a)\mathbf{B}^{u}_{1D} = (0, 0, B_1 z)$, $(b)\mathbf{B}^{p}_{1D} = (0, 0, B_1 x)$.

less particles in a linear potential corresponding to a Hamiltonian

$$H = \frac{p_x^2}{2m} + fx, \tag{4.2}$$

where f is constant. I then apply an algebraic method with the recognition of a group algebra [18]. The linear potential propagator can be obtained in a straightforward way by relating $[\partial_x^2, x] = 2\partial_x$ to $[a^2, a^\dagger] = 2a$, through the substitutions $\partial_x \to a$ and $x \to a^\dagger$. While the exponent in a time-evolution operator $\exp(\frac{iHt}{\hbar})$ involves noncommuting operators, namely $[a, a^\dagger] = 1$, Katriel's formula

$$\exp\left(\alpha a^+ + \beta a^r\right) = e^{\alpha a^+} \exp\left(\sum_{i=0}^{r} \beta\alpha^i \binom{r}{i} \frac{1}{1+i} a^{r-i}\right) \tag{4.3}$$

applied to $r = 2$ makes a separation of the kinetic energy and potential energy term inside the time-evolution operator possible. After some algebraic manipulations, the linear potential propagator is obtained

$$K(x, x_0; t) = \sqrt{\frac{m}{2\pi i\hbar t}} \exp\left(-\frac{m(x-x_0)^2}{2i\hbar t} + \frac{f(x+x_0)t}{2i\hbar} + \frac{f^2t^3}{24i\hbar m}\right). \tag{4.4}$$

It should be noted that in the 1D inhomogeneity case σ_z acts as a place-holder for its diagonal $(+/-)$ elements. Therefore, the potential fx for spinless particles can be

replaced by $\sigma_z fx$ for spin-1/2 particles. With this replacement, Katriel's formula is still valid since $[\sigma_i, \sigma_j] = 2i\epsilon_{ijk}\sigma_k$ and $[\sigma_z, \sigma_z] = 0$. The constant f corresponds to the magnetic term $-\mu B_1 \sigma_z$ in both cases. As a result, the propagator $K^u_{1D}(z, z_0; t)$ for the unphysical field B^u_{1D} and the propagator $K^p_{1D}(x, x_0; t)$ for the physical field B^p_{1D} are

$$\begin{aligned} K^u_{1D}(z, z_0; t) &= \sqrt{\frac{m}{2\pi i\hbar t}} \exp\bigg(-\frac{m(z-z_0)^2}{2i\hbar t} - \frac{\mu B_1 \sigma_z (z+z_0) t}{2i\hbar} \\ &\quad + \frac{\mu^2 B_1^2 t^3}{24 i\hbar m} \bigg), \end{aligned} \tag{4.5}$$

$$\begin{aligned} K^p_{1D}(x, x_0; t) &= \sqrt{\frac{m}{2\pi i\hbar t}} \exp\bigg(-\frac{m(x-x_0)^2}{2i\hbar t} - \frac{\mu B_1 \sigma_z (x+x_0) t}{2i\hbar} \\ &\quad + \frac{\mu^2 B_1^2 t^3}{24 i\hbar m} \bigg). \end{aligned} \tag{4.6}$$

For $\mu B_1 = 0$, Eq.(4.5) and Eq.(4.6) reduce to the free particle propagator

$$K^{free}(x, x_0; t) = \sqrt{\frac{m}{2\pi i\hbar t}} \exp\bigg(-\frac{m(x-x_0)^2}{2i\hbar t} \bigg). \tag{4.7}$$

The free propagator includes quantum mechanical spreading, which will also be observed in external fields.

For 1D inhomogeneity cases, each dimension is independent. The propagator can then be expressed as,

$$K(x, z, x_0, z_0; t) = K(x, x_0; t) K(z, z_0; t). \tag{4.8}$$

As a result, one can extend Eq.(4.5) and Eq.(4.6) to

$$\begin{aligned} K^u_{1D}(x, z, x_0, z_0; t) &= \frac{m}{2\pi i\hbar t} \exp\bigg(-\frac{(x-x_0)^2 + (z-z_0)^2}{2i\hbar t/m} - \frac{\mu B_1 \sigma_z (z+z_0) t}{2i\hbar} \\ &\quad + \frac{\mu^2 B_1^2 t^3}{24 i\hbar m} \bigg) \end{aligned} \tag{4.9}$$

$$\begin{aligned} K^p_{1D}(x, z, x_0, z_0; t) &= \frac{m}{2\pi i\hbar t} \exp\bigg(-\frac{(x-x_0)^2 + (z-z_0)^2}{2i\hbar t/m} - \frac{\mu B_1 \sigma_z (x+x_0) t}{2i\hbar} \\ &\quad + \frac{\mu^2 B_1^2 t^3}{24 i\hbar m} \bigg), \end{aligned} \tag{4.10}$$

where the free particle propagator Eq.(2.11) is used to represent the dimensions where no inhomogeneity is present.

The result Eq. (4.9) disagrees with the expression Eq. (4.11) found in [70] by both the universal signature factor $\frac{\mu^2 B_1^2 t^3}{24i\hbar m}$ for the linear potential and the term linear in t. Eq. (4.9) also differs with the expression found in Eq. (4.12) [71] by the factor $\frac{\mu^2 B^2 t^3}{24i\hbar m}$. One can check that K in Eq. (4.9) satisfies the Pauli-Schrödinger equation. The corresponding expression Eq. (4.11) in [70] and Eq. (4.12) in [71] do not,

$$\begin{aligned} K_{SSM} &= \frac{m}{i\hbar t}\exp\Bigg(-\frac{m\Big((x-x_0)^2+(z-z_0)^2\Big)}{2i\hbar t} \\ &\quad +\frac{m}{2i\hbar t}\Big((z-z_0)\frac{\mu B_1\sigma_z t^2}{m}-\frac{\mu^2 B_1^2 t^4}{4m^2}\Big)\Bigg) \qquad (4.11) \\ K_{SLB} &= \eta(t)\exp\Bigg(\frac{m}{\hbar t}\Big((z-z_0-\frac{\mu\sigma_z B_1 t^2}{2m})^2 \\ &\quad -\frac{2\hbar\mu B_1 t^2 z\sigma_z}{m}\Big)\Bigg). \qquad (4.12) \end{aligned}$$

Once the propagator is obtained, the wavepacket evolution $\psi(x,z,t)$ can be obtained by applying it to an initial wavepacket $\psi(x_0,z_0,0)$

$$\psi(x,z,t)=\int_{-\infty}^{\infty}K(x,x_0,z,z_0;t)\psi(x_0,z_0,0)dx_0dz_0. \qquad (4.13)$$

To show the localization effect in the SGE, I choose $\psi(x_0,z_0,0)$ to be a spinor with Gaussian distribution in space centered at $(x_0,z_0)=(x_i,z_i)$ and with widths in two dimensions w_x and w_z, such that $\psi(x_0,z_0,0)=\frac{1}{\sqrt{\pi w_x w_z}}\exp\Bigg(-\frac{(x_0-x_i)^2}{2w_x^2}-\frac{(z_0-z_i)^2}{2w_z^2}\Bigg)\Bigg(\alpha|\uparrow\rangle+\beta|\downarrow\rangle\Bigg)$ where $|\uparrow\rangle$ and $|\downarrow\rangle$ are up-in-z and down-in-z spin states with constant coefficients α and β chosen to satisfy $|\alpha|^2+|\beta|^2=1$. This is a product state in space and spin. Note that the choice of initial positions (x_0,z_0) will lead to the appearance of different dynamics. In addition to the coherent state case, we also consider the incoherent state case with 50% spin-up states and 50% spin-down states. Because

of the linearity of the Schrödinger equation and of the propagator, the method can be applied to spinors with different spatial localizations for spin-up and spin-down particles (non-product or entangled states). In particular it can be applied repeatedly for arbitrary times in spin separating dynamics without further modifications.

4.2.2 2D Propagator Construction

For the 2D inhomogeneity, complexity arises from the noncommutativity among Pauli matrices, namely $[\sigma_i, \sigma_j] = 2i\epsilon_{ijk}\sigma_k$. This leads to position-dependent eigenspinors in contrast to the global eigenspinors of the 1D case. The nonexistence of global eigenspinors complicates the dynamics. In Fig.4.3 I consider magnetic fields with

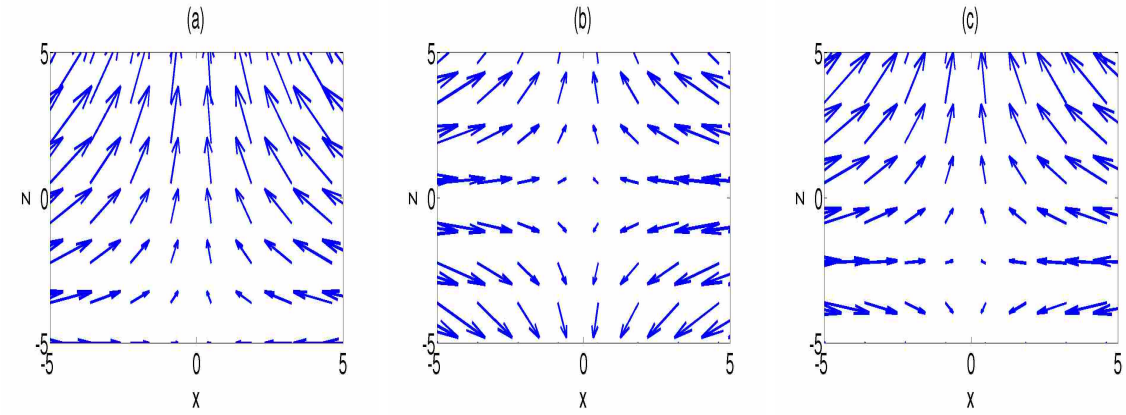

Figure 4.3 Plots of the magnetic field $\mathbf{B} = (-B_1 x, 0, B_1 z + B_0)$ with different inhomogeneity strengths B_1 and homogeneous field B_0. $(a) B_1 = 1.0, B_0 = 5.0$, $(b) B_1 = 1.0, B_0 = 0.0$, $(c) B_1 = 2.0, B_0 = 5.0$.

2D inhomogeneity. The values of the homogeneous component B_0 and the magnitude of the inhomogeneity B_1 can be chosen, so as to move the saddle point $(0, -5)$ in Fig.4.3(a), $(0, 0)$ in Fig.4.3(b), and $(0, -2.5)$ in Fig.4.3(c). Fig.4.3(b) which corresponds to $\mathbf{B} = (-B_1 x, 0, B_1 z)$ is usually used in treating the 2D inhomogeneity problem in the Stern-Gerlach experiment. The Stern-Gerlach magnetic field corre-

sponds to regions of the upper-half of the Fig.4.3. Therefore, the Stern-Gerlach set-up can be described analytically by a beam located at $(0,0)$ in a field with a large homogeneous component B_0 leading to $\mathbf{B} = (-B_1 x, 0, B_0 + B_1 z)$ as in Fig.4.3(a) or by a beam located in the upper-half plane of Fig.4.3(b) without the use of a homogeneous component. This is the choice used below when I select an initial wave packet centered around $z = z_0$ with $z_0 > 0$. This way one covers the historical Stern-Gerlach case and one stays away from the saddle point in the field. Later I will consider what happens when the beam extends beyond the transition axis. This transition axis goes through the saddle point and is perpendicular to the radial vector connecting the center of the initial packet with the saddle point. The radial vector corresponds to the direction of steepest gradient of the inhomogeneous field.

The construction of analytic Stern-Gerlach propagators in 2D inhomogeneities is a difficult task. Note that even with analytic propagators within some approximations, the application of the integral formula can be a daunting task. In order to evaluate the evolution of wave packets in a more efficient way, the Trotter product formula is used such that

$$\exp\Big(-\tau(a_1+a_2)\Big)\psi(x,0) \approx \lim_{n\to\infty}\left(\exp(-\frac{\tau}{2n}a_1)\exp(-\frac{\tau}{n}a_2)\exp(-\frac{\tau}{2n}a_1)\right)^n \psi(x,0). \tag{4.14}$$

This improves upon the simpler assumption

$$\exp\left(-\frac{\tau(a_1+a_2)}{n}\right) \approx \exp\left(-\frac{\tau a_1}{n}\right)\exp\left(-\frac{\tau a_2}{n}\right). \tag{4.15}$$

I set a_1 to be the potential energy term and a_2 to be the kinetic energy term. Instead of using the propagator integral formula, I apply the time-evolution operator directly to the wave packet with a reasonable value n. The Trotter product formula in Eq.(4.14) allows me to operate on the wave packet repeatedly. Since both the wave

packet and the potential are in the coordinate representation, the operation is purely multiplicative. Before applying the kinetic operator to the wave function, one needs to perform a fast Fourier transform on all grid points. After finishing both operations, one performs a fast inverse Fourier transform on all grid points. Once I recover the evolved wave packet in a coordinate representation for a time interval τ/n, I generate spin density plots by projecting wave packets in specific spin directions. As for the limitations of this method, note that in order for Eq.(4.14) to hold, one needs to set τ small enough to ensure the validity of the method. The region also needs to be specified large enough so that effects from the periodic boundaries introduced by the fast Fourier transform do not appear.

This wave packet approach goes beyond the delta distribution approach used in [70]. Unlike [70] and [71], I obtain spin separation.

4.3 Results

4.3.1 Spin Densities for Pure and Mixed States

I obtain $\psi(x, z; t)$ by propagating $\psi(x, z; 0)$. Local spin densities $\langle \mathbf{S} \rangle(x, z)$ can be evaluated, namely $\langle \mathbf{S} \rangle(x, z) = \langle \psi(x, z; t) | \mathbf{S} | \psi(x, z; t) \rangle$. The brackets refer to an integration (summation) over spin variables but *not* over coordinate space. I discuss the features in the local spin densities $\langle \mathbf{S} \rangle$ for both 1D inhomogeneity and 2D inhomogeneity in the magnetic field . In both cases, I label spin states using a subscripted arrow convention. In particular up-in-x ($|\uparrow\rangle_x$) and down-in-x ($|\downarrow\rangle_x$) spin states correspond to a balanced superposition of up-in-z ($|\uparrow\rangle$) and down-in-z ($|\downarrow\rangle$) spin states

$$|\uparrow\rangle_x = \frac{|\uparrow\rangle + |\downarrow\rangle}{\sqrt{2}}, \quad |\downarrow\rangle_x = \frac{|\uparrow\rangle - |\downarrow\rangle}{\sqrt{2}}, \tag{4.16}$$

and similarly for up-in-y ($|\uparrow\rangle_y$) or down-in-y ($|\downarrow\rangle_y$) spin states

$$|\uparrow\rangle_y = \frac{|\uparrow\rangle + i|\downarrow\rangle}{\sqrt{2}}, \quad |\downarrow\rangle_y = \frac{|\uparrow\rangle - i|\downarrow\rangle}{\sqrt{2}}. \tag{4.17}$$

In the simulations, I analyze the spin dynamics for various parameter choices: the initial location of the wave packet (x_0, z_0), the interaction strength μB_1, the widths of the wave packet (w_x, w_z), and the time interval t over which I follow the dynamics.

I choose to combine the magnetic moment and the field into one entity μB_1 because it is the product of μ and B_1 that gives the strength of the effect. The combination μB_1 is a universal Stern-Gerlach "interaction strength" against which different magnetic fields can be chosen for atomic systems with different magnetic moments. It plays a similar role to the spin-orbit Rashba interaction strength in condensed matter systems. I provide plots with natural units $\hbar = 1, m = 1$. Note also that since I am interested in the influence of the width on the dynamics, I select an absolute length unit d such that the width w and the positions x and y are all expressed in terms of d rather than being correlated as a result of the choice of units. I also provide the units for the following variables: μB_1 in units of $\hbar^2/md^3$ and t in units of $md^2/\hbar$. This allows one to recover experimentally accessible values of the magnetic field strength B_1, by substituting realistic value of $\hbar$ and m and by choosing an appropriate length unit d. This also determines a unit width and a unit time, and therefore realistic orders of magnitude for time and for wave packet width.

I also compare results of $\langle S\rangle$ for an initial pure state ($\frac{|\uparrow\rangle+|\downarrow\rangle}{\sqrt{2}}$) and for a mixed state consisting of 50%$|\uparrow\rangle$ and 50%$|\downarrow\rangle$. The propagated spin-up state is

$$\begin{pmatrix} \psi_\uparrow(x,t) \\ \psi_\downarrow(x,t) \end{pmatrix} = \int \begin{pmatrix} K_{\uparrow\uparrow} & K_{\uparrow\downarrow} \\ K_{\downarrow\uparrow} & K_{\downarrow\downarrow} \end{pmatrix} \begin{pmatrix} \psi_\uparrow(x_0,t) \\ 0 \end{pmatrix} dx_0 = \begin{pmatrix} \int K_{\uparrow\uparrow}\psi_\uparrow^0 dx_0 \\ \int K_{\downarrow\uparrow}\psi_\uparrow^0 dx_0, \end{pmatrix} \tag{4.18}$$

where $K_{\uparrow\uparrow}$ and $K_{\downarrow\downarrow}$ are propagators projected onto the same spin state while $K_{\uparrow\downarrow}$ and $K_{\downarrow\uparrow}$ are propagators projected onto the opposite spin state or spin flip-propagators.

Therefore, the density operator ρ_1 from an initial spin-up state is

$$\begin{aligned}\rho_1 &= \begin{pmatrix} \psi_\uparrow(x,t) \\ \psi_\downarrow(x,t) \end{pmatrix} \begin{pmatrix} \psi_\uparrow^*(x,t) & \psi_\downarrow^*(x,t) \end{pmatrix} \\ &= \begin{pmatrix} \psi_\uparrow^*(x,t)\psi_\uparrow(x,t) & \psi_\downarrow^*(x,t)\psi_\uparrow(x,t) \\ \psi_\uparrow^*(x,t)\psi_\downarrow(x,t) & \psi_\downarrow^*(x,t)\psi_\downarrow(x,t) \end{pmatrix}. \end{aligned} \tag{4.19}$$

The density operator ρ_2 for spin-down state $\mid \downarrow \rangle$ can be calculated in the similar manner. By summing up individual density operators, the total density operator ρ_{total} is obtained,

$$\rho_{total} = \rho_1 + \rho_2 = \frac{1}{2} \begin{pmatrix} \rho_{11} & \rho_{12} \\ \rho_{21} & \rho_{22} \end{pmatrix}, \tag{4.20}$$

where

$$\begin{aligned}\rho_{11} &= (\int K_{\uparrow\uparrow}\psi_\uparrow^0 dx_0)(\int K_{\uparrow\uparrow}\psi_\uparrow^0 dx_0)^* + (\int K_{\uparrow\downarrow}\psi_\downarrow^0 dx_0)(\int K_{\uparrow\downarrow}\psi_\downarrow^0 dx_0)^* \\ \rho_{12} &= (\int K_{\uparrow\uparrow}\psi_\uparrow^0 dx_0)(\int K_{\downarrow\uparrow}\psi_\uparrow^0 dx_0)^* + (\int K_{\uparrow\downarrow}\psi_\downarrow^0 dx_0)(\int K_{\downarrow\downarrow}\psi_\downarrow^0 dx_0)^* \\ \rho_{21} &= (\int K_{\downarrow\uparrow}\psi_\uparrow^0 dx_0)(\int K_{\uparrow\uparrow}\psi_\uparrow^0 dx_0)^* + (\int K_{\downarrow\downarrow}\psi_\downarrow^0 dx_0)(\int K_{\uparrow\downarrow}\psi_\downarrow^0 dx_0)^* \\ \rho_{22} &= (\int K_{\downarrow\uparrow}\psi_\uparrow^0 dx_0)(\int K_{\downarrow\uparrow}\psi_\uparrow^0 dx_0)^* + (\int K_{\downarrow\downarrow}\psi_\downarrow^0 dx_0)(\int K_{\downarrow\downarrow}\psi_\downarrow^0 dx_0)^*. \end{aligned} \tag{4.21}$$

This mixed state can not be factorized into a product of two individual states. Consequently, the spin density $\langle S_z \rangle_{mixed}$ =Tr$(\rho_{total} S_z)$ for an incoherent beam gives $(\rho_{11} - \rho_{22})/2$.

For an initial coherent spin state $\mid \uparrow \rangle_x$, the evolved spin state is

$$\begin{pmatrix} \psi_\uparrow(x,t) \\ \psi_\downarrow(x,t) \end{pmatrix} = \frac{1}{\sqrt{2}} \begin{pmatrix} \int K_{\uparrow\uparrow}\psi_\uparrow^0 dx_0 + \int K_{\uparrow\downarrow}\psi_\downarrow dx_0 \\ \int K_{\downarrow\uparrow}\psi_\uparrow^0 dx_0 + \int K_{\downarrow\downarrow}\psi_\downarrow^0 dx_0 \end{pmatrix}. \tag{4.22}$$

The spin density $\langle S_z \rangle_{pure}$ for a pure state can be calculated $\langle S_z \rangle_{pure} = |\psi_\uparrow|^2 - |\psi_\downarrow|^2$. By comparing the spin density $\langle S_z \rangle_{pure}$ and $\langle S_z \rangle_{mixed}$ for both cases, I show that the extra term $\Delta\langle S_z \rangle$ is

$$\begin{aligned}\Delta\langle S_z\rangle &= \langle S_z\rangle_{pure} - \langle S_z\rangle_{mixed} \\ &= (\int K_{\uparrow\uparrow}\psi^0_\uparrow dx_0)(\int K_{\uparrow\downarrow}\psi^0_\downarrow dx_0)^* + (\int K_{\uparrow\downarrow}\psi^0_\downarrow dx_0)(\int K_{\uparrow\uparrow}\psi^0_\uparrow dx_0)^* \\ &\quad -(\int K_{\downarrow\downarrow}\psi^0_\downarrow dx_0)(\int K_{\downarrow\uparrow}\psi^0_\uparrow dx_0)^* - (\int K_{\downarrow\uparrow}\psi^0_\uparrow dx_0)(\int K_{\downarrow\downarrow}\psi^0_\downarrow dx_0)^* \quad (4.23)\end{aligned}$$

Similarly one can calculate $\langle S_x\rangle_{mixed}$ and $\langle S_y\rangle_{mixed}$

$$\langle S_x\rangle_{mixed} = (\rho_{12}+\rho_{21})/2, \quad \langle S_y\rangle_{mixed} = -i(\rho_{12}-\rho_{21})/2 \tag{4.24}$$

for a mixed state, which is the expectation value of the spin operator or $Tr(\rho S_z)$ in the language of density-matrices.

Again I compare results with $\langle S_x\rangle_{pure}$ and $\langle S_y\rangle_{pure}$

$$\langle S_x\rangle_{pure} = \psi^*_\uparrow\psi_\downarrow + \psi^*_\downarrow\psi_\uparrow, \quad \langle S_y\rangle_{pure} = i(\psi^*_\downarrow\psi_\uparrow - \psi^*_\uparrow\psi_\downarrow) \tag{4.25}$$

for a pure state.

I obtain

$$\begin{aligned}\Delta\langle S_x\rangle &= \langle S_x\rangle_{pure} - \langle S_x\rangle_{mixed} \\ &= \frac{1}{2}[(\int K_{\uparrow\uparrow}\psi^0_\uparrow dx_0)^* \int K_{\downarrow\downarrow}\psi^0_\downarrow dx_0 + (\int K_{\downarrow\downarrow}\psi^0_\downarrow dx_0)^* \int K_{\uparrow\uparrow}\psi^0_\uparrow dx_0 \\ &\quad +(\int K_{\uparrow\downarrow}\psi^0_\downarrow dx_0)^* \int K_{\downarrow\uparrow}\psi^0_\uparrow dx_0 + \int K_{\uparrow\downarrow}\psi^0_\downarrow dx_0(\int K_{\downarrow\uparrow}\psi^0_\uparrow dx_0)^*] \\ \Delta\langle S_y\rangle &= \langle S_y\rangle_{pure} - \langle S_y\rangle_{mixed} \\ &= \frac{i}{2}[(\int K_{\downarrow\uparrow}\psi^0_\uparrow dx_0)^* \int K_{\uparrow\downarrow}\psi^0_\downarrow dx_0 - \int K_{\downarrow\uparrow}\psi^0_\uparrow dx_0(\int K_{\uparrow\downarrow}\psi^0_\downarrow dx_0)^* \\ &\quad +(\int K_{\downarrow\downarrow}\psi^0_\downarrow dx_0)^* \int K_{\uparrow\uparrow}\psi^0_\uparrow dx_0 - \int K_{\downarrow\downarrow}\psi^0_\downarrow dx_0(\int K_{\uparrow\uparrow}\psi^0_\uparrow dx_0)^*] \quad (4.26)\end{aligned}$$

Therefore, by using a coherent beam in a field where no spin flipping ($K_{\downarrow\uparrow}$ or $K_{\uparrow\downarrow}$) is possible, the result would be similar to those of incoherent beams. This happens in the two 1D cases.

4.3.2 Spin Evolution Features for 1D-Inhomogeneity

After applying the propagator K^u_{1D} in Eq.(4.9) on an initial spin wavepacket $\psi(x,z;0)$, one obtains an evolved spin wavepacket $\psi^u_{1D}(x,z;t)$ consisting of two components $\psi^u_{\uparrow 1D}(x,z;t)$ and $\psi^u_{\downarrow 1D}(x,z;t)$ corresponding to spin-up and spin-down in z:

$$\begin{aligned}
\psi^u_{\uparrow 1D}(x,z;t) &= \frac{\alpha}{(1+\frac{i\hbar t}{m\sigma^2})\sqrt{\pi}\sigma}\exp\Bigg(-\frac{m\Big(x^2+z^2+\frac{i\hbar t}{m}(x'^2+z'^2)\Big)}{2i\hbar t} \\
&\quad +\frac{m\Big((1+\frac{i\hbar t x'}{m\sigma^2})^2+(1+\frac{i\hbar t z'}{m\sigma^2}-\frac{\mu B_1 t^2}{2m})^2\Big)}{2i\hbar t(1+\frac{i\hbar t}{m\sigma^2})}-\frac{\mu B_1 t z}{2i\hbar}+\frac{\mu^2 B_1^2 t^3}{24i\hbar m}\Bigg) \\
\psi^{\downarrow u}_{1D}(x,z;t) &= \frac{\beta}{(1+\frac{i\hbar t}{m\sigma^2})\sqrt{\pi}\sigma}\exp\Bigg(-\frac{m\Big(x^2+z^2+\frac{i\hbar t}{m}(x'^2+z'^2)\Big)}{2i\hbar t} \\
&\quad +\frac{m\Big((1+\frac{i\hbar t x'}{m\sigma^2})^2+(1+\frac{i\hbar t z'}{m\sigma^2}+\frac{\mu B_1 t^2}{2m})^2\Big)}{2i\hbar t(1+\frac{i\hbar t}{m\sigma^2})}+\frac{\mu B_1 t z}{2i\hbar}+\frac{\mu^2 B_1^2 t^3}{24i\hbar m}\Bigg),
\end{aligned} \tag{4.27}$$

while applying K^p_{1D} in Eq.(4.10) to $\psi(x,z;0)$ gives the two components

$$\begin{aligned}
\psi^p_{\uparrow 1D}(x,z;t) &= \frac{\alpha}{(1+\frac{i\hbar t}{m\sigma^2})\sqrt{\pi}\sigma}\exp\Bigg(-\frac{m\Big(x^2+z^2+\frac{i\hbar t}{m}(x'^2+z'^2)\Big)}{2i\hbar t} \\
&\quad +\frac{m\Big((1+\frac{i\hbar t x'}{m\sigma^2})^2+(1+\frac{i\hbar t x'}{m\sigma^2}-\frac{\mu B_1 t^2}{2m})^2\Big)}{2i\hbar t(1+\frac{i\hbar t}{m\sigma^2})}-\frac{\mu B_1 t x}{2i\hbar}+\frac{\mu^2 B_1^2 t^3}{24i\hbar m}\Bigg) \\
\psi^p_{\downarrow 1D}(x,z;t) &= \frac{\beta}{(1+\frac{i\hbar t}{m\sigma^2})\sqrt{\pi}\sigma}\exp\Bigg(-\frac{m\Big(x^2+z^2+\frac{i\hbar t}{m}(x'^2+z'^2)\Big)}{2i\hbar t} \\
&\quad +\frac{m\Big((1+\frac{i\hbar t x'}{m\sigma^2})^2+(1+\frac{i\hbar t x'}{m\sigma^2}+\frac{\mu B_1 t^2}{2m})^2\Big)}{2i\hbar t(1+\frac{i\hbar t}{m\sigma^2})}+\frac{\mu B_1 t x}{2i\hbar}+\frac{\mu^2 B_1^2 t^3}{24i\hbar m}\Bigg).
\end{aligned} \tag{4.28}$$

With these evolved solutions I construct the spin densities $\langle \mathbf{S}\rangle(x,z)$ and display the results as 2D contour plots (Fig.4.4) and cuts in selected directions as explained below. From the displayed spin density, I observe three interesting features: a Spin-Separating Mechanism (SSM), a Bamboo-Shooting Structure (BSS), and a Persistent Spin Helix (PSH). Note that BSS and PSH are seen only for a coherent beam whereas

SSM appears in both the coherent and the incoherent case. Note that the features provided here are selected snapshots of spin evolution animations.

Spin-Separating Mechanism (SSM)

The spin-separating mechanism occurs when a homogeneous spin density develops into an inhomogeneous spin density, where different spin components occur in different regions of space. One observes the spin-separation mechanism in the plots of $\langle S_z \rangle$ in Fig.4.4. In the 1D case, S_z commutes with the Hamiltonian and their common eigenvectors are global or position-independent. The $\mathbf{B}^u_{1D}$ field leads to the *textbook* Stern-Gerlach effect with vertical separation, while $\mathbf{B}^p_{1D}$ exhibits a horizontal spin separation. Both of them also exhibit entanglement of spin and space. From Fig.4.4,

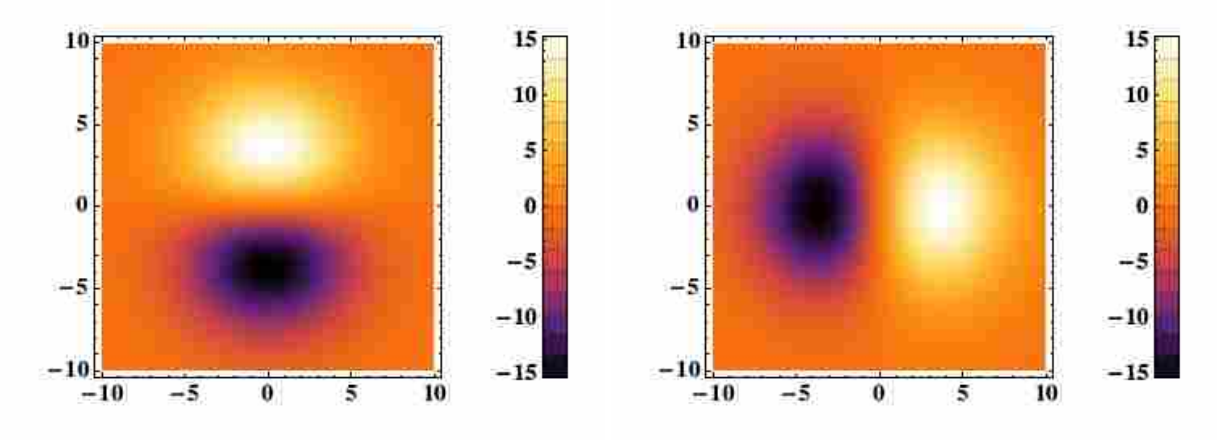

Figure 4.4 Color online. Spin density $\langle S_z \rangle$ for an initial spin state $|\uparrow\rangle_x$ centered around $(x_0, z_0) = (0, 0)$ for $\mu B_1 = 0.1$ (in units of $\hbar^2/md^3$), $w_x = w_z = 1$ (in units of d), and $t = 5$ (in units of $md^2/\hbar$).

the eigenspinors, namely $|\uparrow\rangle$ and $|\downarrow\rangle$ spin states, experience spin separation in the direction of the inhomogeneity. In Fig.4.4(a), one sees a *textbook* Stern-Gerlach effect where inhomogeneity exists in the z direction while in Fig.4.4(b), one sees a horizontal Stern-Gerlach effect where the inhomogeneity is in the x direction.

Note that in Fig.4.4 for the $\mathbf{B}^u_{1D}$ ($\mathbf{B}^p_{1D}$), the x (z)-dimension is not important.

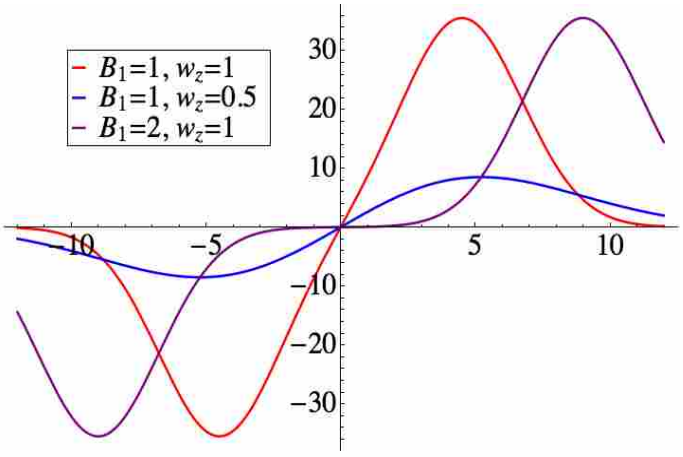

Figure 4.5 Color online. Spin density $\langle S_z \rangle$ for an initial spin state $|\uparrow\rangle_x$ centered around $(x_0, z_0) = (0, 0)$ for $\mu B_1 = 1$ (in units of $\hbar^2/md^3$), $w_x = w_z = 1$ (in units of d), and $t = 3$ (in units of $md^2/\hbar$).

The effect of separation can also be seen clearly by taking $x = 0$ ($z = 0$). In Fig.4.5 I compare the effect of inhomogeneity strength B_1, the width of the packet w on the rate of separation. I plot the spin density $\langle S_z \rangle$ along the central inhomogeneity axis. ($x = 0$ for $\mathbf{B}^u_{1D}$ or $z = 0$ for $\mathbf{B}^p_{1D}$) in Fig.4.5 where the horizontal axis refer to the z (for $\mathbf{B}^u_{1D}$) or x (for $\mathbf{B}^p_{1D}$) dimension. In Fig.4.5, faster separation is observed when one increases the inhomogeneity strength B_1. This is consistent with the semiclassical interpretation where the force is proportional to the gradient of the field. Reducing the width of the packet also leads to a faster spreading and decrease of the amplitude in the plot as expected. In the plots I choose to vary w_i, the width along the inhomogeneity axis only. Reducing the width in the perpendicular direction leads to an overall decrease of the amplitude. Note that the results are the same for both the coherent beam $\frac{|\uparrow\rangle+|\downarrow\rangle}{2}$ and the incoherent beam (50% $|\uparrow\rangle$ and 50% $|\downarrow\rangle$). This can be understood in the system where no spin flippings occur, namely $K_{\uparrow\downarrow} = K_{\downarrow\uparrow} = 0$.

Bamboo-Shooting Structure (BSS)

BSS represents the successive rise of spin polarization at fixed intervals along the axis of inhomogeneity. One sees BSS in Fig.4.6 when observing in a direction not along the eigenspinors of the system, in particular $\langle S_x \rangle$ and $\langle S_y \rangle$. The BSS can be observed for initial coherent states $|\uparrow\rangle_x$ and $|\uparrow\rangle_y$ which are both superpositions of eigenspinors $|\uparrow\rangle$ and $|\downarrow\rangle$. For the mixed state such 50% $|\uparrow\rangle$ and 50% $|\downarrow\rangle$, one can not see BSS. Since the system does not induce spin-flippings for eigenspinors, the final spin polarization remains unchanged and in this case $\langle S_x \rangle = 0$ at all times.

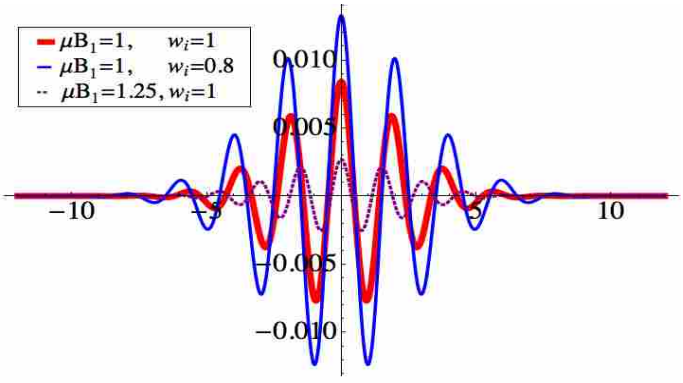

Figure 4.6 Color online. Spin density $\langle S_x \rangle$.

Spin density $\langle S_x \rangle$ is generated for cases where one can manipulate the field strength B_1 and the width of the wavepacket w_z. The parameters B_1 and w_z are chosen for visual readability. The wavepacket extends further as time evolves as a result of quantum spreading. One observes oscillatory motion for the non-eigenspinors. The period of the oscillation decreases as one increases the inhomogeneity strength B_1. For an initial coherent state ($|\uparrow\rangle_x$), one has both $|\uparrow\rangle$ and $|\downarrow\rangle$ spin components. As discussed previously, the two components separate faster with larger B_1. This leads to less overlap between the components, which results in an overall decrease of the amplitude. One should also notice that as the eigenspinors move more rapidly, the non-eigenspinors would experience oscillation with an increase in the frequency or a

decrease in the period. The period increases when the width of the wavepacket is reduced in the direction of inhomogeneity in Fig.4.6.

Persistent Spin Helix (PSH)

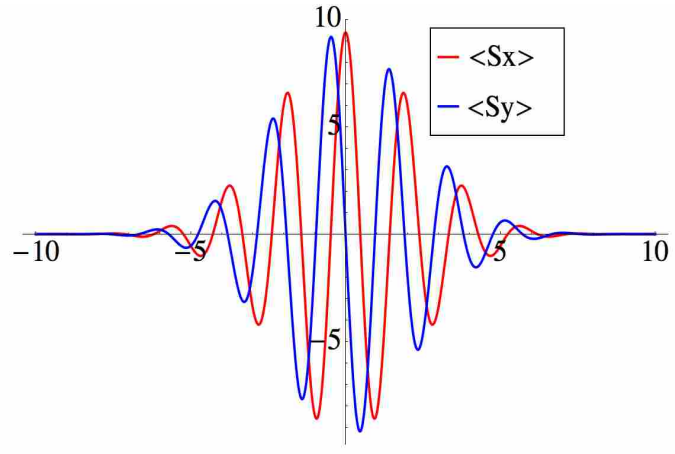

Figure 4.7 Color online. Spin densities $\langle S_x \rangle$ and $\langle S_y \rangle$ at $t = 3$ $w_x = w_z = 1$.

Persistent Spin Helix (PSH) refers to the precessional motion of the spin in the xy plane. One observes a PSH structure by generating the spin densities $\langle S_x \rangle$ and $\langle S_y \rangle$ starting from a coherent state $\mid \uparrow \rangle_x$. This effect can only be observed from a coherent state in the non-eigenspinor basis (up-in-$x(y)$, down-in-$x(y)$). In Fig.4.7, I observe the $\langle S_x \rangle$ exhibits even-symmetry, while $\langle S_y \rangle$ exhibits odd-symmetry with respect to the original location of the packet. The $\langle S_x \rangle$ is shifted with respect to $\langle S_y \rangle$. By following the spin component on the z-axis, one sees that a persistent spin helix forms with clockwise motion to the right. As discussed in the BSS section, the period of the helix can be controlled by manipulating the inhomogeneity strength B_1 and wavepacket width w_z. Therefore one can control the spin polarization at specific locations by manipulating either the inhomogeneity strength B_1 or the wavepacket width w_z.

4.3.3 Spin Evolution Features for 2D-Inhomogeneity

Due to the continuous evolving nature of the wave packet in the 2D case, plots are generated at different times to show explicitly the features individually.

From the spin density contour plots, one observes three interesting features: Radial Spin Separation (RSS), Jellyfish Structure (JFS), and Four-Lobes Structure (FLS). Note that RSS and FLS are observed with an initial spin state $|\uparrow\rangle_x$ and $50\%|\uparrow\rangle$ and $50\%|\downarrow\rangle$ whereas AIC is observed only for an initial coherent spin state $|\uparrow\rangle$.

Radial Spin Separation (RSS)

Plots of spin-density $\langle S_z\rangle$ are generated in a field in Fig.4.3(b) for two cases: a pure state $|\uparrow\rangle_x$ and a mixed state ($50\%\ |\uparrow\rangle$ and $50\%\ |\downarrow\rangle$). I consider both cases with an initial wave packet centered around $x_0 = 0, z_0 = 4$. Both cases exhibit *textbook* Stern-Gerlach effect: vertical spin separation of $|\uparrow\rangle$ and $|\downarrow\rangle$ as seen in Figs.4.8 and 4.9. In both cases, the rate of separation increases when one increases the inhomogeneity strength. By reducing the width in the x direction, the wavepacket spreads faster in x.

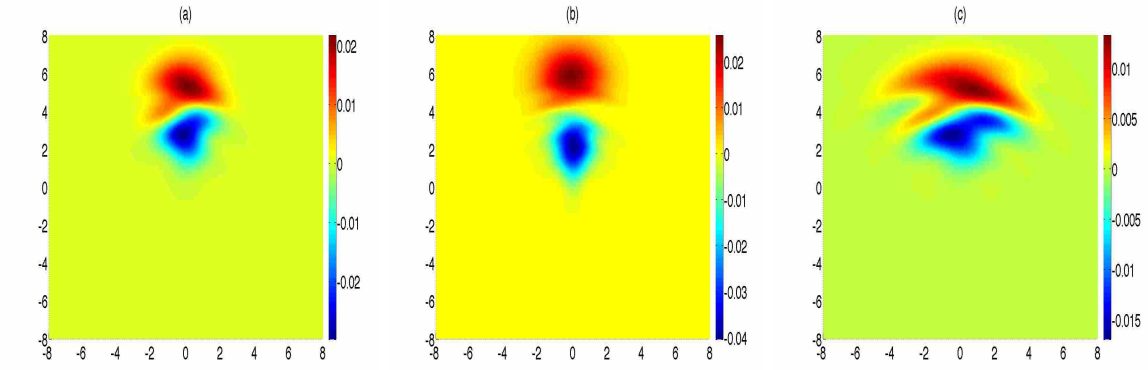

Figure 4.8 Color online. Plot of spin density $\langle S_z\rangle$ at $t = 1.0$ (in units of $md^2/\hbar$) for an initial coherent spin state $|\uparrow\rangle_x$ centered around the initial position at $x_0 = 0, z_0 = 4.0$ with different μB_1 (in units of $\hbar^2/md^3$), w_x and w_z (in units of d). $(a)\mu B_1 = 2.0, w_x = 1.0, w_z = 1.0, (b)\mu B_1 = 4.0, w_x = 1.0, w_z = 1.0, (c)\mu B_1 = 2.0, w_x = 0.5, w_z = 1.0$.

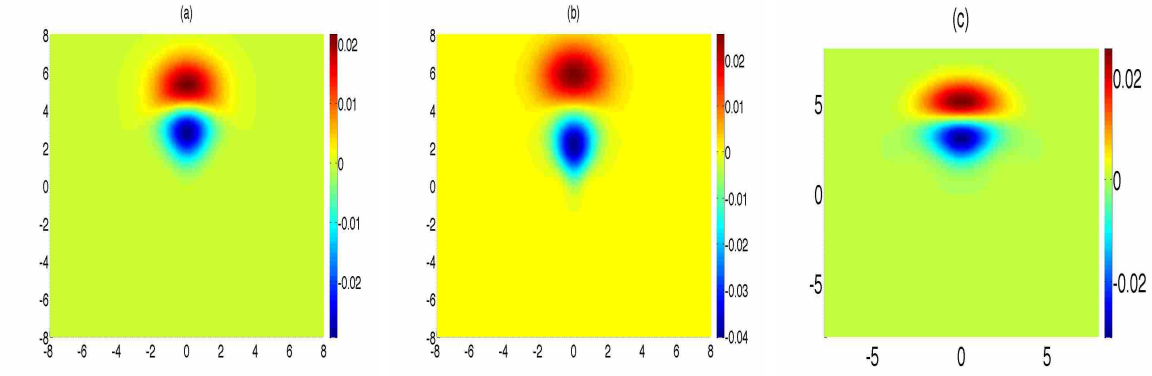

Figure 4.9 Color online. Plot of spin density $\langle S_z \rangle$ at $t = 1.0$ (in units of $md^2/\hbar$) for a mixed spin state (50% $|\uparrow\rangle$ and 50% $|\downarrow\rangle$) centered around the initial position at $x_0 = 0, z_0 = 4.0$ with different μB_1 (in units of $\hbar^2/md^3$), w_x and w_z (in units of d). $(a)\mu B_1 = 2.0, w_x = 1.0, w_z = 1.0, (b)\mu B_1 = 4.0, w_x = 1.0, w_z = 1.0, (c)\mu B_1 = 2.0, w_x = 0.5, w_z = 1.0$.

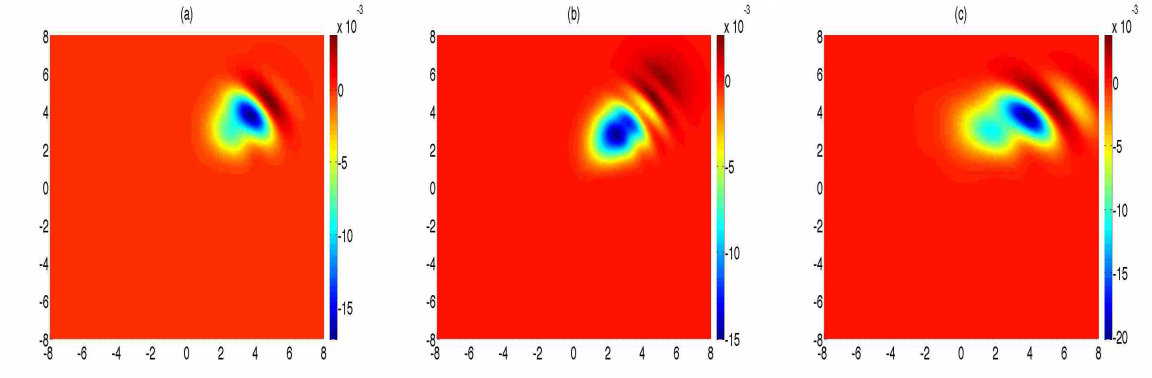

Figure 4.10 Color online. Plot of spin density $\langle S_z \rangle$ at $t = 1.0$ (in units of $md^2/\hbar$) for an initial coherent spin state $|\uparrow\rangle_x$ centered around the initial position at $x_0 = 4.0, z_0 = 4.0$ with different μB_1 (in units of $\hbar^2/md^3$), w_x and w_z (in units of d). $(a)\mu B_1 = 2.0, w_x = 1.0, w_z = 1.0$, $(b)\mu B_1 = 4.0, w_x = 1.0, w_z = 1.0, (c)\mu B_1 = 2.0, w_x = 0.5, w_z = 1.0$.

Comparing an initial pure state (coherent state or C-state) with an initial mixed spin state (incoherent state or IC-state), I notice that IC-states show $x \to -x$ symmetry, whereas C-states do not. At any particular time the plots of C-state wavepackets show an $x \to -x$ asymmetry. This may seem surprising given the symmetric nature of the field in Fig.4.3 . In fact these plots in Fig.4.3 are incomplete since they do

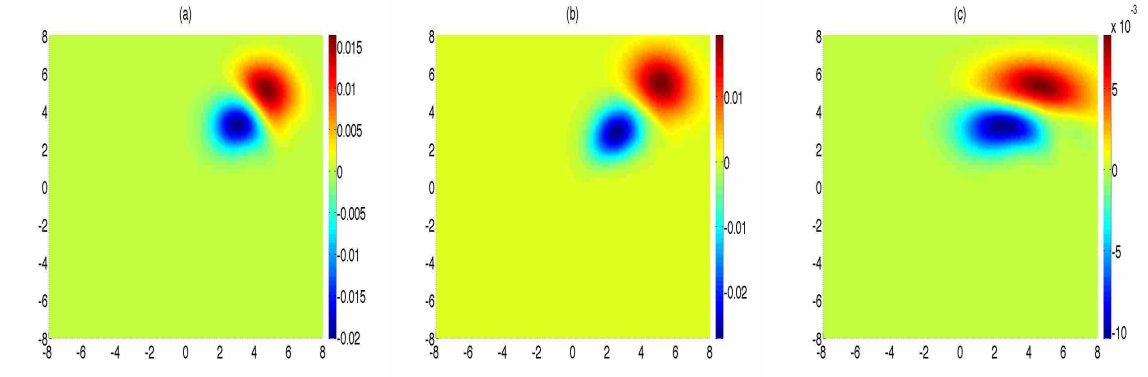

Figure 4.11 Color online. Plot of spin density $\langle S_z \rangle$ at $t = 1.0$ (in units of $md^2/\hbar$) for a mixed spin state (50% $|\uparrow\rangle$ and 50% $|\downarrow\rangle$) centered around the initial position at $x_0 = 4.0, z_0 = 4.0$ with different μB_1 (in units of $\hbar^2/md^3$), w_x and w_z (in units of d). $(a)\mu B_1 = 2.0, w_x = 1.0, w_z = 1.0, (b)\mu B_1 = 4.0, w_x = 1.0, w_z = 1.0, (c)\mu B_1 = 2.0, w_x = 0.5, w_z = 1.0$.

not incorporate the spin direction and therefore miss the asymmetry in the $(\mu \cdot B)$ interaction term. The appearance of this asymmetry can be checked in the following way:

1. By performing a reflection about the z axis only, namely $x \to -x$, I observe that the oscillation is still present but its direction is reversed. Note that the field becomes unphysical under such transformation $B \to B' = (x, 0, z)$.

2. By changing the initial spin state ($|\uparrow\rangle_x \to |\downarrow\rangle_x$) only, I observe that the oscillation is still present but its direction is reversed.

3. By performing both a reflection about the z axis and a reversal of the initial spin state, I observe that the oscillation direction is unchanged.

4. By writing the Trotter formula in a different form, namely $e^{V/2}e^{T}e^{V/2} \to e^{T/2}e^{V}e^{T/2}$, I observe that the oscillation direction is unchanged.

5. By switching the dependence on x and z, namely by starting with a $|\uparrow\rangle$ spin state centered around $x = 4, z = 0$, I observe that the oscillation in time now

displays a vertical asymmetry.

From these observations, I can conclude that a C-state, which is a superposition of eigenstates centered around a non-eigenspinor axis experiences two mechanisms: spin separation and oscillations. For example, this can happen for both a $|\uparrow\rangle_x$ spin state centered around $x = 0$ and a $|\uparrow\rangle$ spin state centered around $z = 0$. Also, this oscillation is short-lived if the wave packet is placed further away from the saddle point. This shows that the oscillation depends on the degree to which the two eigenstates overlap, for example $|\uparrow\rangle$ and $|\downarrow\rangle$ on the z-axis. A complete spin separation is more easily obtained when an initial state enters the field far away from the saddle point. This can be understood as follows: since this is an analysis of wave packet dynamics, it is unavoidable that one has to take the spreading of the wave packet into account. The spreading induces spin-flippings as I discuss in the next subsection.

So far, I have observed a vertical spin-separating mechanism for an initial wave packet centered around $x_0 = 0, z_0 = 4$, where the z inhomogeneity is far greater than the x inhomogeneity. Now, spin density plots are generated for an initial wave packet centered around $x_0 = 4, z_0 = 4$, where the inhomogeneities in both dimensions are equal (Fig.4.11). One notices a Radial Spin Separation (RSS) for $|\uparrow\rangle$ and $|\downarrow\rangle$. RSS occurs when the spin components separate along the radial axis. This is understandable since the eigenenergy of the Hamiltonian $H = \frac{p_x^2+p_z^2}{2m} + \mu B_1(x\sigma_x - z\sigma_z)$ corresponds to a radial linear potential , namely $\pm\mu B_1\sqrt{x^2+z^2}$. Therefore a radial spin separation should be expected. Besides the spin separation mechanism, one also observes a focusing effect of the component moving toward the transition axis. This effect can be attributed to the difference between the unidirectional linear potential (in x or z) and the radial linear potential (in $\mathbf{r}$). One also notices that the amplitude for $|\uparrow\rangle$ and $|\downarrow\rangle$ are very different between the coherent state case and the mixed

state case.

Asymmetry-Induced Contamination (AIC)

Now I investigate the dynamics of an initial spin state $|\uparrow\rangle$. A spin density contour plot $\langle S_z \rangle$ is generated in three different cases. All three cases start from an initial location close to the transition axis $z = 0$. One observes in Fig.4.12 that most spin-ups go up while there is fringe formation between ups and downs close to the $z = 0$ axis, which leads to the Asymmetry-Induced Contamination (AIC). AIC occurs when one finds a spin in the opposite region to what the ideal Stern-Gerlach effect predicts. This only occurs when one starts from an asymmetric initial configuration. In Fig.4.12(a), one observes that successive fringes between spin-up and spin-down appear close to the $z = 0$ axis. In Fig.4.12(b) I notice that there are fewer fringes when one increases the inhomogeneity strength. Also the spin-up state moves upward more rapidly in this case. One sees that by reducing the width w_z, that the wavepacket spreads faster in the z direction and one observes more fringes in both x and z direction.

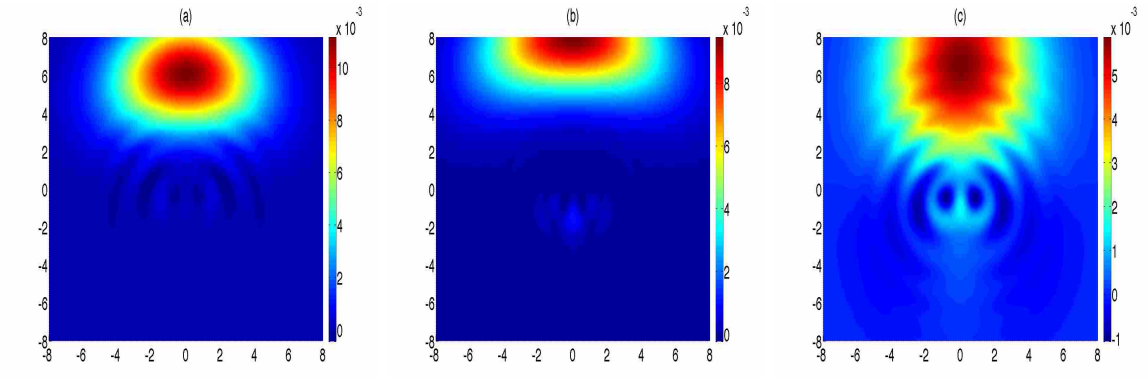

Figure 4.12 Color online. Spin density $\langle S_z \rangle$ for an initial spin state $|\uparrow\rangle$ centered around $x_0 = 0, z_0 = 2.0$ evaluated at $t = 2.0$ (in units of $md^2/\hbar$) for different μB_1 (in units of $\hbar^2/md^3$), w_x and w_z (in units of d). (a) $\mu B_1 = 2.0, w_x = 1.0, w_z = 1.0$, (b) $\mu B_1 = 3.0, w_1 = 1.0, w_z = 1.0$, (c) $\mu B_1 = 2.0, w_x = 1.0, w_z = 0.5$.

In order to visualize the AIC, spin density plots are created for $|\uparrow\rangle$ and $|\downarrow\rangle$ individually in Fig.4.13. The spin-down state, flipped from the spin-up state, leads to fringe formation (the butterfly-like pattern in Fig.4.13). Nevertheless, the spin-down state amplitude is much smaller than the spin-up. Therefore, the spin-downs are only visible in regions where no spin-ups are present.

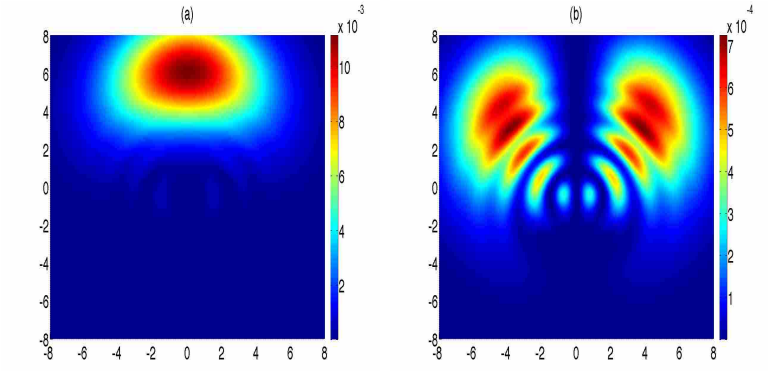

Figure 4.13 Color online. Spin densities for an initial spin state $|\uparrow\rangle$ centered around $(x_0, z_0) = (0.0, 2.0)$ evaluated at $t = 2.0$ (in units of $md^2/\hbar$) with $\mu B_1 = 2.0$ (in units of $\hbar^2/md^3$), $w_x = w_z = 1$ (in units of d). (a) $\langle\uparrow\rangle$, $(b)\langle\downarrow\rangle$.

The field in Fig.4.3(b) corresponds to a Hamiltonian $H = \frac{p_x^2+p_z^2}{2m} + \mu B_1(x\sigma_x - z\sigma_z)$. The inclusion of two Pauli matrices complicates the Heisenberg equations of motion. This leads to difficulties in obtaining analytic solutions. In order to obtain a better understanding of the motion, I set out to consider the motion in a frame moving with the particle. In such a frame, the system Hamiltonian is $H = \mu B_1(x\sigma_x - z\sigma_z)$. The corresponding Heisenberg equations of motions are

$$\begin{aligned} \dot{\hat{p}}_x &= -\hat{\sigma}_x\mu B_1, \quad \dot{\hat{p}}_z = \hat{\sigma}_z\mu B_1, \quad \dot{\hat{x}} = 0, \quad \dot{\hat{z}} = 0, \\ \dot{\hat{\sigma}}_x &= \frac{2\mu B_1\hat{z}\hat{\sigma}_y}{\hbar}, \quad \dot{\hat{\sigma}}_z = \frac{2\mu B_1\hat{x}\hat{\sigma}_y}{\hbar}, \quad \dot{\hat{\sigma}}_y = -\frac{2\mu B_1(\hat{x}\hat{\sigma}_z + \hat{z}\hat{\sigma}_x)}{\hbar}. \end{aligned} \tag{4.29}$$

It is clear that the position operators are constants of the motion, namely $x(t) = x(0)$ and $z(t) = z(0)$. It follows that it is easier to calculate the spin dynamics in such a

frame. If one assumes an initial $|\uparrow\rangle$ spin state $\langle\sigma_z(0)\rangle = 1$, the solution for the three spin operators are

$$\begin{aligned}\langle\sigma_x(t)\rangle &= -\frac{2xz\sin(\frac{\mu B1t\sqrt{x^2+z^2}}{\hbar})^2}{x^2+z^2}, \quad \langle\sigma_y(t)\rangle = -\frac{x\sin(\frac{2\mu B1t\sqrt{x^2+z^2}}{\hbar})}{\sqrt{x^2+z^2}}, \\ \langle\sigma_z(t)\rangle &= \frac{z^2+x^2\cos(\frac{2\mu B1t\sqrt{x^2+z^2}}{\hbar})}{x^2+z^2}. \end{aligned} \tag{4.30}$$

In Fig.4.14, I display the solutions on three different contour plots respectively. This is a different frame at all times.

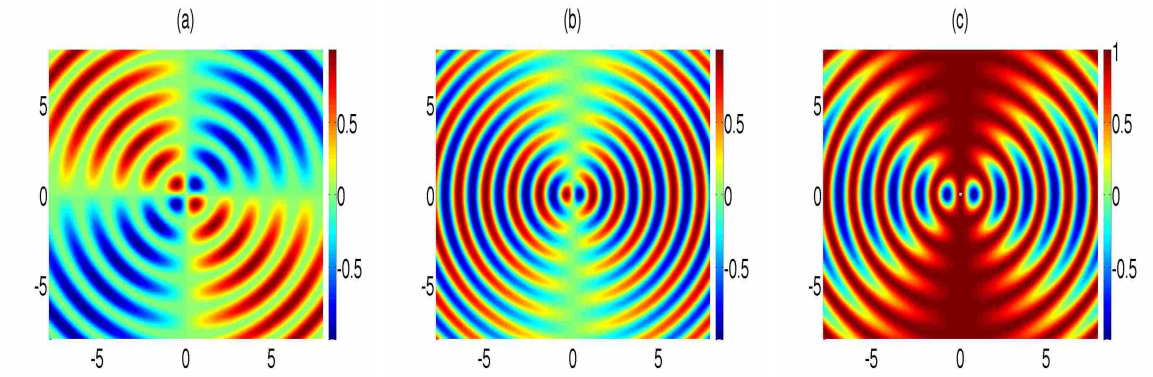

Figure 4.14 Color online. For an initial spin state $|\uparrow\rangle$ in the rest frame. (a) $\sigma_x(t)$, (b) $\sigma_y(t)$, (c) $\sigma_z(t)$.

The $\sigma_z(t)$ is responsible for the AIC. Recall that the solution in Eq.(4.30) is in a frame where the particle is not "moving". "Spin-up goes up" is iconic for the Stern-Gerlach effect. All three figures demonstrate in a local field similar to the Stern-Gerlach field, the spin-up state could have a possibility of moving downward if the initial point is closer to the transition axis $z = 0$. This is also an example of the Non-Ideal Stern-Gerlach effect.

Four-Lobes Structure

In Fig.4.15 a fringe pattern is formed for $\langle S_x\rangle$ evaluated at $t = 1$, where the initial state is a coherent state $|\uparrow\rangle$ centered around the z axis, where the eigenspinors of

S_z are present. One can also check for $x = 0$ and compare it with the BSS structure. There exists reflection asymmetry across the axis $x = 0$ for $\langle S_x \rangle$. In Fig.4.15(b), I plot $\langle S_x \rangle$ evaluated at $t = 1.2$, where the initial state is a mixture (50% $| \uparrow \rangle$ and 50 % $| \downarrow \rangle$) centered around the z axis. It is clear that one cannot see fringe formation which is consistent with the argument that BSS occurs for coherent initial states. The $| \uparrow \rangle_x$ and $| \downarrow \rangle_x$ states appear on the right and on the left and both of them exhibit a *Zitterbewegung*-like motion in the vertical direction, namely oscillatory motion around one point. Note also this motion is also observed for spin-flipping from $| \uparrow \rangle$ to $| \downarrow \rangle$ or vice-versa. The mixed state currently in use is in the z-basis.

In the 1D inhomogeneity case, the up and the down states go up and down respectively in a symmetric way, and the BSS appears while the polarization is fixed at specific locations. In the 2D inhomogeneity case, the polarization is not fixed at specific locations but making periodic oscillations. The only difference between the coherent and mixed states is the asymmetric motion for both spin-up and spin-down components displayed by a coherent state. For an initial mixed state, one observes Zitterbewegung of two blobs appearing sideways in the 2D inhomogeneity case. From the simulations, this Zitterbewegung can also be seen when an initial spin-up flipped to spin-down. This does not happen in the 1D inhomogeneity case. Therefore, the Zitterbewegung of two blobs might be the consequence of possible spin flipping and asymmetry.

Now, Figs.4.16(a) and (b) refer to the same initial condition as in Fig.4.15 with the time extended to $t = 2$. The Four-Lobes Structure (FLS) shows separation of $\langle S_x \rangle$ in 4 quadrants with the same sign across the diagonal. One observes the FLS close to the transition axes. The FLS can be understood in the following way: From the results in the 1D inhomogeneity, the eigenspinors move toward the corresponding inhomogeneity direction. In the 2D inhomogeneity case, the $| \uparrow \rangle$ is moving upwards

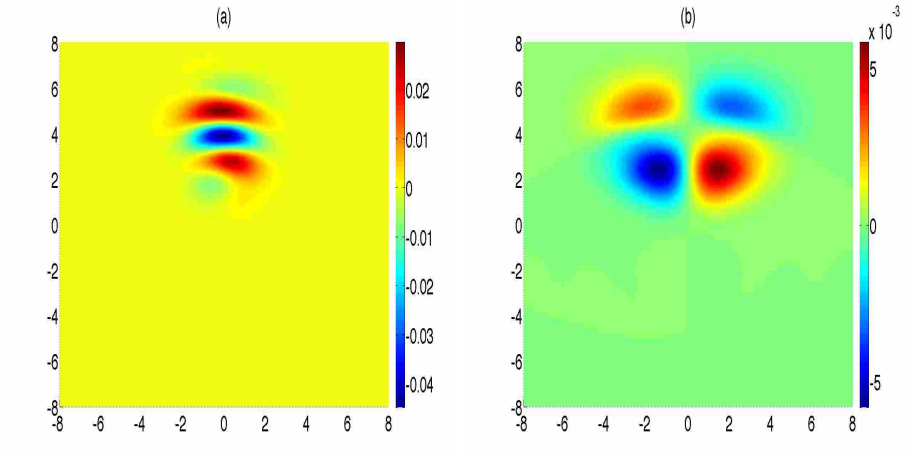

Figure 4.15 Color online. Spin density $\langle S_x \rangle$ for an initial wave packet centered around at $x_0 = 0, z_0 = 4.0$ (in units of d) with the following parameter choices: $\mu B_1 = 2.0$ (in units of $\hbar^2/md^3$), $w_x = 1.0, w_z = 1.0$ (in units of d), and $t = 1.0$ (in units of $md^2/\hbar$) for an initial spin state (a) $|\uparrow\rangle_x$, (b) 50% $|\uparrow\rangle$ and 50%$|\downarrow\rangle$

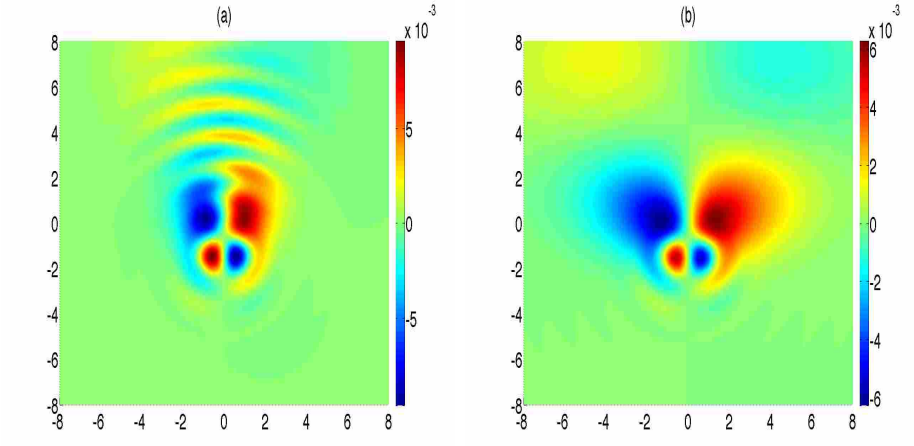

Figure 4.16 Color online. Spin density $\langle S_x \rangle$ for an initial wave packet centered around at $x_0 = 0, z_0 = 4.0$ (in units of d) with the following parameter choices: $\mu B_1 = 2.0$ (in units of $\hbar^2/md^3$), $w_x = 1.0, w_z = 1.0$ (in units of d), and $t = 2.0$ (in units of $md^2/\hbar$) for an initial spin state (a) $|\uparrow\rangle_x$, (b) 50% $|\uparrow\rangle$ and 50%$|\downarrow\rangle$

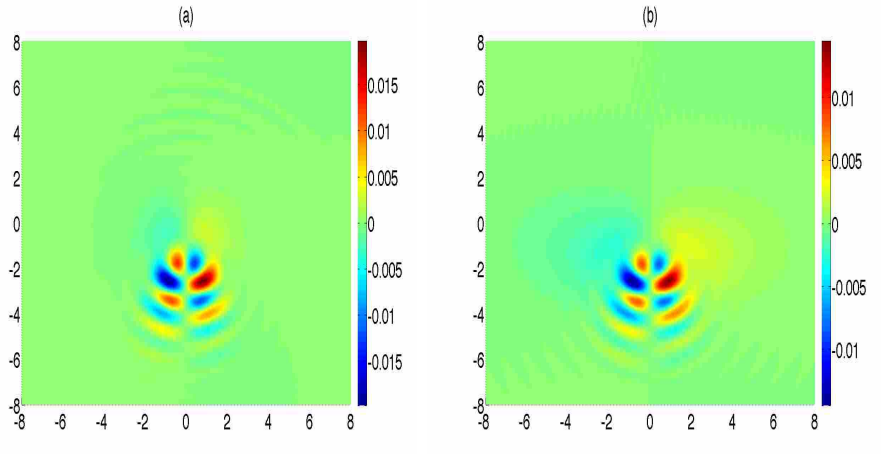

Figure 4.17 Color online. Spin density $\langle S_x \rangle$ for an initial wave packet centered around at $x_0 = 0, z_0 = 4.0$ (in units of d) with the following parameter choices: $\mu B_1 = 2.0$ (in units of $\hbar^2/md^3$), $w_x = 1.0, w_z = 1.0$ (in units of d), and $t = 3.0$ (in units of $md^2/\hbar$) for an initial spin state (a) $|\uparrow\rangle_x$, (b) 50% $|\uparrow\rangle$ and 50%$|\downarrow\rangle$.

if one starts from a $|\uparrow\rangle$ centered around the z axis. However, as pointed out in the radial spin separation, the $|\uparrow\rangle$ goes up and also expands in the x direction. This is very different from the 1D inhomogeneity case where the symmetry is preserved. The consequence of the asymmetry in the shape of $|\uparrow\rangle$ and $|\downarrow\rangle$ leads to a more complex feature than the BSS on the axis $x = 0$ in the 1D inhomogeneity case. The $|\downarrow\rangle$ is focused while moving towards the transition axis where the eigenspinors of S_x are present while $|\uparrow\rangle$ is spreading. The $|\downarrow\rangle$ state can be a superposition of two eigenspinors of S_x. It should be noted that the $|\uparrow\rangle_x$ moves to the left while $|\downarrow\rangle_x$ moves to the right as predicted from the inhomogeneity rule. In order to preserve the focusing effect for the $|\downarrow\rangle$, the $|\uparrow\rangle_x$ has to be on the right-hand side of $x = 0$ and likewise for $|\downarrow\rangle_x$. Similarly, for a $|\uparrow\rangle$ centered on the z axis, one expects to see the $|\uparrow\rangle_x$ on the left-hand side of $x = 0$ and on the right-hand side for $|\downarrow\rangle_x$. After moving across the transition axis for $|\downarrow\rangle$, one expects to see the $|\uparrow\rangle_x$ and $|\downarrow\rangle_x$ states swap sides. This happens because after crossing, the $|\downarrow\rangle$ state will expand in size for $z < 0$ in the x direction like $|\uparrow\rangle$ for $z > 0$. As a result, one can expect a FLS

close to the transition axis.

4.4 Mixing Entropy and Entanglement

4.4.1 Introduction

So far I have found the dynamics of spin wave packets in Stern-Gerlach systems, including the Stern-Gerlach effect (SGE) (both horizontal and vertical separation), Radial Spin Separation, and others. The SGE is also famous for introducing entanglement [75]. This is the subject of quantum information. In what follows I explore some of these concepts in view of what I have learned from SGE dynamics.

In a Stern-Gerlach experiment, an initial beam described by a pure state is prepared. The evolution of the beam in the magnet is determined by quantum mechanics. From the calculation, the state becomes entangled and can be expressed as $|+\uparrow\rangle + |-\downarrow\rangle$ where $+(-)$ in the ket refers to the upward(downward) momentum and $\uparrow$ ($\downarrow$) refers to the spin-up (spin-down) state. To understand the entanglement qualitatively, I calculate the von-Neumann mixing entropy, since it is known to be a measure of entanglement [16]. This concept is based on the mixing entropy accounts for both entanglement and partial-tracing. In particular, if the mixing entropy is zero, there is no entanglement.

4.4.2 Numerical Calculation of the von Neumann mixing Entropy

A useful decomposition for the Hermitian density operator ρ is provided using a complete set of orthonormal eigenstates $|\bar{p}_j\rangle$ and its eigenvalues $\bar{p}_j$. The von Neumann mixing entropy is denoted by $S_v(\rho)$ and defined as $S_v(\rho) = -\sum_{i=1}^{n} \bar{p}_i ln \bar{p}_i =$

$-\text{trace}(\rho \ln \rho)$.

After evolving the spin-up wave packet $\psi_\uparrow$ and the spin-down wave packet $\psi_\downarrow$ individually at a specific time, a density operator is generated based on the wavepacket amplitude $\psi_\uparrow$ and $\psi_\downarrow$ by tracing out the spatial degree of freedom

$$\rho = \begin{pmatrix} \int \psi_\uparrow^*(\mathbf{x})\psi_\uparrow(\mathbf{x})d\mathbf{x} & \int \psi_\uparrow^*(\mathbf{x})\psi_\downarrow(\mathbf{x})d\mathbf{x} \\ \int \psi_\downarrow^*(\mathbf{x})\psi_\uparrow(\mathbf{x})d\mathbf{x} & \int \psi_\downarrow^*(\mathbf{x})\psi_\downarrow(\mathbf{x})d\mathbf{x} \end{pmatrix}. \tag{4.31}$$

I then integrate over all space and double check that the wavepacket has not leaked out through the boundary to decrease the overall probability to less than 100%. Once ρ at time $t = \tau$ is obtained, one can simply find the two eigenvalues λ_1 and λ_2 which provide us with the information on the von Neumann entropy S_v as

$$S_v = -\lambda_1 \log_2 \lambda_1 - \lambda_2 \log_2 \lambda_2. \tag{4.32}$$

4.4.3 Results

I show the results both from a SG mixure (50%$|\uparrow\rangle$ and 50%$|\downarrow\rangle$) and a pure state $(|\uparrow\rangle + |\downarrow\rangle)/\sqrt{2}$ for different parameter choices of the interaction strength μB_1 and the wave packet widths (w_x, w_z). I also generate results for wavepackets starting from different initial positions.

Fig.4.18 shows the entropy change in an unphysical 1D Stern-Gerlach experiment starting from a pure state (top) and a mixed state (bottom).

Note that the von Neumann mixing entropy is a good measure of entanglement for an initial pure state but a bad one for an initial mixed state. An initial mixed state starts from a perfect mixture, while for an initial pure state, the mixing happens simultaneously with the spatial entanglement. Therefore the entanglement process is not visible through the von Neumann mixing entropy for an initial mixed state. I therefore label "Entanglement" and "Entropy" on initial pure state and mixed state

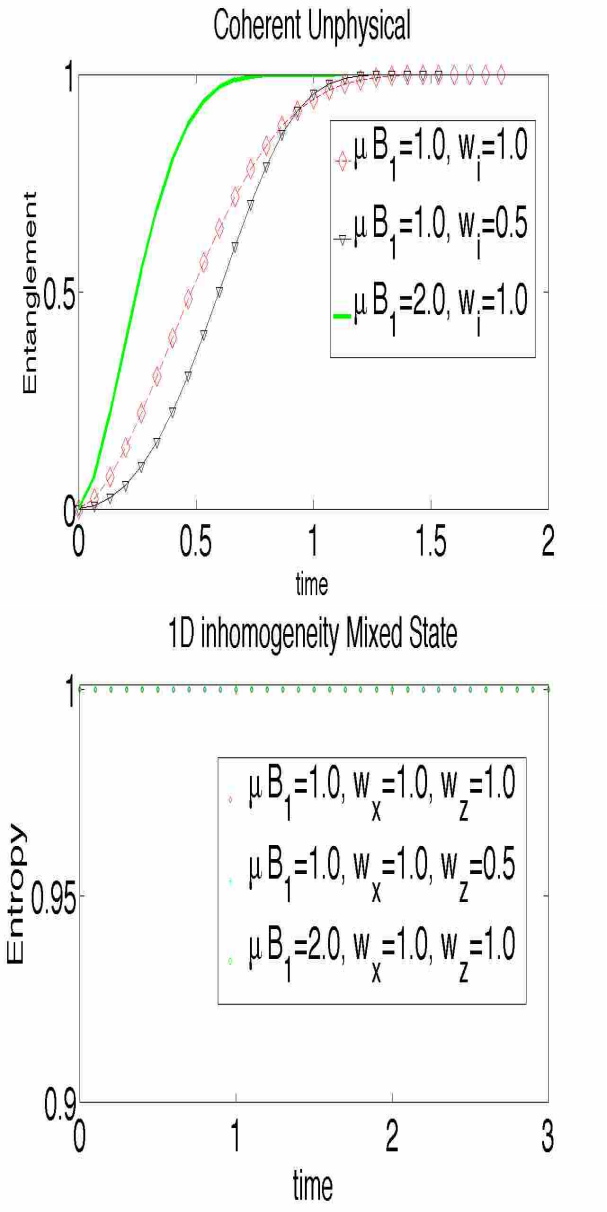

Figure 4.18 Color online

cases.

In the 1D Stern-Gerlach field, one obtains complete entanglement (CE) after some time for an initial coherent state. One gets a constant value for the von Neumann mixing entropy of a mixed state. For an initial coherent state, the rate to CE can vary as a function of the interaction strength μB_1, and the wave packet width in the inhomogeneity direction w_i. One reaches CE more rapidly when one applies larger μB_1 for a fixed width. This is because the larger the interaction strength, the faster the separation of the two wave packets. I also notice that for a fixed interaction strength, the entanglement in the case of a smaller w_i catches up with the larger w_i after some time. The wave packet spreads faster for a smaller w_i and therefore the overlapping area is smaller. For an initial mixed state, the von Neumann mixing entropy remains constant. This can be explained from the fact that there are still $50\%|\uparrow\rangle$ and $50\%|\downarrow\rangle$ spin states. Indeed, no spin flipping has occurred.

Fig.4.19 refers to the entropy change in a Stern-Gerlach experiment with 2D inhomogeneity starting from a pure state (top) and a mixed state (bottom). In the 2D Stern-Gerlach field, plots are generated for wave packets starting from $(x_0, z_0) = (0.0, 1.0)$ in Fig.4.19 and from $(x_0, z_0) = (0.0, 3.0)$ in Fig.4.20. Since two inhomogeneity axes are involved, I choose to compare the effect from w_x and w_z. For an initial pure state, one can see from Fig.4.19 that the interaction strength μB_1 determines the time to first reach CE. However after CE is obtained, one observes a reduction in the entanglement. This can be attributed to the spin flipping when crossing the transition axis. One also sees that the entanglement drops by about the same amount for identical values of w_z whereas the case with smaller w_z is closer to CE after the entanglement drop. For an initial mixed state, the von Neumann mixing entropy is no longer a constant throughout the experiment. One observes from the Fig.4.19 that the larger μB_1 is, the earlier the entropy decreases. This is understandable since as

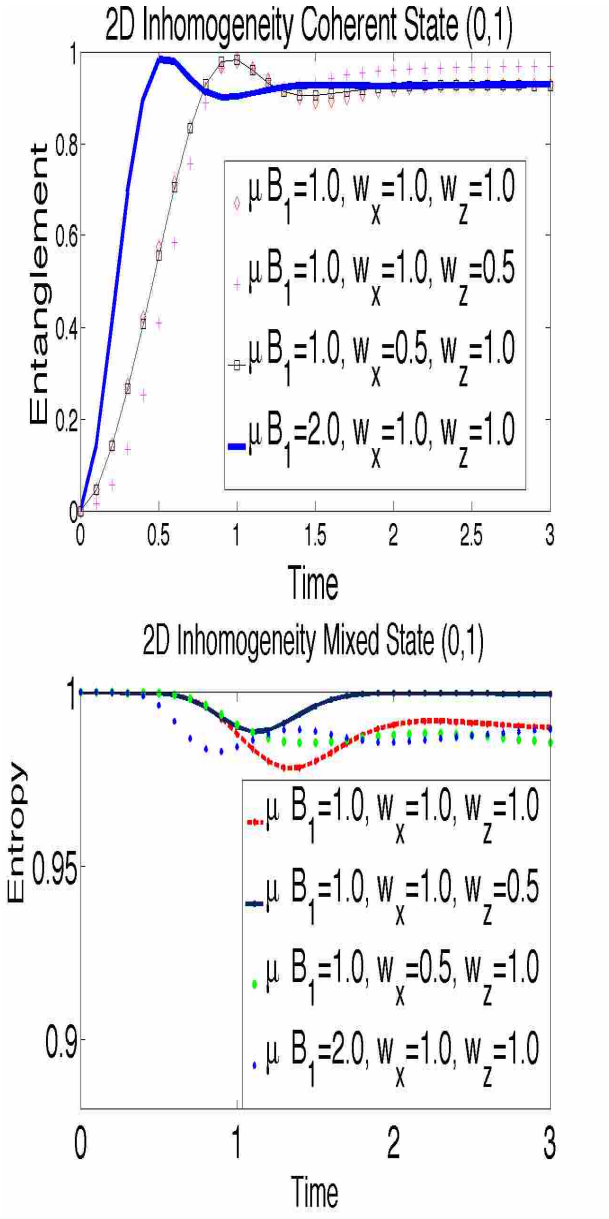

Figure 4.19 Color online

one increases the interaction strength, the down component moves faster through the transition axis where spin flipping occurs. As a result, the dip happens faster than in the other three cases.

Fig.4.20 refers to the entropy change in a Stern-Gerlach experiment with 2D inhomogeneity starting from a pure state (top) and a mixed state (bottom) at an initial location $(x_0, z_0) = (0, 3)$.

In the 1D unphysical SGE from a coherent state $(|\uparrow\rangle + |\downarrow\rangle)/2$, one can calculate the density

$$\begin{aligned} \rho &= \begin{pmatrix} \int \psi_\uparrow^*(\mathbf{x})\psi_\uparrow(\mathbf{x})d\mathbf{x} & \int \psi_\uparrow^*(\mathbf{x})\psi_\downarrow(\mathbf{x})d\mathbf{x} \\ \int \psi_\downarrow^*(\mathbf{x})\psi_\uparrow(\mathbf{x})d\mathbf{x} & \int \psi_\downarrow^*(\mathbf{x})\psi_\downarrow(\mathbf{x})d\mathbf{x} \end{pmatrix} \\ &= \begin{pmatrix} 1/2 & \int \psi_\uparrow^*(\mathbf{x})\psi_\downarrow(\mathbf{x})d\mathbf{x} \\ \int \psi_\downarrow^*(\mathbf{x})\psi_\uparrow(\mathbf{x})d\mathbf{x} & 1/2 \end{pmatrix}. \end{aligned} \tag{4.33}$$

Since there is no spin flipping, one would expect the diagonal terms to be both 1/2. As a result, the eigenvalues $\lambda_\pm$ can be obtained as

$$\begin{aligned} \lambda_\pm &= \frac{1}{2} \pm |\int \psi_\downarrow^*(\mathbf{x})\psi_\uparrow(\mathbf{x})d\mathbf{x}| \\ &= \frac{1}{2} \pm \rho_{\downarrow\uparrow}. \end{aligned} \tag{4.34}$$

One can then calculate the von Neumann mixing entropy S_v [1]

$$\begin{aligned} S_\rho &= -\lambda_+ \log_2 \lambda_+ - \lambda_- \log_2 \lambda_- \\ &= -\frac{1}{2}\log_2(\frac{1}{4} - \rho_{\downarrow\uparrow}^2) - \rho_{\downarrow\uparrow}\log_2(\frac{\frac{1}{2} + \rho_{\downarrow\uparrow}}{\frac{1}{2} - \rho_{\downarrow\uparrow}}). \end{aligned} \tag{4.35}$$

4.5 Discussion

I have studied Stern-Gerlach dynamics in both 1D and 2D magnetic-field inhomogeneities using analytic and numerical propagators respectively. This propagator

[1] This expression is different from the one used by Caldeira $E = 1 - \rho_{\downarrow\uparrow}^2$ [76].

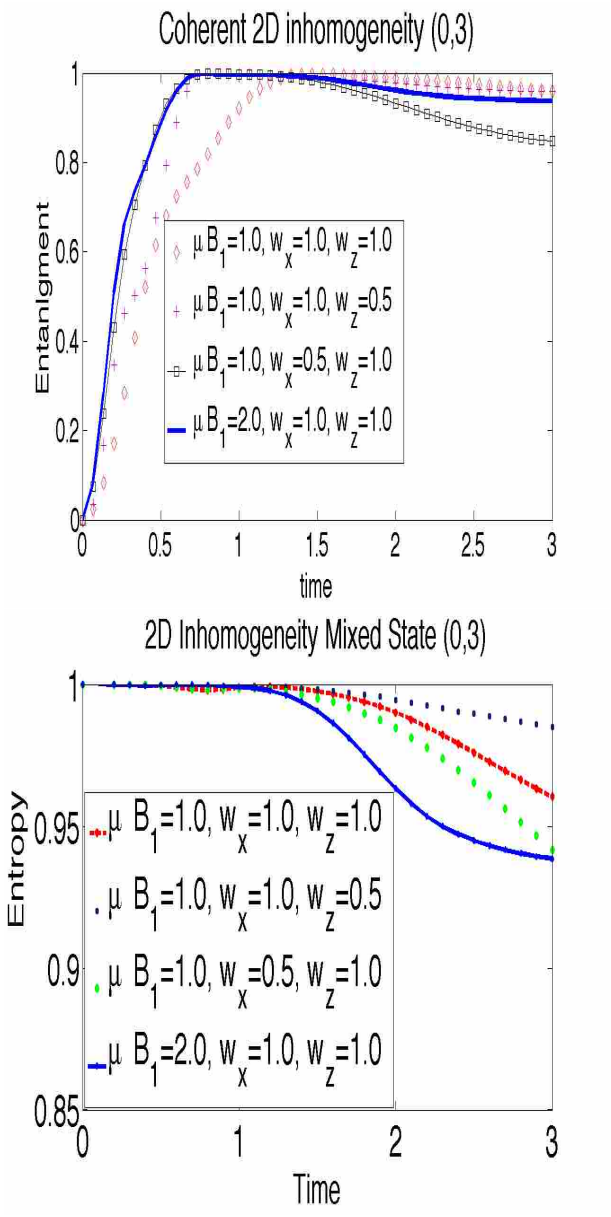

Figure 4.20 Color online

method enables one to track spin dynamics in time, as shown in spin density $\langle S_i \rangle$ contour plots. I have constructed the analytic propagators for 1D inhomogeneity and have obtained analytic forms for evolved wave packets after applying the integral formula to Gaussian wave packets. In the case where 2D inhomogeneity is present, a difficulty arises with respect to the construction and the application of propagators. The non-commutativity between two Pauli matrices results in the challenge of obtaining an exact solution for the propagators. There simply does not exist a transformation that can decouple the two inhomogeneity directions. Attempting to use the analytic propagators within a short time approximation is inconvenienced by the fact that additional numerical integrations have to be performed. Instead, I use a numerical propagation method to propagate the wave packets. This method relies on the use of the Trotter product formula and repeated operations on the wave packet without any space integration.

I have recovered the textbook Stern-Gerlach effect for specific parameter choices. For example, this separation can be obtained in the following two cases. Case I: The beam can enter anywhere in an unphysical (Maxwell's law violating) magnetic field from either an initial coherent state or an initial mixture. Case II: The beam enters the magnetic field (2D inhomogeneity with large local magnetic field in $\hat{z}$) as long as it enters far above $z = 0$ and close to $x = 0$. One just has to measure the outcome before the wave packet gets too close to the transition axis. In case I, the field has global eigenspinors and eigenenergies. As a result, symmetry is preserved and one recovers the vertical Stern-Gerlach separation. In case II, the presence of two Pauli matrices couple the two dimensions and the field gives position-dependent eigenspinors and eigenenergies. As a result, to get a vertical Stern-Gerlach separation requires a careful choice of initial locations. Indeed, I have shown that a radial separation is obtained when one chooses an arbitrary initial location. Therefore I have shown that vertical

separation is *not an automatic feature* in a Stern-Gerlach configuration.

I compare the wave packet evolution of an initial spin state in either a coherent-state (CS) representation ($|\uparrow\rangle_x$) or a mixed-state(MS) representation ($50\%|\uparrow\rangle$ and $50\%|\downarrow\rangle$). Initial coherent states are widely used in the literature. However, this does *not* reflect the historical Stern-Gerlach experiment where a beam of unpolarized silver atoms is produced out of the oven. The difference between the initial CS and MS spin states lead to different features in both 1D and 2D cases. In 1D inhomogeneity, I have shown that both CS and MS exhibit the *textbook* Stern-Gerlach separation. Nonetheless, the BSS and PSH features only appear with an initial CS. One sees that the spin polarization is correlated with position and can be controlled by manipulating the interaction strength and wavepacket width of the packet. This makes it a good candidate for a spintronics device. In 2D inhomogeneity, an initial CS leads to oscillating patterns.

I have also presented a short analysis of quantum entanglement based on Stern-Gerlach dynamics. It is well-known that in a Stern-Gerlach experiment, an initial pure state will be transformed into a completely mixed state, and therefore the von Neumann mixing entropy $S_v(\rho)$ (after partial tracing over spatial degrees of freedom) goes from 0 to 1. The measure of entanglement of an initial pure state is based on $S_v(\rho)$. This can be understood as follows: $S_v(\rho)$ reaches its maximum when the spin-up and the spin-down states are completely separated from each other, and no off-diagonal contributions survive in the density operator. Therefore one concludes that there is complete entanglement: when the spin-up and the spin-down states are completely separated, spin is fully entangled with space.

Nevertheless, the above statement fails in two major aspects according to the analysis provided in this thesis: (i) $S_v(\rho)$ is a good measure of entanglement for an initial pure state but not a good one for an initial mixed state (50% spin-up and 50% spin-

down). An initial mixed state starts out with maximum entropy, namely $S_v(\rho) = 1$, since the state is fully mixed. Therefore one is not able to see the entanglement process for an initial mixed state. Again, the scheme to measure the entanglement for an initial mixed state is different from that for an initial pure state and needs to be established more clearly. This can be further strengthened by the argument that an initial mixed state was used in the historical Stern-Gerlach experiment. (ii) For an initial pure state, I have shown in the dynamics that spin-flipping will occur in places such as the saddle point of the field. Therefore, complete entanglement can not be achieved. This uneven spin-flipping leads to a non-ideal Stern-Gerlach effect, contradicting the textbook Stern-Gerlach effect and the Stern-Gerlach quantum entanglement process. What happens if we have balanced spin-flipping (equal amounts of $|\uparrow\rangle$ to $|\downarrow\rangle$ and $|\downarrow\rangle$ to $|\uparrow\rangle$) ? Interestingly enough, $S_v(\rho)$ would be unaffected by the flipping after partial-tracing over all space. However, this balanced- spin-flipping would contradict both the textbook discussion of the Stern-Gerlach effect and of the Stern-Gerlach quantum entanglement. I have presented a situation where the von Neumann mixing entropy is not a good measure of entanglement.

I have thus shown that the von Neumann mixing entropy is not a good genereal measure of entanglement for mixed states. Based on the plots generated for mixed states, it is impossible to see the entanglement process since the state starts from a complete mixture. I have also shown that the entanglement of an initial pure state would decrease after a time interval. This reduction is attributed to the uneven spin flipping close to the transition axis.

Chapter 5

Conclusions

I have constructed analytic propagators for various systems including some exhibiting spin-orbit couplings (atomic spin-orbit and Rashba effect) and some involving inhomogeneous magnetic fields (Stern-Gerlach field). For systems with one degree of freedom in spin space, the analytic propagators can be constructed in a straightforward manner. However, for systems with two or more degree of freedom in spin space, the analytic propagator is difficult to obtain due to the noncommutativity between spin operators. I have used the Trotter formula to obtain approximate analytic propagators in the 2D Rashba case. In the 2D Stern-Gerlach case, I have used a numerical propagation method to propagate the initial wave packet without generating analytic propagators. Note that an analytic propagator can be obtained for the 2D Stern-Gerlach systems using the Trotter formula, as was used toward constructing the propagators for the 2D Rashba system. The consistency of the two methods was checked for the Rashba case although it has not been included in this manuscript.

These analytic propagators have been applied to localized wave packets in order to generate plots to display spin evolution. This is an improvement over Scully's treatment [71] of Stern-Gerlach systems, where an initial delta-like wave function was

assumed. For 1D Stern-Gerlach and Rashba systems, the results are exact, since an analytic Gaussian integration can be performed. For systems involving two or more degrees of freedom in spin space, it is challenging to perform analytic integrations. Therefore alternative routes have been sought. For the 2D Rashba system, a Monte-Carlo integration is used to address the difficulty of integration. For the 2D Stern-Gerlach system, I have used a numerical propagation method to propagate the initial wave packet. With these propagation methods I have been able to obtain the following results.

Various features have been identified in the local spin density plots for Rashba systems. The following features occur in 1D Rashba systems: Spin Separation (SS), Bamboo-Shooting Structure (BSS), Persistent Spin Helix (PSH), and Spin Accumulation (SA). These features have been interpreted using the eigenstates for the Rashba 1D system, since global eigenspinors exist in the 1D Rashba case. These features agree with results in the literature. I have also discovered that the features strongly depend on the width of the wave packet and on the strength of the Rashba coefficient.

For the 2D Rashba system I have observed: Ripple Formation Structure (RFS), Triangular Oscillations (TO), Asymmetric Spin Rotation (ASR), Diagonal Symmetry Structure (DSS). In the 2D case, eigenspinors are momentum-dependent. Since I start from a localized wave packet in space and in momentum, the packet covers different sets of eigenspinors. These features have also been discussed in function of their dependence on the widths of the wave packet and the Rashba coefficient. Thus in both 1D and 2D Rashba systems one can control the parameters to achieve features for specific purposes.

Several features have also been identified in the local spin density plots for Stern-Gerlach systems. I have considered initial spin states to be either pure or mixed (50% up and 50% down). While a pure state is widely used in the literature to

treat the Stern-Gerlach effect, mixed states have not been discussed extensively. This somehow is not consistent with the historical Stern-Gerlach experiment, where a beam of unpolarized silver atoms is produced from an oven before collimation towards the magnet. I have found out that an initial pure state leads to distinctive new features in a Stern-Gerlach system.

From the generated plots, I have observed three features in 1D Stern-Gerlach systems: Spin-Separating Mechanism (SSM), Bamboo-Shooting Structure (BSS), and Persistent Spin Helix (PSH). These three features have been explained and interpreted using the concept of global eigenspinors in 1D Stern-Gerlach systems. I have also generated plots for 2D Stern-Gerlach systems and I have observed: Radial Spin Separation (RSS), Non-ideal Stern-Gerlach effect (NSGE), and Fringe formation and Four-Lobe Structure (FFLS). From all of these features I conclude that the statement "spin-up goes up, and spin-down goes down" is an oversimplification. This simplified model which is widely used for pedagogical purposes could be referred to as the ideal Stern-Gerlach effect in analogy to ideal (massless) springs and frictionless inclined planes from elementary mechanics.

I have used the results of Stern-Gerlach dynamics to understand the quantum entanglement in the Stern-Gerlach experiment. It has been stated repeatedly that in a Stern-Gerlach experiment, an initial pure state will be transformed into a completely mixed state, and therefore the von Neumann mixing entropy $S_v(\rho)$ (after partial tracing over spatial degree of freedom) goes from 0 to 1. The measure of entanglement of an initial pure state is based on $S_v(\rho)$. This can be understood as follows: $S_v(\rho)$ reaches its maximum when the spin-up and the spin-down states are completely separated from each other, and no off-diagonal contributions survive in the density operator. Therefore one obtains complete entanglement, since when the spin-up and the spin-down states are separated, they are fully entangled with space.

Nevertheless, the above statement fails in two major aspects according to the analysis provided in this thesis: (i) $S_v(\rho)$ is a good measure of entanglement for an initial pure state but not a good one for an initial mixed state (50% spin-up and 50% spin-down). An initial mixed state starts out with maximum entropy, namely $S_v(\rho) = 1$, since the state is fully mixed. Therefore one is not able to see the entanglement process for an initial mixed state. Again, the scheme to measure the entanglement for an initial mixed state is different from that for an initial pure state and needs to be established more clearly. This can be further strengthened by the argument that an initial mixed state was used in the historical Stern-Gerlach experiment. (ii) For an initial pure state, I have shown in the dynamics that spin-flipping will occur in places such as the saddle point of the field. Therefore, complete entanglement can not be achieved. This uneven spin-flipping leads to a non-ideal Stern-Gerlach effect, contradicting the textbook Stern-Gerlach effect and the Stern-Gerlach quantum entanglement process. What happens if we have even spin-flipping? Interestingly enough, $S_v(\rho)$ would be unaffected by the flipping after partial-tracing over all space. However, this even- spin-flipping would contradict both the textbook discussion of the Stern-Gerlach effect and of the Stern-Gerlach quantum entanglement. I have presented a situation when the von Neumann mixing entropy is not a good measure of entanglement.

I have also derived displacement formulas involving noncommutative operators in Appendix A. This work is motivated by the manipulation of noncommuting operators in exponents, in analogy to the noncommutativities discussed in the construction of propagators. The noncommutativity results in three characteristic effects: the appearance of phase factors, space-modulated displacements and staggered spin-dependent displacements. The modified displacement formulas reveal an underlying symmetry beyond simple translational symmetry for quantum systems to which they

are applicable, namely noncommutative ones. The staggered spin-dependent displacements can be connected to the current spintronics technology.

Finally, I have applied this propagator approach to option pricing theory. Extensive research has been done in the area of quantum finance which connects the financial market and quantum mechanics [77, 78]. It can be shown that the Black-Scholes formula for European option pricing can be reduced to a time-dependent Schrödinger equation. Therefore, it is appropriate to derive quantum propagators and apply them to specific distributions. I have also speculated on the existence of spin-like variable in the financial market. This is motivated by the formal similarity between the Black-Scholes Schrödinger equation and the Schrödinger equation with Rashba interactions.

Beyond this work there are further applications for spin propagators. For example, this propagator method can be extended to additional spin-dependent systems, such as monolayer graphene. The Hamiltonian for monolayer graphene is very similar to that of the Rashba system. It couples spin operators to momentum operators. In fact, monolayer graphene should be easier to work with than Rashba, since it lacks the mass dependence. One could, of course, construct analytic propagators for monolayer graphene based on the Trotter formula to a given order of accuracy. However, I believe it is preferable to derive a general formula for a time-evolution operator with terms $\sum_i p_i \sigma_i$ in the exponent in order to operate directly on a spatial distribution along the lines of what I have done in Appendix A.

In this thesis, I have not considered systems involving interactions higher than quadratic terms, or including nonlinearity in the wave function. The construction of such propagators would be more difficult. First, the higher-order terms would possibly lead to non-terminating terms in the Zassenhaus formula. Second, the nonlinear terms would lead to a different form for the time-evolution operator and thus would

require a new method to construct the time-evolution operator before constructing the propagators. The propagator method has proven to be extensible to spin systems and to give interesting results in the few cases that I covered in this spin-current analysis.

Bibliography

[1] R. Winkler, *Spin-orbit Coupling Effects in Two-Dimensional Electron and Hole Systems*, 1st ed. (Berlin: Springer, 2003).

[2] P. Grünberg, R. Schreiber, Y. Pang, M. B. Brodsky, and H. Sowers, Phys. Rev. Lett. **57** 19, 2442V2445 (1986).

[3] S. Bandyopadhyay 2008 *Introduction to Spintronics*, 1st ed. (Boca Rota, FL: CRC, 2008).

[4] D. Awschalom, *Semiconductor Spintronics and Quantum Computation*, 1st ed. (New York: Springer, 2002).

[5] J. Shi, P. Zhang, D Xiao, and Q. Niu, Phys. Rev. Lett. **96**, 076604 (2006).

[6] H. Kleinert, *Path Integrals in Quantum Mechanics, Statistics, and Polymer Physics, and Financial Markets*, 3rd ed. (New York: World Scientific, 2004).

[7] L. S. Schulman, *Techniques and Applications of Path Integration*, 1st ed. (New York: Dover, 2005).

[8] E. B. Manukian, *Quantum Theory: A Wide Spectrum*, 1st ed. (Springer, New York, 2006).

[9] R. P. Feynman, *Quantum Mechanics and Path Integrals* (McGraw-Hill, New York, 1965).

[10] J. Schwinger, *Quantum Mechanics*, (Berlin: Springer, 2001).

[11] K. M. Poon and G. Munoz, Am. J. Phys. **67**, 547 (1999).

[12] K. Gottfried, *Quantum Mechanics: Fundamentals*, 2nd ed. (New York: Springer, 2004).

[13] G. P. Arrighini, N. L. Durante, and C. Guidotti, Am. J. Phys. **64**, 8, 1036-1041 (1996).

[14] E. Kennard. Z. Phys. **44**. 326 (1927).

[15] L. S. Brown and Y. Zhang, Am. J. Phys. **62**, 9, 806-808 (1994).

[16] Eugen Merzbacher, *Quantum Mechanics*, 3rd ed. (Wiley, New York, 1998).

[17] F.A. Barone *et al.*, Am. J. Phys. **71**, 483-491 (2003).

[18] Q. Wang, J. Phys. A **20**, 5041 (1987).

[19] G. Y. Tsaur and J. Wang, Am. J. Phys. **74**, 7, 600-606 (2006).

[20] M. Suzuki, Physica A **117**, 103 (1983).

[21] D. R. Truax, Phys. Rev. D. **31**, 1988 (1985).

[22] R. A. Fisher, N. M. Nieto, and V. D. Sandberg, Phys. Rev. D **29**, 1107 (1984).

[23] Hans A. Bethe and Edwin E. Salpeter, *Quantum Mechanics of One- and Two-Electron Atoms*, 1st ed. (Dover Publications, 1977).

[24] A. K. Geim and K. S. Novoselov, Nature Mat. **6**, 183 (2007).

[25] J. Y. Vaishnav and Charles W Clark Charles, Phys. Rev. Lett. **100**, 153002 (2008).

[26] E. I. Rashba, Fiz. Tverd. Tela (Leningrad) 2, 1224 (1960) (Sov. Phys. Solid State 2, 1109 (1960)).

[27] Yu. A. Bychkov and E. I. Rashba, J. Phys. C **17**, 6039-6045 (1984).

[28] G. Dresselhaus, Phys. Rev. **100**, 580-586 (1955).

[29] B. A. Bernevig, J. Orenstein, and S.C. Zhang, Phys. Rev. Lett. **97**, 236601 (2006).

[30] J. Schliemann J, J. C. Egues, and D. Loss, Phys. Rev. Lett. **90**, 146801 (2003).

[31] K. Suzuki and S. Kurihara, arXiv:cond-mat/0611013 v2 (2006).

[32] B. A. Bernevig and Shou-Cheng Zhang, Phys. Rev. Lett. **96**, 106802 (2006).

[33] Xi Fu, Wenhu Liao, and Guanghui Zhou, Advances in Condensed Matter Physics, **2008**, 152731 (2008).

[34] J. Sinova *et al*, Phys. Rev. Lett. **92**, 126603 (2004).

[35] J. Schliemann, D. Loss, and R. M. Westervelt, Phys. Rev. Lett. **94**, 206801 (2005).

[36] S. Datta and B. Das, Appl. Phys. Lett. **56**, 665 (1990).

[37] I. Zutic, J.Fabian and S. D. Sarma, Rev. Mod. Phys. **76**, 323 (2004).

[38] S-Q Shen, Phys. Rev. B., **70**, 081311(R) (2004).

[39] Y. K. Kato, R. C. Myers, A. C. Gossard, D. D. Awschalom, Science, **306**, 5703, 1910 - 1913 (2004).

[40] M. H. Liu *et al*, Phys. Rev. B **74**, 235322 (2006).

[41] J. Schliemann *et al*, Phys. Rev. B **73**, 085323 (2006).

[42] P. Brusheim and H. Q. Xu, Phys. Rev. B **74**, 205307 (2006).

[43] A. Sarkar and T. K. Bhattacharyya, J. Appl. Phys. **101**, 036108 (2007).

[44] A. Sarkar and T. K. Bhattacharyya, J. Appl. Phys. **90**, 173101 (2007).

[45] J Chen *et al*, Proceedings of the 2004 11th IEEE International Conference, 195-198 (2004).

[46] M. Pletyukhov and A. Shnirman, Phys. Rev. B. **79**, 033303 (2009).

[47] A. Csordás *et al*, Eur. Phys. J. B **54**, 189-200 (2006).

[48] Y-Y Chin *et al*, J. Magn. Magn. Mater. **310**, e702-e704 (2007).

[49] J Brüning *et al*, J. Phys. A **40**, F697-F704 (2007).

[50] W. Jing *et al*, Chin. Phys. Lett. **25**, 8 3001 (2008).

[51] V. Ya. Demikhovskii, G. M. Makisimova, and E. V. Frolova, Phys. Rev. B **78**. 115401 (2008).

[52] K. Bencheikh and G. Vignale, Phys. Rev. B **77**, 155315 (2008).

[53] J. A. Lock, Am. J. Phys. **47**, 797 (1979).

[54] J. Schliemann, Phys. Rev. B **75**, 045304 (2007).

[55] W Zawadzki and T. M. Rusin, arXiv:0909.0463v1 (2009).

[56] B. C. Hsu and J.-F. S. Van Huele, J. Phys. A: Math. Theo. **42**, 475304 (2009).

[57] Hans De Raedt and Bart De Raedt, Phys. Rev. A. **28**, 3575-3580 (1983).

[58] J. Wang *et al*, Phys. Rev. B **73**, 033316 (2006).

[59] J. E. Hirsch, Phys. Rev. Lett. **83**, 1834 (1999).

[60] J. D. Koralek *et al*, Nature **458**, 610-613 (2009).

[61] A. Manchon and S. Zhang, Phys. Rev. B **79**, 094422 (2008).

[62] W. Gerlach and O. Stern, Z. Phys. **8**, 110 (1922).

[63] A. Sommerfeld, *Atombau Und Spektrallinien*, (Friedr. Viweg & Sohn, 1924).

[64] H. Haken and H. C. Wolf, *The physics of atoms and quanta: Introduction to experiments and theory*, 6th ed. (Springer, New York, 2000).

[65] L. I. Schiff, *Quantum mechanics*, 3rd ed. (McGraw-Hill, New York, 1968).

[66] D. Bohm, *Quantum Theory* (Prentice-Hall, Englewood Cliffs, 1951).

[67] D. Griffith, *Introduction to Quantum Mechanics*, 2nd ed. (Pearson Prentice Hall, 2005).

[68] G. Potel, F. Barranco, S Cruz-Barrios, and J. Gomez-Camacho, Phys. Rev. A, **71**, 052196 (2005).

[69] J. Diaz Bulnes and I. S. Oliveira, Braz. J. Phys. **31**, 3, 488-495 (2001).

[70] M.O. Scully, R. Shea and J.D. McCullen, Phys. Rep. **43**, 485-498 (1978).

[71] M.O. Scully, W.E. Lamb,Jr., and A.O. Barut, Found. Phys. **17**, 575-583 (1987).

[72] J. S. Townsend, *A modern approach to quantum mechanics*, (University Science Books, Sausalito, 2000).

[73] B. C. Hsu and J.-F. S. Van Huele, Phys. Rev. B. **80** 235309 (2009).

[74] D. Home, A. K. Pan, M. M. Ali, and A. S. Majumdar, J. Phys. A **40**, 13975 (2007).

[75] G. B. Roston, M. Cases, A. Plastino, and A. R. Plastino, Eur. J. Phys. **26**, 657 (2005).

[76] T. R. de Oliveira, A. O. Caldeira, arXiv:quant-ph/0608192 (2006).

[77] Belal E. Baaquie, *Quantum Finance: Path Integrals and Hamiltonians for Options and Interest Rates*, 1st ed. (Cambridge University Press, 2007).

[78] Eugene Stanley, *"Econophysics and the Current Economic Turmoil"*, http://polymer.bu.edu/hes/articles/s08a.pdf. (Accessed Jan 2009).

Appendix A

Displacement Formulae for Noncommutative Operators

This paper is published in Physical Scripta **80** 065011 (2009).

IOP Publishing Physica Scripta
Phys. Scr. **80** (2009) 065011 (7pp) doi:10.1088/0031-8949/80/06/065011

Displacement formulae for noncommutative operators

Bailey C Hsu and Jean-François S Van Huele

Department of Physics and Astronomy, Brigham Young University Provo, UT 84602, USA

E-mail: bailey.c.hsu@gmail.com and vanhuele@byu.edu

Received 18 June 2009
Accepted for publication 20 October 2009
Published 1 December 2009
Online at stacks.iop.org/PhysScr/80/065011

Abstract
We present analytical expressions for displacements that involve noncommutative operators. We generalize the standard displacement formula $D_a f(x) = f(x-a)$ by considering successively the displacement effect of momentum operators in noncommutative quantum mechanics $[p_i, p_j] = \mathrm{i}\theta_{ij}$, d-dimensional radial momentum operators $p_r^{(d)} = -\mathrm{i}\hbar(\partial_r + (d-1)/2)$ and spin-dependent operators. The noncommutativity results in three characteristic effects: the appearance of phase factors, space-modulated displacements and staggered spin-dependent displacements.

PACS numbers: 02.20.−a, 03.65.Fd

1. Introduction

Displacement (or translation) operators play an important role in quantum physics. The displacement operator D_a acts on a wave function $\psi(x)$ by translating its argument by a so that $D_a\psi(x) = \psi(x-a)$. The use of the displacement operator is usually associated with the existence of translational symmetry, such as the symmetry that occurs in periodic structures. Analytic expressions for displacement operators and a discussion of the method to obtain them are well known [1]. We can exponentiate the derivative operator $\partial/\partial x$, or the momentum operator p_x, which is related to it, to obtain the displacement operator D_a. The momentum operator is said to generate the displacement. This procedure applies in an arbitrary number of dimensions. In d dimensions the generator of translations is the d-dimensional momentum vector $\vec{p}$.

Noncommutativity and noncommuting operators pervade quantum theory. They express the mutual incompatibility of pairs of physical observables. One consequence of noncommutativity is the need to develop rules for the ordering of observables. For example the noncommutativity of operators A and B, $[A, B] = AB - BA \neq 0$ implies in general that $f(A)f(B) \neq f(B)f(A)$ and in particular that $\mathrm{e}^A\mathrm{e}^B \neq \mathrm{e}^B\mathrm{e}^A \neq \mathrm{e}^{B+A}$. Expressions relating exponentials of sums of noncommuting operators to products of exponentials of these operators and of their nested commutators are given in the literature [2, 3], and are generally known under the name of Baker–Campbell–Hausdorff formulae ([4] and references therein).

In this paper, we combine the two properties of displacement and noncommutativity and extend the familiar displacement formulae to cases where the operators in the exponent do not commute. In particular, we look at three different cases where the operators associated with the momenta, or the generators of the displacement operator, do not commute. After a review of displacement operators in section 2, we consider the action of Cartesian momentum operators in noncommutative quantum mechanics in section 3. The resulting displaced function exhibits multiplicative local phase factors proportional to the commutator of the two momentum operators. In section 4, we work out the similar formulae for the radial momentum operator in two dimensions and then generalize to the radial momentum in d dimensions. The displaced function now exhibits space-dependent factors. Finally in section 5, we consider the displacements that arise from coupling noncommuting spin operators to a single Cartesian momentum operator. The result of this situation is to combine spin-dependent complex factors with staggered displacements corresponding to the eigenvalues of the spin operators.

The formulae in this paper can be used to study the evolution of physical systems that exhibit some type of noncommutativity: noncommutative toy models in high-energy physics, in particular those where the commutation relation between momenta in different dimensions differs from

zero [5–7], condensed matter systems that include spin–orbit coupling, which leads to spin separation that may help control future spintronics devices [8, 9] as well as ultracold atomic physics systems that mimic those condensed matter interactions [10].

2. Standard displacement operators

The displacement operator D_a displaces the argument of the function $f(x)$ so that,

$$D_a f(x) = f(x-a). \tag{1}$$

By developing the function $f(x-a)$ in a Taylor series for small displacements a and summing the resulting operator series, we obtain an expression for the displacement operator as an exponential of the momentum operator

$$\begin{aligned} f(x-a) &= f(x) - a\frac{\mathrm{d}}{\mathrm{d}x}f(x) + \frac{a^2}{2!}\frac{\mathrm{d}^2}{\mathrm{d}x^2}f(x) + \cdots \\ &= \exp\left(-a\frac{\mathrm{d}}{\mathrm{d}x}\right) f(x) = \exp\left(-\frac{\mathrm{i}ap}{\hbar}\right) f(x), \end{aligned} \tag{2}$$

where the coordinate representation of the momentum operator $p = \frac{\hbar}{\mathrm{i}}\frac{\mathrm{d}}{\mathrm{d}x}$ has been introduced.

The family of displacement operators form a group with the null displacement as neutral element of the group and the inverse displacement operator given by

$$D_{-a} f(x) = f(x+a). \tag{3}$$

For a displacement in two independent dimensions, we can similarly define the operators

$$D_{(a,b)} f(x, y) = f(x-a, y-b), \tag{4}$$

which, again, form a group. The displacement formula in two dimensions becomes

$$\begin{aligned} f(x-a, y-b) &= f(x) - a\frac{\partial}{\partial x}f(x, y) - b\frac{\partial}{\partial y}f(x, y) \\ &\quad + \frac{a^2}{2!}\frac{\partial^2}{\partial x^2}f(x) + \frac{b^2}{2!}\frac{\partial^2}{\partial y^2}f(x, y) + ab\frac{\partial}{\partial x\partial y}f(x, y) + \cdots \\ &= \exp\left(-a\frac{\partial}{\partial x} + b\frac{\partial}{\partial y}\right) f(x, y) \\ &= \exp\left(-\frac{\mathrm{i}(ap_x + bp_y)}{\hbar}\right) f(x, y) \end{aligned} \tag{5}$$

for $f(x, y)$ a well-behaved (Schwarzian) function of two variables. This procedure can be repeated for any number of dimensions as long as the corresponding momentum operators commute among themselves. In the next subsection, we consider what happens when we add noncommutativity between the momentum operators. In what follows we read equation (5) from right to left and find out how noncommuting generators affect the displacement formula.

3. Displacement formula involving momentum operators in noncommutative space

In the momentum–momentum algebra (MMA) version of noncommutative quantum mechanics (NCQM) [11], momentum operators corresponding to different coordinates obey a nonstandard (deformed) commutation relation

$$[p_i, p_j] = \mathrm{i}\theta_{ij},$$

with θ_{ij} antisymmetric constants. The other (space–space and space–momentum) commutation relations are unaffected. To find out what happens to the displacement formula, we calculate $\exp(-\frac{\mathrm{i}(ap_i+bp_j)}{\hbar})f(x, y)$. However, the usual coordinate representation of the momentum operators $p_i = \frac{\hbar}{\mathrm{i}}\frac{\mathrm{d}}{\mathrm{d}x_i}$ is now incompatible with the nonstandard commutation relation, $[\partial_i, \partial_j] \neq \mathrm{i}\theta_{ij}$. Instead we transform the MMA coordinates and momenta such that (using the Einstein summation convention)

$$x_i = \tilde{x}_i, \tag{6}$$

$$p_i = \tilde{p}_i + \frac{\theta_{il}}{2\hbar}\tilde{x}_l, \tag{7}$$

where $\tilde{x}_i$ and $\tilde{p}_i$ satisfy the usual (Heisenberg) algebra and are thus compatible with the standard representation $\tilde{p}_i = \frac{\hbar}{\mathrm{i}}\frac{\mathrm{d}}{\mathrm{d}\tilde{x}_i}$. In this case, we can use the Zassenhaus formula [12, 13], which expresses the exponential of the sum of two noncommuting operators in terms of a product of exponentials containing increasingly complex nested commutators of the two original operators

$$\mathrm{e}^{t(X+Y)} = \mathrm{e}^{tX}\,\mathrm{e}^{tY}\,\mathrm{e}^{-\frac{t^2}{2!}[X,Y]}\,\mathrm{e}^{\frac{t^3}{3!}(2[Y,[X,Y]]+[X,[X,Y]])}\cdots \tag{8}$$

In the right-hand side of this expression (ignoring the two left-most factors whose exponents do not involve commutators), the exponential of the nth factor contains terms with exactly n-nested commutators of $n+1$ operators, with X and Y appearing at least once each. It should be pointed out that there is no known general analytic form for the coefficients of the different terms appearing in the exponents of equation (8), but that the coefficients up to order 17 have been evaluated explicitly, and also that all the coefficients of the last term in each exponent are exactly equal to one [14]. In the present case, the formula reduces to a product of three factors since both p_i and p_j commute with their commutator and all the nested commutators vanish

$$\begin{aligned} \mathrm{e}^{-\mathrm{i}/\hbar(ap_i+bp_j)} &= \mathrm{e}^{-\mathrm{i}ap_i/\hbar}\,\mathrm{e}^{-\mathrm{i}bp_j/\hbar}\,\mathrm{e}^{ab/2\hbar^2[p_i,p_j]} \\ &= \mathrm{e}^{-\mathrm{i}ap_i/\hbar}\,\mathrm{e}^{-\mathrm{i}bp_j/\hbar}\,\mathrm{e}^{(ab/2\hbar^2)\mathrm{i}\theta_{ij}}. \end{aligned} \tag{9}$$

By applying this operator to a function $f(x_i, x_j)$, first transforming to the Heisenberg operators, reordering the exponentials to bring the momenta $\tilde{p}_i = \frac{\hbar}{\mathrm{i}}\frac{\mathrm{d}}{\mathrm{d}\tilde{x}_i}$ to the right to act on the function, and collecting the extra factors to the left, one shows that

$$\begin{aligned} \mathrm{e}^{-\mathrm{i}/\hbar(ap_i+bp_j)} f(x_i, x_j) &= \mathrm{e}^{(-\mathrm{i}a/2\hbar^2)\theta_{ik}x_k}\mathrm{e}^{(-\mathrm{i}b/2\hbar^2)\theta_{jk}x_k} \\ &\quad \times f(x_i - a, x_j - b). \end{aligned} \tag{10}$$

The effect of noncommutativity in this case leads to local phases proportional to the commutator and multiplying the displaced function. The property can be extended to noncommuting momentum operators and functions in d dimensions through repeated application of the procedure for two noncommuting operators because the phase factors commute among themselves.

4. Displacement formula involving the radial momentum operators

In quantum mechanics the radial momentum operator in two dimensions, p_r is defined as $\frac{\hbar}{\mathrm{i}}(\partial_r + \frac{1}{2r})$, an expression that guarantees the symmetry (but not the self-adjointness [16]) of the operator [1]. When thus written as a sum, p_r consists of two parts that do not commute $[\partial_r, \frac{1}{2r}] \neq 0$. We consider the effect of applying the exponential of the radial momentum operator, $\exp(\frac{\mathrm{i}ap_r}{\hbar})$ on a radial function $f(r)$. We introduce the inverse of the radial coordinate, $x = 1/r$, relate the two partial derivatives $\partial_r = -x^2\partial_x$, and we set out to expand $\exp(\frac{\mathrm{i}ap_r}{\hbar}) = \exp(-a(x^2\partial_x - \frac{x}{2}))$ by applying the Zassenhaus product formula equation (8). Unlike in the previous section the product of exponentials of sums of nested commutators does not terminate because the commutators do not vanish for any power of x. However, the particular structure of the operators involved leads to a simplification that allows the expression to be evaluated in closed form, as we now show. We identify $t \to -a$, $X \to x^2\partial_x$, $Y \to -\frac{x}{2}$ in equation (8) and evaluate all the commutators. First we notice that any nested commutator consisting of more than one Y factor vanishes since Y itself commutes with $[X, Y] = -2Y^2$. The only remaining terms are of the form $[X, [X, [\ldots, [X, Y]]\ldots]]$ with the lone Y operator in the right-most position. We now evaluate these terms by induction. Denoting the commutator with exactly n X operators to the left of the single Y operator as $[X, Y]_{(n)}$, it is a simple matter to check that

$$[X, Y]_{(1)} = [X, Y] = \left[x^2\partial_x, -\frac{x}{2}\right] = -\frac{x^2}{2} = -\frac{1!x^{1+1}}{2},$$

$$[X, Y]_{(2)} = [X, [X, Y]] = \left[x^2\partial_x, -\frac{x^2}{2}\right] = -x^3 = -\frac{2!x^{2+1}}{2},$$

and by assuming

$$[X, Y]_{(n)} = -\frac{n!x^{n+1}}{2},$$

it follows that

$$[X, Y]_{(n+1)} = \left[x^2\partial_x, -\frac{n!x^{n+1}}{2}\right] = -\frac{(n+1)!x^{n+2}}{2}, \quad (11)$$

which completes the proof by induction. It has been shown [15] that the coefficients of the terms with one Y operator in the nth factor equals $\frac{1}{n!}$ and as a result,

$$\exp\left(-a\left(x^2\partial_x - \frac{x}{2}\right)\right) = \mathrm{e}^{-ax^2\partial_x}\mathrm{e}^{ax/2}\mathrm{e}^{a^2/2![x^2\partial_x, \frac{x}{2}]}\mathrm{e}^{a^3/3![x^2\partial_x, [x^2\partial_x, \frac{x}{2}]]}\ldots. \quad (12)$$

All but the first factor commute among themselves because the nested commutators result in powers of x only, and equation (11) allows us to rearrange equation (12) as

$$\begin{aligned}\exp\left(-a\left(x^2\partial_x - \frac{x}{2}\right)\right) &= \mathrm{e}^{-ax^2\partial_x}\mathrm{e}^{ax/2}\mathrm{e}^{\sum_{n=1}^{\infty}\frac{(ax)^{n+1}}{2(n+1)}} \\ &= \mathrm{e}^{-ax^2\partial_x}\mathrm{e}^{ax/2}\mathrm{e}^{-ax/2}\mathrm{e}^{-[\ln(1-ax)]/2} \\ &= \mathrm{e}^{-ax^2\partial_x}\frac{1}{\sqrt{1-ax}}, \end{aligned} \quad (13)$$

where we have used the power series for the logarithm $\sum_{n=0}^{\infty}\frac{(ax)^{n+1}}{2(n+1)} = -\frac{\ln(1-ax)}{2}$. This is a formal expression involving operators. Note that, as a series, the exponent in the first line of equation (13) converges when $|ax| < 1$.

We now proceed to commute the two operators appearing in the right-hand side of equation (13). The Baker–Campbell–Hausdorff formula [2]

$$\mathrm{e}^{\lambda A}B\mathrm{e}^{-\lambda A} = B + \frac{\lambda}{1!}[A, B] + \frac{\lambda^2}{2!}[A, [A, B]] + \frac{\lambda^3}{3!}[A, [A, [A, B]]] + \cdots \quad (14)$$

can be transformed by multiplication by $\mathrm{e}^{\lambda A}$ on the right into

$$\mathrm{e}^{\lambda A}B = B\mathrm{e}^{\lambda A} + \frac{\lambda}{1!}[A, B]\mathrm{e}^{\lambda A} + \frac{\lambda^2}{2!}[A, [A, B]]\mathrm{e}^{\lambda A} + \frac{\lambda^3}{3!}[A, [A, [A, B]]]\mathrm{e}^{\lambda A} + \cdots. \quad (15)$$

We now consider the action of $\mathrm{e}^{-ax^2\partial_x}$ on arbitrary powers x^n. We start off with $n = 1$. By substituting $\lambda \to -a$, $A \to x^2\partial_x$, $B \to x$, working out the commutators in equation (15) and summing, we obtain a closed form

$$\begin{aligned}\mathrm{e}^{-ax^2\partial_x}x &= x\mathrm{e}^{-ax^2\partial_x} + \frac{-a}{1!}x^2\mathrm{e}^{-ax^2\partial_x} + \frac{a^2}{2!}2x^3\mathrm{e}^{-ax^2\partial_x} + \frac{-a^3}{3!}6x^4\mathrm{e}^{-ax^2\partial_x} + \cdots \\ &= x\sum_{n=0}^{\infty}(-ax)^n\mathrm{e}^{-ax^2\partial_x} = \frac{x}{1+ax}\mathrm{e}^{-ax^2\partial_x}. \end{aligned} \quad (16)$$

Similarly for general n, we substitute $\lambda \to -a$, $A \to x^2\partial_x$, $B \to x^n$, and obtain

$$\begin{aligned}\mathrm{e}^{-ax^2\partial_x}x^n &= x^n\mathrm{e}^{-ax^2\partial_x} + \frac{-a}{1!}nx^{n+1}\mathrm{e}^{-ax^2\partial_x} + \frac{a^2}{2!}n(n+1)x^{n+2}\mathrm{e}^{-ax^2\partial_x} + \frac{-a^3}{3!}n(n+1)(n+2)x^{n+3}\mathrm{e}^{-ax^2\partial_x} + \cdots \\ &= \sum_{j=0}^{\infty}\frac{x^n(-ax)^j}{j!}\frac{(n+j-1)!}{(n-1)!}\mathrm{e}^{-ax^2\partial_x} \\ &= x^n(1+ax)^{-n}\mathrm{e}^{-ax^2\partial_x}. \end{aligned} \quad (17)$$

Now that we have found the effect of $\mathrm{e}^{-ax^2\partial_x}$ on arbitrary powers of x, we consider its action on more general functions of x by relating these functions to a power series in x. We thus work out the binomial expansion of $(1-ax)^n$ which converges for $|ax| < 1$

$$(1-ax)^n = \sum_{k=0}^{\infty}\frac{(-n)_k(ax)^k}{k!}, \quad (18)$$

where $(n)_k$ is the Pochhammer symbol, $(n)_k = n(n+1)\ldots(n+k-1)$. For the special case $n = -1/2$, which enters the expression equation (13) of the exponentiated radial

momentum operator, equation (18) becomes

$$\frac{1}{\sqrt{1-ax}} = \sum_{k=0}^{\infty} \frac{\left(\frac{1}{2}\right)_k}{k!}(ax)^k, \tag{19}$$

we obtain

$$\begin{aligned} \mathrm{e}^{-ax^2\partial_x}\frac{1}{\sqrt{1-ax}} &= \mathrm{e}^{-ax^2\partial_x}\sum_{k=0}^{\infty}\frac{\left(\frac{1}{2}\right)_k}{k!}(ax)^k \\ &= \sum_{k=0}^{\infty}\frac{\left(\frac{1}{2}\right)_k}{k!}a^k\mathrm{e}^{-ax^2\partial_x}x^k \\ &= \left(\sum_{k=0}^{\infty}\frac{\left(\frac{1}{2}\right)_k}{k!}(ax)^k(1+ax)^{-k}\right)\mathrm{e}^{-ax^2\partial_x} \\ &= \sqrt{1+ax}\,\mathrm{e}^{-ax^2\partial_x}. \end{aligned} \tag{20}$$

In this formula, we have succeeded in bringing the radial displacement operator $\mathrm{e}^{a\partial_r} = \mathrm{e}^{-ax^2\partial_x}$ to the right-most position of the expression.

Transforming back to the radial coordinate, we find

$$\mathrm{e}^{a\partial_r}\frac{1}{\sqrt{1-\frac{a}{r}}} = \sqrt{1+\frac{a}{r}}\,\mathrm{e}^{a\partial_r}, \tag{21}$$

which can be applied directly to any radial function $f(r)$. Finally, we see that the effect of applying the radial momentum in two dimensions onto a function is to shift its argument and to multiply it by a radial-dependent factor

$$\begin{aligned} \mathrm{e}^{\mathrm{i}ap_r/\hbar}f(r) &= \left(\sum_{k=0}^{\infty}\frac{\left(\frac{1}{2}\right)_k}{k!}\left(\frac{a}{r}\right)^k\left(1+\frac{a}{r}\right)^{-k}\right)\mathrm{e}^{a\partial_r}f(r) \\ &= \sqrt{1+\frac{a}{r}}\,f(r+a). \end{aligned} \tag{22}$$

The space modulation decreases with the distance to the origin. The combination of the shift and the modulation is to increase the value of the function at short distances and to decrease it at large distances for positive values of a. The reverse applies to negative values of a.

The result in equation (22) can be obtained more elegantly by writing the radial momentum p_r in product form with three noncommuting factors, $p_r = \frac{1}{\sqrt{r}}\partial_r\sqrt{r}$. Powers now take on a simple form since

$$p_r^2 = \frac{1}{\sqrt{r}}\partial_r\sqrt{r}\frac{1}{\sqrt{r}}\partial_r\sqrt{r} = \frac{1}{\sqrt{r}}(\partial_r)^2\sqrt{r}$$

and similarly

$$p_r^n = \frac{1}{\sqrt{r}}(\partial_r)^n\sqrt{r}$$

leading to

$$\begin{aligned} \mathrm{e}^{\mathrm{i}ap_r/\hbar}f(r) &= \sum_{n=1}^{\infty}\frac{\left(\frac{1}{\sqrt{r}}a\partial_r\sqrt{r}\right)^n}{n!}f(r) \\ &= \frac{\frac{1}{\sqrt{r}}\sum_{n=1}^{\infty}(a\partial_r)^n\sqrt{r}}{n!}f(r) \\ &= \frac{1}{\sqrt{r}}\mathrm{e}^{a\partial_r}\sqrt{r}\,f(r) \\ &= \frac{1}{\sqrt{r}}\sqrt{r+a}\,f(r+a) \\ &= \sqrt{1+\frac{a}{r}}\,f(r+a). \end{aligned} \tag{23}$$

The fortuitous cancelation of the opposite powers of r when taking simple powers of p_r in the second line of equation (23) does not occur in general. In the case where the radial operator multiplies the radial momentum operator, $rp_r = r\partial_r + 1$, the substitution $r = \frac{1}{x}$ leads to $rp_r = -x\partial_x + 1$ and we see that the action of the operator results in a dilatation rather than in a displacement [17, 18]

$$\mathrm{e}^{ax\partial_x}f(x) = f(\mathrm{e}^a x). \tag{24}$$

Now we proceed to generalize equation (22) to d dimensions. The radial momentum p_r in d-dimensional Euclidean space is given by

$$p_r^{(d)} = \frac{\hbar}{\mathrm{i}}\left(\partial_r + \frac{d-1}{2r}\right). \tag{25}$$

By using the same transformation $r = 1/x$, we obtain

$$\begin{aligned} &\exp\left(a\left(\partial_r + \frac{d-1}{2r}\right)\right) = \exp\left(-a\left(x^2\partial_x - \frac{(d-1)x}{2}\right)\right) \\ &= \mathrm{e}^{-ax^2\partial_x}\mathrm{e}^{[a(d-1)x]/2}\mathrm{e}^{(a^2/2)[x^2\partial_x,\frac{(d-1)x}{2}]}\ldots \\ &= \mathrm{e}^{-ax^2\partial_x}\mathrm{e}^{[a(d-1)x]/2}\mathrm{e}^{\sum_{n=1}^{\infty}\frac{(ax)^{n+1}}{2(n+1)}(d-1)} \\ &= \mathrm{e}^{-ax^2\partial_x}\mathrm{e}^{[a(d-1)x]/2}\mathrm{e}^{-[a(d-1)x]/2}\mathrm{e}^{-[\ln(1-ax)(d-1)]/2} \\ &= \mathrm{e}^{-ax^2\partial_x}(1-ax)^{(1-d)/2}. \end{aligned} \tag{26}$$

Applying equation (18) with $n = \frac{1-d}{2}$

$$(1-ax)^{(1-d)/2} = \sum_{k=0}^{\infty}\frac{\left(\frac{d-1}{2}\right)_k(ax)^k}{k!} \tag{27}$$

and as a result

$$\begin{aligned} &\exp\left(-a\left(x^2\partial_x - \frac{(d-1)x}{2}\right)\right) \\ &= \mathrm{e}^{-ax^2\partial_x}\sum_{k=0}^{\infty}\frac{\left(\frac{d-1}{2}\right)_k(ax)^k}{k!} = \sum_{k=0}^{\infty}\frac{\left(\frac{d-1}{2}\right)_k a^k}{k!}\mathrm{e}^{-ax^2\partial_x}x^k. \end{aligned} \tag{28}$$

Using equation (17)

$$\mathrm{e}^{-ax^2\partial_x}x^k = x^k(1+ax)^{-k}\mathrm{e}^{-ax^2\partial_x}, \tag{29}$$

we obtain

$$\begin{aligned} \sum_{k=0}^{\infty}\frac{\left(\frac{d-1}{2}\right)_k a^k}{k!}\mathrm{e}^{-ax^2\partial_x}x^k &= \sum_{k=0}^{\infty}\frac{\left(\frac{d-1}{2}\right)_k(ax)^k}{k!}(1+ax)^{-k}\mathrm{e}^{-ax^2\partial_x} \\ &= (1+ax)^{(d-1)/2}\mathrm{e}^{-ax^2\partial_x}. \end{aligned} \tag{30}$$

By transforming back to the radial variable $r = \frac{1}{x}$ we obtain

$$\exp\left(\frac{\mathrm{i}ap_r^{(d)}}{\hbar}\right) = \left(1+\frac{a}{r}\right)^{(d-1)/2}\mathrm{e}^{a\partial_r}. \tag{31}$$

Therefore the generalized formula in d dimensions is

$$\exp\left(\frac{\mathrm{i}ap_r^{(d)}}{\hbar}\right) f(r) = \left(1+\frac{a}{r}\right)^{(d-1)/2} \mathrm{e}^{a\partial_r} f(r) = \left(1+\frac{a}{r}\right)^{(d-1)/2} f(r+a). \quad (32)$$

This result can again be obtained using the product form of the radial momentum operator $p_r^{(d)} = r^{-(d-1)/2}\partial_r r^{(d-1)/2}$ with a similar cancelation of the radial operator factors in d dimension.

We note that we have developed the operator in a series. The question of convergence of the series appears once the operator is applied on a specific function. Suzuki [19] has studied the conditions under which the Zassenhaus formula converges in general. The series expansions for $1/2ln|1-ax|$ and $1/\sqrt{1-ax}$ are valid when $|ax|<1$. However, when $|ax|>1$ these expressions can still be written as convergent series in the variable $1/|ax|$ by first extracting a factor $\sqrt{|ax|}$. The derivation of equation (23) using the product form of the radial momentum and which proceeds without series development confirms the general validity of the result. Thus a justification of the Zassenhaus method involving infinite series is given *a posteriori* from the independent derivation using the product form of the radial momentum operator that does not involve infinite sums explicitly.

5. Displacement formula involving spin operators

We now focus on the translation resulting from combining momentum operators and the generators of SU(2), the Pauli spin operators σ_i, $i=1,2,3$. We consider the exponentiation of two noncommuting Pauli operators multiplying one momentum operator, as in the expression $\exp(\frac{\mathrm{i}p_x(a\sigma_x+b\sigma_y)}{\hbar}) f(x)$, where $f(x)$ is a spinor function.

We start with the case $a=b=1$ and generalize later. In the derivation we only use the commutation rule for Pauli operators

$$[\sigma_i,\sigma_j] = 2\epsilon_{ijk}\mathrm{i}\sigma_k \quad (33)$$

and Euler's formula

$$\mathrm{e}^{\mathrm{i}\gamma\sigma_j} = \cos\gamma + \mathrm{i}\sigma_j\sin\gamma. \quad (34)$$

All the results that follow can of course be checked explicitly in the standard representation of the Pauli matrices

$$\sigma_x = \begin{pmatrix}0&1\\1&0\end{pmatrix}, \quad \sigma_y = \begin{pmatrix}0&-\mathrm{i}\\\mathrm{i}&0\end{pmatrix}, \quad \sigma_z = \begin{pmatrix}1&0\\0&-1\end{pmatrix}.$$

Using the two properties equations (33) and (34), we can relate the exponential of two Pauli operators to exponentials of single Pauli operators by considering a spin rotation around the third (z) axis to align the spin with the x-axis

$$\exp\left(\frac{\mathrm{i}\phi(\cos\theta\sigma_x+\sin\theta\sigma_y)}{2}\right) = \exp\left(\frac{\mathrm{i}\theta\sigma_z}{2}\right)\exp\left(\frac{\mathrm{i}\phi\sigma_x}{2}\right)\exp\left(-\frac{\mathrm{i}\theta\sigma_z}{2}\right) \quad (35)$$

and select values of ϕ and θ to match the original expression $\exp(\frac{\mathrm{i}p_x(\sigma_x+\sigma_y)}{\hbar})$ namely $\phi = \frac{2\sqrt{2}p_x}{\hbar}$, $\theta = \frac{\pi}{4}$

$$\exp\left(\frac{\mathrm{i}p_x(\sigma_x+\sigma_y)}{\hbar}\right) = \exp\left(-\frac{\mathrm{i}\theta\sigma_z}{2}\right)\exp\left(\frac{\mathrm{i}\phi\sigma_x}{2}\right)\exp\left(\frac{\mathrm{i}\theta\sigma_z}{2}\right) = \exp\left(-\frac{\mathrm{i}\pi\sigma_z}{8}\right)\exp\left(\frac{\mathrm{i}\sqrt{2}p_x\sigma_x}{\hbar}\right)\exp\left(\frac{\mathrm{i}\pi\sigma_z}{8}\right). \quad (36)$$

Since

$$\exp(\gamma\sigma_x) = \cosh\gamma + \sigma_x\sinh\gamma \quad (37)$$

and the Pauli operators anticommute, $\sigma_x\sigma_z = -\sigma_z\sigma_x$, we find that

$$\exp(\gamma\sigma_x)\exp(\delta\sigma_z) = \mathrm{e}^{\delta\sigma_z}\left(\frac{\mathrm{e}^{\gamma}+\mathrm{e}^{-\gamma}}{2}\right) + \mathrm{e}^{-\delta\sigma_z}\sigma_x\left(\frac{\mathrm{e}^{\gamma}-\mathrm{e}^{-\gamma}}{2}\right). \quad (38)$$

Substituting equation (38) into (36) and distributing, we obtain

$$\begin{aligned}&\exp\left(-\frac{\mathrm{i}\pi\sigma_z}{8}\right)\exp\left(\frac{\mathrm{i}\sqrt{2}p_x\sigma_x}{\hbar}\right)\exp\left(\frac{\mathrm{i}\pi\sigma_z}{8}\right)\\ &= \exp\left(-\frac{\mathrm{i}\pi\sigma_z}{8}\right)\left(\exp\left(\frac{\mathrm{i}\pi\sigma_z}{8}\right)\left(\frac{\mathrm{e}^{\mathrm{i}\sqrt{2}p_x/\hbar}+\mathrm{e}^{-\mathrm{i}\sqrt{2}p_x/\hbar}}{2}\right)\right)\\ &\quad+\exp\left(-\frac{\mathrm{i}\pi\sigma_z}{8}\right)\left(\exp\left(-\frac{\mathrm{i}\pi\sigma_z}{8}\right)\right.\\ &\quad\left.\times\sigma_x\left(\frac{\mathrm{e}^{\mathrm{i}\sqrt{2}p_x/\hbar}-\mathrm{e}^{-\mathrm{i}\sqrt{2}p_x/\hbar}}{2}\right)\right)\\ &= \frac{\mathrm{e}^{\mathrm{i}\sqrt{2}p_x/\hbar}+\mathrm{e}^{-\mathrm{i}\sqrt{2}p_x/\hbar}}{2}+\exp\left(-\frac{\mathrm{i}\pi\sigma_z}{4}\right)\\ &\quad\times\sigma_x\left(\frac{\mathrm{e}^{\mathrm{i}\sqrt{2}p_x/\hbar}-\mathrm{e}^{-\mathrm{i}\sqrt{2}p_x/\hbar}}{2}\right). \end{aligned} \quad (39)$$

Now that the exponentials containing single momentum operators have been isolated to the right of the expression, we can apply the simple Cartesian displacement equation (2) to obtain

$$\begin{aligned}&\exp\left(\frac{\mathrm{i}p_x(\sigma_x+\sigma_y)}{\hbar}\right)f(x) = \left(\frac{\mathrm{e}^{\mathrm{i}\sqrt{2}p_x/\hbar}+\mathrm{e}^{-\mathrm{i}\sqrt{2}p_x/\hbar}}{2}\right)f(x)\\ &\quad+\exp\left(-\frac{\mathrm{i}\pi\sigma_z}{4}\right)\sigma_x\left(\frac{\mathrm{e}^{\mathrm{i}\sqrt{2}p_x/\hbar}-\mathrm{e}^{-\mathrm{i}\sqrt{2}p_x/\hbar}}{2}\right)f(x)\\ &= \frac{f(x+\sqrt{2})+f(x-\sqrt{2})}{2}+\exp\left(-\frac{\mathrm{i}\pi\sigma_z}{4}\right)\\ &\quad\times\sigma_x\frac{f(x+\sqrt{2})-f(x-\sqrt{2})}{2}. \end{aligned} \quad (40)$$

In order to consider the case $a = b \neq 1$, we select the value $\phi = \frac{a2\sqrt{2}p_x}{\hbar}$. It is then straightforward to show that

$$\exp\left(\frac{\mathrm{i}ap_x(\sigma_x+\sigma_y)}{\hbar}\right) f(x) = \frac{f(x+a\sqrt{2})+f(x-a\sqrt{2})}{2} + \exp\left(-\frac{\mathrm{i}\pi\sigma_z}{4}\right)\sigma_x\frac{f(x+a\sqrt{2})-f(x-a\sqrt{2})}{2}.$$

Finally, we extend the formula to the case of unequal scalar coefficients $a \neq b$ by selecting $\phi = \frac{2\sqrt{a^2+b^2}p_x}{\hbar}$ and $\theta = \arctan(\frac{b}{a})$ to obtain

$$\begin{aligned}
&\exp\left(\frac{\mathrm{i}p_x(a\sigma_x+b\sigma_y)}{\hbar}\right)\\
&= \exp\left(\frac{\mathrm{i}\sqrt{a^2+b^2}p_x}{\hbar}\left(\frac{a}{\sqrt{a^2+b^2}}\sigma_x+\frac{b}{\sqrt{a^2+b^2}}\sigma_y\right)\right)\\
&= \exp\left(-\frac{\mathrm{i}\theta\sigma_z}{2}\right)\exp\left(\frac{\mathrm{i}\phi\sigma_x}{2}\right)\exp\left(\frac{\mathrm{i}\theta\sigma_z}{2}\right)\\
&= \exp\left(-\frac{\mathrm{i}\sigma_z\arctan\left(\frac{b}{a}\right)}{2}\right)\exp\left(\frac{\mathrm{i}\sqrt{a^2+b^2}p_x\sigma_x}{\hbar}\right)\\
&\quad\times\exp\left(\frac{\mathrm{i}\sigma_z\arctan(\frac{b}{a})}{2}\right)\\
&= \frac{\mathrm{e}^{(\mathrm{i}\sqrt{a^2+b^2}p_x)/\hbar}+\mathrm{e}^{-(\mathrm{i}\sqrt{a^2+b^2}p_x)/\hbar}}{2}\\
&\quad+\exp\left(-\mathrm{i}\sigma_z\arctan\left(\frac{b}{a}\right)\right)\\
&\quad\times\sigma_x\left(\frac{\mathrm{e}^{(\mathrm{i}\sqrt{a^2+b^2}p_x)/\hbar}-\mathrm{e}^{-(\mathrm{i}\sqrt{a^2+b^2}p_x)/\hbar}}{2}\right).
\end{aligned}\tag{41}$$

By applying this operator to a function $f(x)$, we obtain the following staggered displacement

$$\begin{aligned}
&\exp\left(\frac{\mathrm{i}p_x(a\sigma_x+b\sigma_y)}{\hbar}\right) f(x)\\
&= \frac{\mathrm{e}^{(\mathrm{i}\sqrt{a^2+b^2}p_x)/\hbar}+\mathrm{e}^{-(\mathrm{i}\sqrt{a^2+b^2}p_x)/\hbar}}{2} f(x)\\
&\quad+\exp\left(-\mathrm{i}\sigma_z\arctan\left(\frac{b}{a}\right)\right)\\
&\quad\times\sigma_x\left(\frac{\mathrm{e}^{(\mathrm{i}\sqrt{a^2+b^2}p_x)/\hbar}-\mathrm{e}^{-(\mathrm{i}\sqrt{a^2+b^2}p_x)/\hbar}}{2}\right) f(x)\\
&= \frac{f(x+\sqrt{a^2+b^2})+f(x-\sqrt{a^2+b^2})}{2}\\
&\quad+\exp\left(-\mathrm{i}\sigma_z\arctan\left(\frac{b}{a}\right)\right)\\
&\quad\times\sigma_x\frac{f(x+\sqrt{a^2+b^2})-f(x-\sqrt{a^2+b^2})}{2}.
\end{aligned}\tag{42}$$

We see that the coupling of noncommutative Pauli operators to a momentum operator results in two displacements given by $\pm\sqrt{a^2+b^2}$ corresponding to the eigenvalues of the Pauli operator $a\sigma_x + b\sigma_y$. The displaced functions are weighted by spin-dependent factors related to the original spin operator. In effect the eigenspinors of $a\sigma_x + b\sigma_y$ become separated in space by an amount $2\sqrt{(a^2+b^2)}$ as well as weighted by a factor proportional to their overlap with the original spinor.

This result can be extended to the case where a single momentum operator multiplies three spin operators. This follows from the fact that three Pauli operators can be reduced to one by the use of two successive rotations. Extending the formula to two or more momentum operators is not straightforward, however.

6. Discussion

Our main result, the effect of noncommutativity on displacement, is given in equations (10), (32) and (42). The origin of the noncommutativity is different in the three cases and so is the way to overcome the difficulty in applying the translational formula.

In all three cases, we obtain a displacement formula where displacement in the argument of the function is combined with the multiplication by a factor. In section 3 (equation (10)), this factor is a local phase proportional to the commutator of the noncommuting momenta, in section 4 (equation (32)), this factor varies and decreases with r, and in section 5 (equation (42)) two shifts take place in opposite directions and are modulated by spin-dependent constants.

The results obtained in this paper use several existing formulae for changing the order of exponentials of noncommuting operators. In addition to the Baker–Campbell–Hausdorff formula, we use the Zassenhaus formula. In section 3, this formula simplifies to a closed form due to vanishing commutators. In section 4, the Zassenhaus formula is combined with the substitution $r = \frac{1}{x}$ and can be summed exactly because of the resulting limited noncommutativity. In section 5, a spin rotation is used to reduce the noncommutativity in the following way: a sum of noncommuting operators in the exponent is replaced by a simple product of exponentials that are commuted one by one. In all cases, the displacement formula is modified by the noncommutativity. The fact that the noncommutativity is limited allows a displacement formula to be derived analytically. The modified displacement formulae reveal an underlying symmetry beyond simple translational symmetry for quantum systems to which they are applicable, namely noncommutative ones.

The noncommutativity that we have considered in this paper is between different operator terms in a *sum* in an exponent. This is precisely the way that noncommutativity enters in the study of the evolution of quantum systems mentioned in the introduction. How the noncommutativity between *factors* in an exponential $\mathrm{e}^{AB} \neq \mathrm{e}^{BA}$ might affect displacement formulae is a separate question that we did not address in this note except in the special case of the radial momentum operator where it provides an alternative derivation for a formula involving a sum of noncommutative terms.

Acknowledgments

We thank Eric Hirschmann for pointing out the use of the product form of the radial momentum operator and

members of the Theoretical Physics Group at BYU for helpful comments on the manuscript.

References

[1] Merzbacher E 1998 *Quantum Mechanics* 3rd edn (New York: Wiley)
[2] Louisell W H 1973 *Quantum Statistical Properties of Radiation* (New York: Wiley)
[3] Wilcox R M 1967 *J. Math. Phys.* **8** 962
[4] Gilmore R 1974 *J. Math. Phys.* **15** 2090
[5] Douglas M R and Nekrasov N A 2001 *Rev. Mod. Phys.* **73** 977
[6] Ho P M and Kao H C 2002 *Phys. Rev. Lett.* **88** 151602
[7] Zhang J-Z, Gao K-L and Ning C-G 2008 *Phys. Rev.* D **78** 105021
[8] Winkler R 2003 *Spin–Orbit Coupling Effects in Two-Dimensional Electron and Hole Systems* (Berlin: Springer)
[9] Bernevig B A, Orenstein J and Zhang S C 2006 *Phys. Rev. Lett.* **97** 236601
[10] Vaishnav J Y and Clark Charles W 2008 *Phys. Rev. Lett.* **100** 153002
[11] Yin Q-J and Zhang J-Z 2005 *Phys. Lett.* B **613** 91
[12] Zassenhaus H 1939 *Abh. Math. Sem. Univ. Hamburg* **13** IV 1
[13] Witschel W 1975 *J. Phys. A: Math. Gen.* **8** 143
[14] Scholz D and Weyrauch M 2006 *J. Math. Phys.* **47** 033505
[15] Volkin H C 1968 *NASA Technical Note* TN D4857
[16] Paz G 2002 *J. Phys. A: Math. Gen.* **35** 3727
[17] Wang Q 1987 *J. Phys. A: Math. Gen.* **20** 5041
[18] Suzuki M 1983 *Physica* A **117** 103
[19] Suzuki M 1977 *Comm. Math. Phys.* **57** 193

Appendix B

Propagator in Spintronics

This paper is published in the Journal of Utah Academy of Science, Arts, and Letters (2007).

Propagators in Spintronics

Bailey C. Hsu and Jean-Francois S. Van Huele
Department of Physics and Astronomy, Brigham Young University

1. Introduction

Spintronics, spin-electronics, or magneto-electronics is currently the focus of an intense research effort [1]. In spintronics, we manipulate the spin degree of freedom of an electron as opposed to, or in addition to, manipulating the charge as we do in conventional electronics. Spin is a quantum two-level system; states are quantum superpositions of "up" and "down", the two basis states in which the physical system can be found. Spin reflects the quantum nature of an electron so that the remarkable property of quantum parallelism, which is so useful in quantum computation, for instance, can be achieved with spin states. Although spintronics is not expected to replace traditional electronics, it will likely play a complementary role to electronics, in particular in the domain of quantum information. Research in spintronics has been proceeding at a rapid pace, both experimentally and theoretically. New effects have been predicted, and then detected in the lab. As new experimental data become available, new interpretations are required. Although the study of the motion of charges can serve as a guide, the methods need to be adapted to the specifics of the spin degree of freedom.

In this paper we introduce and illustrate the use of propagators in spintronics. In section 2 we review some properties of the physical variable spin. In section 3 we mention how electronics needs to be extended by including spin explicitly. In section 4 we introduce two classes of spintronics effects that are particularly promising, spin-orbit couplings, and spin Hall effects. In section 5 we introduce propagators and mention some methods for constructing them. In section 6 we combine what we have learned about propagators and about spin to introduce the spin propagator. We choose to apply the propagator in two particular cases: the Stern-Gerlach system and the Rashba system. We conclude by displaying the result: the evolution of the spin components in space. Since our main goal is to motivate and then illustrate the use of spin propagators, we leave out most of the derivations and keep the technicalities to a minimum. The formulas displayed are there for illustrative purpose only and can be skipped without losing the thread of our argument. Additional information on spintronics and on propagator methods can be found in the references.

2. Spin

Spin $\boldsymbol{S}$ is an angular momentum with the physical dimension of action, i.e., energy-time. Like charge, spin is an intrinsic property of an electron. Its magnitude is fixed once and for all, but its orientation is not. This is unlike the orbital angular momentum $\boldsymbol{L}$, whose classical counterpart is familiar from merry-go-round physics, and which depends on the position $\mathbf{r}$ and the linear momentum $\boldsymbol{P}$ through the relation $\boldsymbol{L} = \mathbf{r} \times \boldsymbol{P}$ and can therefore

take on many values depending on the spatial distribution of the electron.

The electron spin is expressed as

$$\vec{S} = \frac{\hbar}{2}\vec{\sigma},$$

where $\hbar$ (h-bar), Planck's fundamental quantum of action, provides the dimension, the factor ½ determines the magnitude of the spin and ■, the Pauli spin operator, determines its properties. The spin freedom reduces to the duplicity of "up" and "down", although in typical quantum fashion, it is the observer, namely the spintronics physicist in her lab, who determines what exactly is meant by "up" or "down" in any specific experiment. Where does spin show up? The spin affects atomic spectral lines and the collective behavior of electrons, as dictated by the Pauli exclusion principle. Spin is especially tangible in a magnetic environment, because every spin has a magnetic moment associated with it and the magnetic moment is not indifferent to magnetic fields. A conspicuous illustration of the spin degree of freedom is the Stern-Gerlach Effect (SGE).

In the SGE a beam of silver atoms passing between the poles of an inhomogeneous magnetic field is split in two parts. One goes up and one goes down according to the up-or-down state of the spin of the lone 47th electron in the silver atom [2]. The 46 other electrons in the atoms' filled inner shells do not contribute since their spins add up to zero. So whereas spin itself is rather elusive (and should not be associated with a classical rigid self-rotation), its effect can be dramatic. Spin does not typically appear explicitly in traditional electronic devices. The lack of magnetic fields means that the device is insensitive to the spin state of the individual electrons. In what follows we discuss how we can explicitly manipulate the spin and help unlock the great potential of spintronics.

3. From Electronics to Spintronics

Our daily lives have been dramatically affected by the many possible applications of electronics. Simply put, in electronic devices we create a network of electric currents so that we may perform Boolean logic by controlling the current flow. In order to achieve faster computation, the size of electronic building blocks is reduced. Moore's law [3] indicates the rate at which this miniaturization is proceeding. In semiconductors, we control the conductivity of a well-defined area by doping the sample and by controlling the electric voltage, thus building transistors. We then assemble them into complex circuits, like microprocessors. By varying the doping, we can also control the optical properties of the device and make a light-emitting diode (LED). Electronics devices are both cheaper and less bulky than prior technologies but the trade-offs of minimization have to be negotiated constantly. As the size of a single transistor keeps shrinking, we ineluctably reach the quantum regime. Consequently, quantum phenomena, spin among them, surface and need to be addressed. Can we turn spin into a technological asset? Spintronics aims at recreating in the world of spin some of the building blocks and

associated logical functions from charge electronics. For example, in a Field Effect Transistor (FET), we apply gate voltages to control the charge transport and tie it to the on-and-off states of a logic device. The concept of a Spin Field Effect Transistor (SPINFET) was proposed in 1990 [4]. However, separating spin states remains a challenge for theorists and for experimentalists. Electrical currents are created by separating positive and negative charges. By analogy we want to create "spin currents" for logic devices. To illustrate the fact that the transition from electronics to spintronics is not straightforward, we point out that unlike charge, spin by itself is not conserved. This creates an ambiguity in the definition of the spin current. The SGE separates neutral atomic beams in vacuum by using an inhomogeneous magnetic field, and spin-up and spin-down atoms each go their own way, thus effectively creating spin currents. Until now the SGE has never been achieved with electrons however [5]. Due to the bulkiness of magnets, researchers have looked into controlling spin with electric fields. This can be achieved by using the mechanism of Spin-Orbit Coupling (SOC): in bulk materials asymmetries can lead to a coupling between the spin and the electric fields.

4. Spintronics Effects

4.1. Spin-Orbit Coupling

In atomic physics, an orbiting electron experiences the electric field of the nucleus. As Einstein explained, considered from a relativistic point of view, the electron experiences a magnetic field in its rest frame. The magnetic moment of the spin of the electron can now interact with this magnetic field. This is spin-orbit coupling (SOC). In certain materials the Rashba [6, 7] and Dresselhaus [8] effects originate respectively in Structure Inversion Asymmetry (SIA) and Bulk Inversion Asymmetry (BIA). SIA arises from the asymmetric doping of the quantum well which creates an electric field, while BIA stems from the asymmetry of the zinc-blende crystal lattice structure. As a result of these two SOC-type effects, we can control the spin without using magnetic fields. The Rashba and Dresselhaus Hamiltonians, which describe the energy and evolution of electrons of mass m in two-dimensional materials, involve both linear momenta $\boldsymbol{P}$ and spin variables,

$$H_{Rashba} = \frac{P_x^2 + P_y^2}{2m} + \frac{\alpha}{\hbar}(P_y\sigma_y - P_x\sigma_x)$$

$$H_{Dresselhaus} = \frac{P_x^2 + P_y^2}{2m} + \frac{\beta}{\hbar}(P_x\sigma_x - P_y\sigma_y),$$

where $\boldsymbol{x}$ and $\boldsymbol{y}$ refer to the two spatial dimensions and the parameters $\boldsymbol{\alpha}$ and $\boldsymbol{\beta}$ indicate the Rashba and Dresselhaus coupling strengths. We can control the Rashba coupling strength by changing the gate voltage. To maximize SOC we have to increase $\boldsymbol{\alpha}$. However the Rashba effect also tends to destroy the coherence of the spin states [9]. Physicists need to carefully balance the strength of the spin separation with the need to maintain quantum coherence. Quantum coherence, the ability of microscopic systems to remain in nonclassical superposition states, is a critical ingredient of quantum technology.

4.2. Spin Hall Effect

A second exciting area of spintronics centers on the Spin Hall Effect (SHE). In 1879, long before the advent of quantum mechanics, Edwin Hall, then a doctoral student, discovered what came to be known as the Hall effect [10].

Fig. 1 The Hall effect, with charge separation and accumulation

In the original Hall effect, opposite charges accumulate on opposite edges of a conductor (top and bottom in Fig. 1) because of the pull **F** of a magnetic field **B** (pointing into the page in Fig.1) which acts on the particles of charge q moving at velocity **v** (to the right in Fig.1) as described by the microscopic Lorentz force **F** = q **(v x B)**. The potential resulting from this charge separation leads to the Hall current. Fifty years later and now retired, Edwin Hall was again studying electrons in metals [11-13], using quantum mechanics and the statistical properties that spin forces upon them. Could he have predicted that several decades later, spintronics would open a new chapter in Hall effect physics? In 2003, Murakami et al. [14] and Sinova et al. [15] predicted the existence of an intrinsic Spin Hall Effect (SHE) as a result of Rashba SOC. Earlier Hirsch [16] had predicted an extrinsic SHE effect resulting from spin-dependent scattering due to defects in the sample. In 2004, Kato et al. [17] observed the SHE in semiconductors with spin accumulation on opposite edges of the semiconductor as illustrated in Fig.2.

Fig. 2 The spin Hall effect with spin separation and accumulation

And there is more. The Quantum Hall Effect (QHE), a quantized version of the Hall Effect, was unexpectedly discovered in 1980 [19]. A Quantized Spin Hall Effect (QSHE) was predicted in 2005 [22] and discovered just recently [23]. Clearly there are several mechanisms that can generate spin currents. In what follows we address the description of spin dynamics in space and time using the technique of quantum propagators.

5. Propagators

Propagator theory is a powerful technique in quantum mechanics and quantum field theory used to visualize the dynamics of waves and particles. A quantum propagator $K(x, t / x_0, t_0)$ describes the conditional probability amplitude of the transition of the system, from location x_0 at time t_0 to location x at time t, so that

$$\psi(x,t) = \int K(x,t|x_0,t_0)\psi(x_0,t_0)dx_0,$$

where the wavefunction $\psi(x, t)$ is the probability amplitude for finding the system at location x at time t. It can be shown that the propagator must satisfy the Schrödinger equation of quantum mechanics. Several methods exist to construct quantum propagators [20] and we mention two of them. An operator method, originally due to Schwinger consists in finding the time-dependent position and momentum operators in the Heisenberg representation of quantum mechanics [18]. We recall that position and momentum operators are incompatible in quantum mechanics. By eliminating the momentum operators from the solution, we retain only position information as needed for constructing the propagator $\mathbf{K}(x ; t / x_0 ; t_0)$. As an example the purely kinetic energy Hamiltonian of a free particle

$$\hat{H} = \frac{\hat{P}_x^2}{2m}$$

becomes exclusively position-dependent once the solution for the momentum operator

$$\hat{P}_x = \frac{m(\hat{x(t)} - \hat{x(0)})}{t}$$

has been substituted back in the free-particle Hamiltonian expression

$$\hat{H} = \frac{1}{2m}\left(\frac{m(\hat{x(t)} - \hat{x(0)})}{t}\right)^2.$$

One can now apply this evolution generating operator in the coordinate bases at the initial and final times to obtain the propagator directly. In the process the ordering of the incompatible position operators at different times needs to be treated with care. In a second method, the classical action method [20] the propagator is obtained as a Feynman path-integral formula which ads all the possible paths coherently

$$K(x,t|x_0,t_0) = C\int exp(\frac{i}{\hbar}S[x(t)])D[x(t)]$$

and reduces by approximation to

$$K(x,t|x_0,t_0) = C(t-t_0)exp(\frac{i}{\hbar}S[x(t)])$$

where $S\,[\,x(t)\,]$ is the classical action, which contains the dynamics of the classical system, and the normalization C takes care of the quantum fluctuations. The constant C can be found by imposing physical requirements such as considering what happens in no time at all $(t = t_0)$ or when the system propagates from x_0 to x and then back to x_0. These are just two of the many methods that have been developed to construct propagators. So far however, the propagator does not contain any spin information and, as such, it is not very useful for spintronics applications. A remedy is proposed in the next section.

6. Spin Propagators

Spin propagators, i.e., propagators which include the spin degree of freedom, are needed for spin-dependent transport. How can a spin propagator describe the separation of spin states as it occurs in the SGE for example? To our knowledge no correct analytic expression for SGE propagators involving the spin variable can be found in the literature. We have derived the expression for several propagators for specific magnetic and spin-orbit configurations. In this contribution we give a flavor of our approach and we illustrate some of the results. Details will be presented in a comprehensive paper elsewhere [24]. The quantum incompatibility (or noncommutativity) between different Pauli matrices complicates the calculations further. This intricacy can be illustrated as follows: quantum dynamics implies an incompatibility between position and momentum (as illustrated by the Heisenberg uncertainty relation) or, equivalently, an incompatibility between position operators at different times as we discovered in the previous section. The spin description carries its own incompatibility between the different spin components (or noncommutativity of Pauli matrices). Spin and position (or momentum) are compatible, but their simultaneous appearance in the Hamiltonian (r and for SGE, P and for SOC) means that the position-momentum noncommutativity and the spin-components noncommutativity get entangled. Our challenge is to disentangle them in

order to be able to use Schwinger's method and find the propagator. Once this is done we can apply the propagator on an initial quantum state, a wave packet, and we can then follow the evolution of the quantum state. We find that the beam separates in the two spin components as observed in SGE. This is illustrated in Fig.3 where a vertical separation of the two components corresponding to opposite spins develops in the ***xz***-plane (i.e., perpendicular to the beam) as time progresses (from top left to bottom right in the figure).

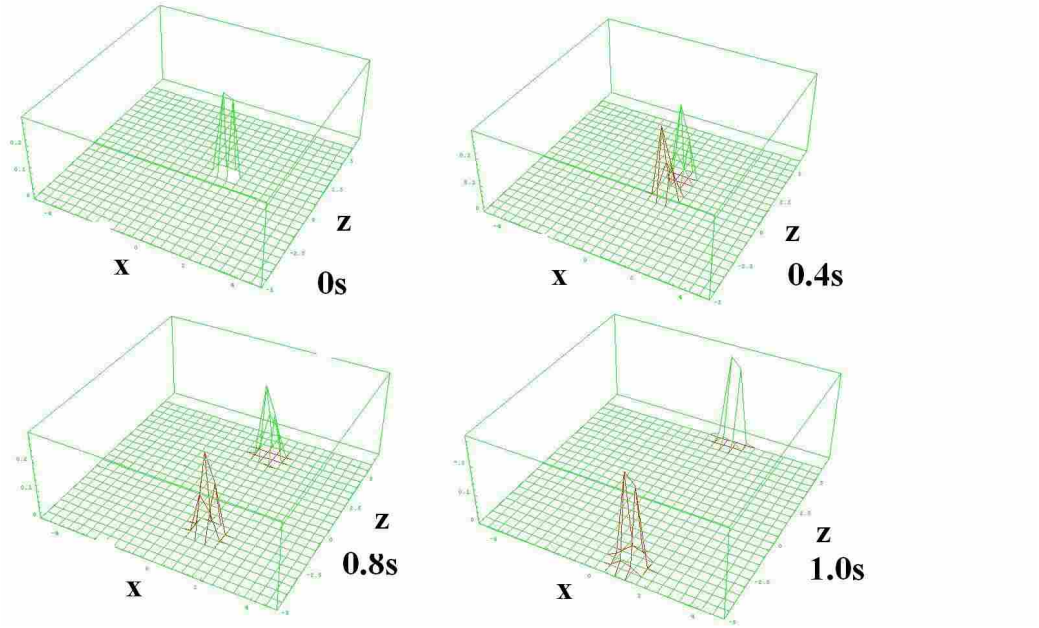

Fig.3 Spin component separation obtained using a Stern-Gerlach propagator

In spin-orbit coupled systems, i.e., Rashba and Dresselhaus materials, the momenta P_x and P_y become coupled through the spins and this leads to higher order equations. Whereas the lowest order approximation is too crude to give spin separation, higher order terms exhibit spin separation.

Finally we have verified that a semiclassical "effective" potential method [21] leads to an interesting result for the Rashba and Dresselhaus systems: a repeated application of the Heisenberg prescription for time-dependence of the position gives the acceleration of the particle, therefore the force, and by space integration also the potential acting on the particle. For time-independent (or frozen) spin operators this potential yields precisely a spin-orbit coupling term

$$H_{eff} = \frac{P_x^2 + P_y^2}{2m} + C\vec{\sigma} \cdot \vec{L}$$

where C depends on the coupling strength α. Starting with a Rashba system which mixes $\boldsymbol{P}$ and [redacted], the effective potential method produces a familiar spin-orbit term [redacted]$\cdot\boldsymbol{L}$ for which we can construct the propagator in the way described above by expressing the

momenta in terms of the positions and by freezing the spin degrees of freedom. Applying the propagator matrix to a Gaussian wave packet with spin-up and spin-down components we obtain indeed spin separation. The result is illustrated in Fig. 4, where both the probability density plot of the spin-up (green) and spin-down (red) components of the wave packet are indicated at successive times from top to bottom. The spin-up and spin-down waves are seen to have opposite chirality, as one moves clockwise and the other one counterclockwise in the **xy**-plane. It is interesting to note that a recent discussion on the QSHE [22] that traces the effect to the strain of the material, uses a Hamiltonian of the same form as in Eq.(7), and shows opposite chirality for spin-up and spin-down in agreement with our result.

7. Summary

SHE and SOC effects are exciting developments in the new field of spintronics. Traditionally spin has been affected by magnetic fields through their interaction with its associated magnetic moment as in the SGE, but now SOC opens the way for spin control with electrical fields in some bulk materials. A consistent theoretical description of spin currents and spin evolution will greatly help interpret the physical phenomena taking place in all these systems. Techniques from mathematical physics originally designed to construct spinless propagators can be extended to include the spin degree of freedom. These spin propagators can then be used to follow the time evolution of wave packets and follow spin distributions in coordinate spaces. Both vacuum SGE and bulk Rashba and Dresselhaus SOC can be described with these spin propagators. In this contribution we have given two brief illustrations of the construction and the power of spin propagators: one led to spin separation in a SGE situation and one showed the chirality separation in a Rashba-type SOC interaction with the help of an effective potential. In the general case, however, the construction of these propagators can be quite challenging as the complexity increases with the number of incompatible degrees of freedom and more creative solutions will have to be developed. Spin proves once again to be a useful, if tricky, quantum property.

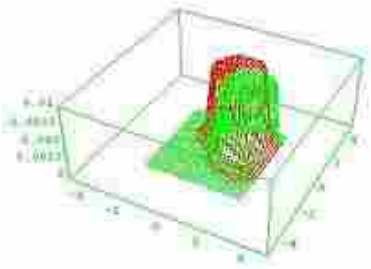

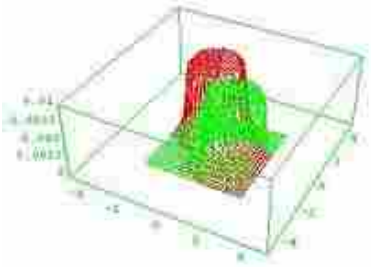

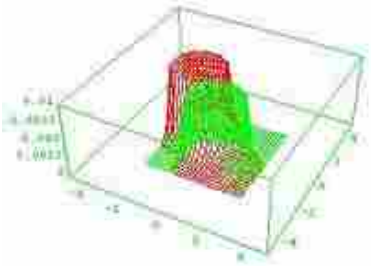

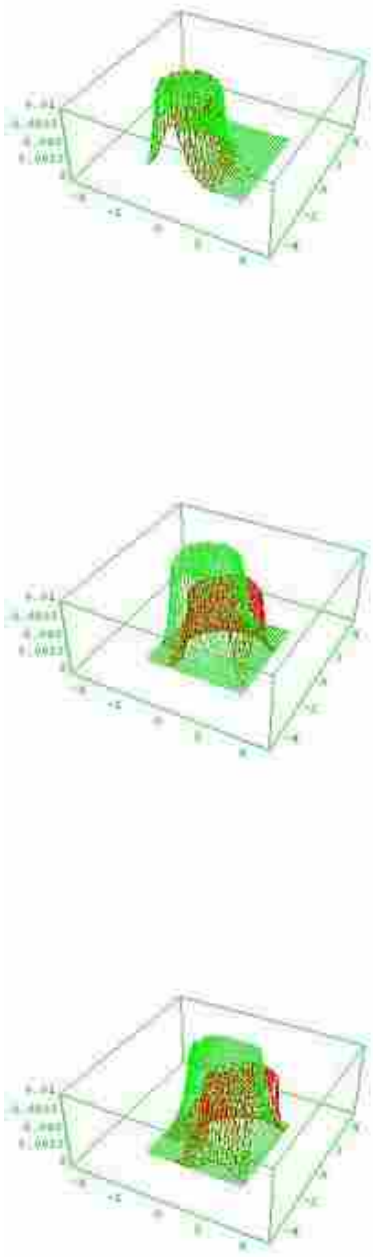

Fig. 4 Six snapshots of the counter rotating spin component wave packets for a Rashba interaction

References

[1] D. D. Awschalom and N. Samarth (editors), *Semiconductor, Spintronics, and Quantum Computation,* (Springer-Verlag, Berlin, 2001).
[2] J-F. S. Van Huele and J. R. Stenson, "*Stern-Gerlach Experiments: Past, Present, and Future*", Journal of the Utah Academy of Sciences, Arts & Letters, 81, 206-212 (2004).
[3] G. E. Moore, "*Cramming more components onto integrated circuits*", Electronics, 38, 8, 114-117 April 19 (1965).
[4] S. Datta and B. Das, "*Electronic analog of the electro-optic modulator*", Appl. Phys. Lett. 56, 665 (1990).
[5] H. Batelaan, T. J. Gay, and J. J. Schwendiman, "*Stern-Gerlach Effect for Electron Beams*", Phys. Rev. Lett. 79, 4517-4521 (1997).
[6] Yu. A. Bychkov and E. I. Rashba, "*Oscillatory effects and the magnetic susceptibility of carriers in inversion layers*", J. Phys. C 17, 6039-6045 (1984).
[7] E. I. Rashba, Fiz. Tverd. Tela (Leningrad) 2, 1224 (1960) (Sov. Phys. Solid State 2, 1109 (1960)).
[8] G. Dresselhaus, "*Spin-Orbit Coupling Effects in Zinc Blende Structures*", Phys. Rev. 100, 580-586 (1955).
[9] B.A. Bernevig, J. Orenstein, and S.-C. Zhang, "*An Exact SU(2) Symmetry and Persistent Helix in a Spin-Orbit Coupled System*", Phys. Rev. Lett. (2006) and references herein.
[10] E.H. Hall, "*On a New Action of the Magnet on Electric Currents*", Am. J. Mathematics. 2, 287-292 (1879).
[11] E.H. Hall, "*The Fermi Statistical Postulate; Examination of the Evidence in Its Favor* ", Proc. Natl. Acad. Sci. 14, 365-370 (1928).
[12] E.H. Hall, "*Sommerfeld's Electron-Theory of Metals* ", Proc. Natl. Acad. Sci. 14, 370-377 (1928).
[13] E.H. Hall, "*On electrons that are "pulled out" from metals*", Proc.Natl. Acad. Sci. 15, 241-251 (1929).
[14] S. Murakami, N. Nagaosa and S.-C. Zhang, "*Dissipationless Quantum Spin Current at Room Temperature*", Science 301, 1348 (2003).
[15] J. Sinova, D. Culcer, Q. Niu, N.A. Sinitsyn, T. Jungwirth, and A.H. MacDonald, "*Universal Intrinsic Spin Hall Effect*", Phys. Rev. Lett. 93, 46602 (2004).
[16] J. E. Hirsch, "*Spin Hall Effect*", Phys. Rev. Lett. 83, 1834-1837 (1999).
[17] Y. K. Kato, R. C. Myers, A. C. Gossard, D. D. Awschalom, "*Observation of the Spin Hall Effect in Semiconductors*", Science 10 Dec. 2004: 306 5703, 1910-1913 (2004).
[18] F. A. Barone, H. Boschi-Filho, C. Farina, "*Three Methods for Calculating the Feynman Propagators,*" Am. J. Phys. 71, 483-491 (2003).
[19] K. von Klitzing, G. Dorda, and M. Pepper, "*New Method for High-Accuracy Determination of the Fine-Structure Constant Based on Quantized Hall Resistance*", Phys. Rev. Lett. 45, 494-497 (1980).
[20] Eugen Merzbacher, *Quantum Mechanics*, 3rd ed. (Wiley, New York, 1998).
[21] K. Suzuki and S. Kurihara, "Spin *accumulation caused by confining potential*", arXiv:cond-mat/0611013 v2 (2006).
[22] B.A. Bernevig and Shou-Cheng Zhang, "*Quantum Spin Hall Effect*", Phys. Rev. Lett. 96, 106802 (2006).

[23] M. König, S. Wiedmann, C. Brüne, A. Roth, H. Buhmann, L.W. Molenkamp, X.-L. Qi, S.-C. Zhang, "*Quantum Spin Hall Insulator State in HgTe Quantum Wells"*, Science 318, 5851, 766 – 770 (2007).
[24] B. C. Hsu and J-F.S. Van Huele (in preparation).

Appendix C

Analytic Propagators for Spin-Orbit Interactions

This paper is published in Journal of Physics A: Theory and Mathematical **42** 475304 (2009).

IOP PUBLISHING JOURNAL OF PHYSICS A: MATHEMATICAL AND THEORETICAL

J. Phys. A: Math. Theor. **42** (2009) 475304 (17pp) doi:10.1088/1751-8113/42/47/475304

Analytic propagators for spin–orbit interactions

Bailey C Hsu and Jean-François S Van Huele

Department of Physics and Astronomy, Brigham Young University, Provo, UT 84602, USA

E-mail: bailey.c.hsu@gmail.com and vanhuele@byu.edu

Received 22 June 2009, in final form 28 September 2009
Published 6 November 2009
Online at stacks.iop.org/JPhysA/42/475304

Abstract

We derive analytic expressions for propagators in spin–orbit coupled systems. In addition to their kinetic energy, these systems exhibit a potential energy that mixes position, momentum and spin operators. We consider Hamiltonians with limited noncommutativities: the confined spin–orbit coupled Hamiltonian $H^c_{\mathrm{SO}} = \frac{\mathbf{p}^2}{2m} + \gamma\boldsymbol{\sigma}\cdot\mathbf{L} + \frac{1}{2}m\eta^2(x^2+y^2)$, the confined Equal–Strength–Rashba–Dresselhaus Hamiltonian $H^c_{\mathrm{ESRD}} = \frac{\mathbf{p}^2}{2m} + \frac{\alpha}{\hbar}(p_x+p_y)(\sigma_x-\sigma_y) + \frac{1}{2}m\eta^2(x^2+y^2)$ and the confined Opposite–Strength–Rashba–Dresselhaus Hamiltonian $H^c_{\mathrm{OSRD}} = \frac{\mathbf{p}^2}{2m} + \frac{\alpha}{\hbar}(p_x-p_y)(\sigma_x+\sigma_y) + \frac{1}{2}m\eta^2(x^2+y^2)$. We use both a classical action method and an algebraic method in our derivations. We mention specific applications for these propagators and illustrate their significance with examples of wavepacket evolution.

PACS numbers: 03.65.Fd, 31.15.aj, 72.25.Dc

(Some figures in this article are in colour only in the electronic version)

1. Introduction

The spin–orbit coupling (SOC) occurs in many areas of physics. Discovered in the fine structure of atomic spectra, later introduced to explain the nuclear structure, it is now also of great interest in condensed matter systems, such as graphene [1] and semiconducting materials with promising spintronics applications [2, 3]. It is also found in the physics of optical lattices mimicking condensed matter systems [4]. The SOC is characterized by interaction terms that contain position **r**, momentum **p** and spin operators **S**. In nuclear and atomic systems, the spin–orbit interaction is given in the form $H_{\mathrm{SO}} = \gamma(r)\mathbf{S}\cdot\mathbf{L}$, where $\mathbf{L} = \mathbf{r}\times\mathbf{p}$. The coupling strength γ is determined in atomic systems by the Coulomb potential $V(r)$ such that

$$\gamma(r) \sim \frac{1}{r}\frac{\mathrm{d}V(r)}{\mathrm{d}r}. \tag{1}$$

H_{SO} can be derived in the nonrelativistic approximation of relativistic electron–atom interactions. In spintronics, the spin–orbit coupling is manifest as Rashba and Dresselhaus

interactions [5]. The Rashba interaction is the signature of structure inversion asymmetry (SIA) present in essentially two-dimensional materials [6, 7]. Its Hamiltonian

$$H_R = \frac{\alpha}{\hbar}(p_y\sigma_x - p_x\sigma_y) \tag{2}$$

combines components of the spin operator $\mathbf{S}$ (related to the Pauli matrices by $\mathbf{S} = \frac{\hbar}{2}\boldsymbol{\sigma}$) and the momentum operator $\mathbf{p}$. Its overall strength, the Rashba coupling constant α, can be controlled experimentally. The Dresselhaus interaction, with coupling strength β, originates in bulk inversion asymmetry (BIA) which is inherent to zinc-blende structures [8]

$$H_D = \frac{\beta}{\hbar}(p_x\sigma_x - p_y\sigma_y). \tag{3}$$

Interesting features such as spin accumulation [9], spin-Hall effect [10], quantum spin-Hall effect [11], *Zitterbewegung* motion of the wavepacket [12] and persistent spin helix [13] have been predicted and observed for spin–orbit coupled systems. It is our goal here to derive SOC propagators in order to get a better handle on the evolution of the corresponding physical systems. To our knowledge, the propagator method has not been applied explicitly to these specific SOC systems.

The propagator method is a powerful tool to study the evolution of systems [15, 16]. The quantum propagator $K(\mathbf{r}, \mathbf{r}_0; t)$ is the conditional transition amplitude between a state $|\mathbf{r}_0\rangle$ corresponding to an initial position $\mathbf{r}_0$ and a state $|\mathbf{r}\rangle$ corresponding to a final position $\mathbf{r}$ over a time interval t

$$K(\mathbf{r}, \mathbf{r}_0; t) = \langle \mathbf{r}|T(t)|\mathbf{r}_0\rangle = \langle\ \mathbf{r}|\ \mathrm{e}^{\frac{Ht}{\mathrm{i}\hbar}}|\mathbf{r}_0\rangle, \tag{4}$$

where $|\mathbf{r}\rangle$ represents a position eigenvector, $\langle\mathbf{r}|$ is its conjugate and $T(t)$ is the time-evolution operator which evolves a function from one time to another $T(t)|\psi(\mathbf{r}, 0)\rangle = |\ \psi(\mathbf{r}, t)\rangle$ [17]. Since we are interested in spin systems, we construct propagators for the evolution of spin distributions. By applying the propagators on a spin wavefunction $\psi(\mathbf{r}_0, 0)$ at $t = 0$, we gain information on the final spin wavefunction $\psi(\mathbf{r}, t)$ at any time

$$\psi(\mathbf{r}, t) = \int_{-\infty}^{\infty} K(\mathbf{r}, \mathbf{r}_0; t)\psi(\mathbf{r}_0, 0)\,\mathbf{dr}_0. \tag{5}$$

There are several methods for constructing spinless propagators. In this paper, we select a classical action method [17] and an algebraic method [18] and extend them to spin-dependent problems. The inclusion of the spin degree of freedom introduces a new level of noncommutativity which can considerably complicate the analysis of the systems. We give specific examples from 2D electron gas spin–orbit systems with limited noncommutativity and obtain analytic expressions for the propagators. By limited we mean that we consider powers and combinations of position, momentum and spin operators that allow some factorization of exponentials so that Baker–Campbell–Hausdorff-type formulae take on simplified forms. First, we consider particles moving under the influence of the spin–orbit coupling and isotropic parabolic horizontal (xy) confinement

$$H = \frac{\mathbf{p}^2}{2m} + \gamma\boldsymbol{\sigma}\cdot\mathbf{L} + \frac{1}{2}m\eta^2(x^2 + y^2), \tag{6}$$

where γ and η are real constants. This Hamiltonian has been shown to exhibit different chiralities for spin components [11]. We also consider specific spin–orbit-type interactions from condensed matter systems, namely specific superpositions of Rashba and Dresselhaus interactions. When both Rashba and Dresselhaus are present and balanced in strength, a simplification occurs as the degrees of freedom decouple. We consider nonrelativistic free

particles with spin under the influence of H_R and H_D and define the Equal–Strength–Rashba–Dresselhaus (ESRD) Hamiltonian for $\alpha = \beta$

$$H_{\mathrm{ESRD}} = \frac{p_x^2 + p_y^2}{2m} + \frac{\alpha}{\hbar}(p_y\sigma_x - p_x\sigma_y + p_x\sigma_x - p_y\sigma_y), \tag{7}$$

and the Opposite–Strength–Rashba–Dresselhaus (OSRD) Hamiltonian for $\alpha = -\beta$

$$H_{\mathrm{OSRD}} = \frac{p_x^2 + p_y^2}{2m} + \frac{\alpha}{\hbar}(p_y\sigma_x - p_x\sigma_y - p_x\sigma_x + p_y\sigma_y). \tag{8}$$

Equal–Strength–Rashba–Dresselhaus has been shown to exhibit helicoidal motion leading to a so-called persistent spin helix [13] and is relevant to the development of the nonballistic spin-field-effect transistor [14]. We also consider the case where an isotropic parabolic confinement is added to both ESRD and OSRD systems. Confinement terms can represent the finite spatial extension of realistic semiconducting samples.

The confined spin–orbit Hamiltonian corresponds to an atomic spin–orbit interaction with the Coulomb potential in equation (1) replaced by a simple harmonic oscillator (SHO) potential. Because the motion is limited to the plane, this particular coupling only brings in the z component of the spin. Similarly the Rashba interaction can also be obtained from equation (1) with a linear potential corresponding to a constant electric field [2]. These Hamiltonians operate on a space of spin distributions or spinorial functions $\psi(x, y)$ defined in two dimensions characterized by the coordinates x and y, and with a spin degree of freedom in 3D. These spinors obey time-dependent Pauli–Schrödinger equations.

This paper is organized as follows. We construct the quantum propagators for the atomic spin–orbit Hamiltonians (in section 2) and for specific spintronics Hamiltonians (in section 3) using both the classical action method and the algebraic method. In section 4, we illustrate the power of using these propagators to study the evolution of spin wavepackets in two particular cases of confined atomic and ESRD systems. In section 5, we weigh the relative advantages of our two methods in view of their applicability to the particular physical realizations discussed in this paper.

2. Atomic spin–orbit coupling propagator

The Hamiltonian for the confined atomic spin–orbit coupling in the xy-plane is given by

$$H_{\mathrm{SO}}^{c} = \frac{p_x^2 + p_y^2}{2m} + \sigma_z\gamma(xp_y - yp_x) + \frac{1}{2}m\eta^2(x^2 + y^2). \tag{9}$$

Since only one Pauli operator occurs in the Hamiltonian, it corresponds to a constant of the motion. The classical action method [17] can be extended to a 2×2 spin formalism. The successive steps consist in finding the corresponding Lagrangian, solving the Euler–Lagrange equations, substituting the motion into the Lagrangian, integrating over time to find the action and exponentiating to find the quantum propagator in two dimensions

$$K(x, x_0, y, y_0; t) = C \exp\left(\frac{\mathrm{i}S}{\hbar}\right), \tag{10}$$

where S is the classical action and C is a c-number determined by the initial conditions.

Since only σ_z is present, the Hamiltonian in equation (9) is diagonal in the standard representation of the Pauli matrices. In what follows, we use the symbol σ_z as a place holder for $(+1)$ and (-1) of the diagonal elements of the Pauli matrix σ_z. Therefore, our calculation proceeds in the usual way with a scalar Lagrangian.

We find Hamilton's equations

$$\dot{x} = \frac{p_x}{m} + \sigma_z \gamma y, \qquad \dot{y} = \frac{p_y}{m} - \sigma_z \gamma x, \tag{11}$$

perform a Legendre's transformation

$$L = \sum_i p_i \dot{q}_i - H, \tag{12}$$

and obtain the Lagrangian

$$L = \tfrac{1}{2} m(\dot{x}^2 + \dot{y}^2) - m\gamma\sigma_z(\dot{x}y - \dot{y}x) + \tfrac{1}{2} m(\gamma^2 - \eta^2)(x^2 + y^2). \tag{13}$$

The equations of motions are obtained

$$\begin{aligned} \frac{\mathrm{d}}{\mathrm{d}t}\frac{\partial L}{\partial \dot{x}} - \frac{\partial L}{\partial x} &= m\ddot{x} - 2m\sigma_z\gamma\dot{y} - (\gamma^2 - \eta^2)mx = 0 \\ \frac{\mathrm{d}}{\mathrm{d}t}\frac{\partial L}{\partial \dot{y}} - \frac{\partial L}{\partial y} &= m\ddot{y} + 2m\sigma_z\gamma\dot{x} - (\gamma^2 - \eta^2)my = 0, \end{aligned} \tag{14}$$

and solved for $x(t')$ and $y(t')$ (which also provides $\dot{x}(t')$ and $\dot{y}(t')$) using the boundary conditions

$$x(0) = x_0, \qquad x(t) = x, \qquad y(0) = y_0, \qquad y(t) = y. \tag{15}$$

The classical action,

$$S = \int_0^t L \, \mathrm{d}t', \tag{16}$$

is found by substituting the solutions into the Lagrangian and performing a partial integration

$$\begin{aligned} S &= \frac{m}{2}(x\dot{x} + y\dot{y})|_0^t - \int_0^t \left(\frac{m}{2}(x\ddot{x} + y\ddot{y}) + m\gamma\sigma_z(\dot{x}y - \dot{y}x) - \frac{1}{2}m(\gamma^2 - \eta^2)(x^2 + y^2) \right) \mathrm{d}t' \\ &= \frac{1}{2} m(x(t)\dot{x}(t) + y(t)\dot{y}(t) - x(0)\dot{x}(0) - y(0)\dot{y}(0)). \end{aligned} \tag{17}$$

Note that the integrand in equation (17) vanishes as a result of the equations of motions [19].

We distinguish three cases $\eta = 0$, $\eta = \gamma$ and arbitrary η corresponding to respectively no confinement, spin–orbit from the confinement potential and the general case. In this last, general, case, we use the algebraic method because it leads to the analytic result more elegantly than the classical action method. That result reduces to the results found in the first two cases when taking the proper limits.

2.1. Unconfined case: $\eta = 0$

For the unconfined Hamiltonian

$$H = \frac{p_x^2 + p_y^2}{2m} + \sigma_z\gamma(xp_y - yp_x), \tag{18}$$

we solve the equations of motions in equation (14) with $\eta = 0$. The action in equation (17) gives

$$S = \frac{m}{2t}\left(x^2 + x_0^2 + y^2 + y_0^2 - 2(xx_0 + yy_0)\cos\gamma t + 2\sigma_z(-xy_0 + x_0y)\sin\gamma t\right) \tag{19}$$

and, as a result, the unconfined spin–orbit propagator is

$$\begin{aligned} K_{\mathrm{SO}}^{(\eta=0)}(x, x_0, y, y_0; t) = \frac{m}{2\pi\mathrm{i}\hbar t} \exp\Bigg(\frac{\mathrm{i}m}{2\hbar t}\big(x^2 + x_0^2 + y^2 + y_0^2 - 2(xx_0 + yy_0)\cos\gamma t \\ + 2\sigma_z(-xy_0 + x_0y)\sin\gamma t\big)\Bigg), \end{aligned} \tag{20}$$

where the front coefficient is determined by the initial condition on the propagator

$$\lim_{t\to 0} K(x, x_0, y, y_0; t) = \delta(x - x_0)\delta(y - y_0). \tag{21}$$

This result can be checked against the free-particle propagator [17] by taking the limit $\gamma \to 0$

$$K^{\text{Free}}(x, x_0, y, y_0; t) = \frac{m}{2\pi \mathrm{i}\hbar t} \exp\left(-\frac{m(x - x_0)^2 + m(y - y_0)^2}{2\mathrm{i}\hbar t}\right). \tag{22}$$

2.2. *Larmor case (confined and balanced): $\eta \neq 0, \eta = \gamma$*

When the confinement strength η matches the SOC strength γ such that $\eta = \gamma$, the Hamiltonian

$$H = \frac{p_x^2 + p_y^2}{2m} + \sigma_z \gamma (x p_y - y p_x) + \frac{1}{2} m \gamma^2 (x^2 + y^2) \tag{23}$$

can be recognized as describing a charged particle in a homogeneous magnetic field, where γ plays the role of the Larmor frequency but exhibits an additional factor σ_z ($\sigma_z^2 = 1$). The propagator (without the σ_z factor) has been obtained for this Larmor case [20]

$$K(x, x_0, y, y_0; t) = \frac{m}{2\pi \mathrm{i}\hbar t} \frac{\gamma t}{\sin \gamma t} \exp\left(\frac{\mathrm{i}m\gamma}{2\hbar}\left(\frac{(x - x_0)^2 + (y - y_0)^2}{\tan \gamma t} + 2(x_0 y - x y_0)\right)\right), \tag{24}$$

where the front coefficient is found using the Feynman trick [21].

The propagator including the σ_z factor is now obtained by replacing γ by $\gamma\sigma_z$, $\gamma \cot \gamma t$ by $\gamma\sigma_z \cot \gamma\sigma_z t = \gamma \cot \gamma t$, and $\sin \gamma t$ by $\sin \gamma\sigma_z t = \sigma_z \sin \gamma t$. As a result

$$K_{\text{SO}}^{(\eta=\gamma)}(x, x_0, y, y_0; t) = \frac{m}{2\pi \mathrm{i}\hbar t} \frac{\gamma t}{\sin \gamma t} \exp\left(\frac{\mathrm{i}m\gamma}{2\hbar}\left(\frac{(x - x_0)^2 + (y - y_0)^2}{\tan \gamma t} + 2\sigma_z(x_0 y - x y_0)\right)\right). \tag{25}$$

In the limit $\gamma \to 0$, equation (25) reduces also to the free-particle propagator. Note that the propagators in the section can also be obtained following the same steps as in section 2.1.

2.3. *General case: $\eta \neq \gamma$*

For arbitrary η solving the equations of motions is cumbersome. Instead we use an algebraic method introduced by Wang [18] to calculate the propagator. In the Hamiltonian in equation (9), the spin–orbit term, which is linear in x, commutes with the sum of the confining term, which is quadratic in x, and the kinetic term. Because of this limited noncommutativity, the time-evolution operator T can be expressed as

$$\begin{aligned} T &= \exp\left(-\frac{\mathrm{i}Ht}{\hbar}\right) \\ &= \exp\left(-\frac{\mathrm{i}t}{\hbar}\left(\frac{\mathbf{p}^2}{2m} + \sigma_z\gamma(x p_y - y p_x) + \frac{1}{2}m\eta^2(x^2 + y^2)\right)\right) \\ &= \exp\left(-\frac{\mathrm{i}t}{\hbar}\sigma_z\gamma(x p_y - y p_x)\right) \exp\left(-\frac{\mathrm{i}t}{\hbar}\left(\frac{\mathbf{p}^2}{2m} + \frac{1}{2}m\eta^2(x^2 + y^2)\right)\right). \end{aligned} \tag{26}$$

Note that we have isolated to the right of this expression the complete simple harmonic oscillator evolution.

By applying equation (26) to a wavefunction, we obtain

$$\begin{aligned}\psi(x,y,t) &= T(t,0)\psi(x,y,0)\\ &= \exp\left(-\frac{\mathrm{i}t}{\hbar}\sigma_z\gamma(xp_y - yp_x)\right)\exp\left(-\frac{\mathrm{i}t}{\hbar}\left(\frac{\mathbf{p}^2}{2m}+\frac{1}{2}m\eta^2(x^2+y^2)\right)\right)\psi(x,y;0),\end{aligned} \tag{27}$$

where $\exp\left(-\frac{\mathrm{i}t}{\hbar}\left(\frac{\mathbf{p}^2}{2m}+\frac{1}{2}m\eta^2(x^2+y^2)\right)\right)\psi(x,y;0)$ is known since it represents the result of SHO evolution,

$$\begin{aligned}\psi(x,y,t) &= T^{\mathrm{SHO}}(t,0)\psi(x,y,0)\\ &= \exp\left(-\frac{\mathrm{i}t}{\hbar}\left(\frac{\mathbf{p}^2}{2m}+\frac{1}{2}m\eta^2(x^2+y^2)\right)\right)\psi(x,y,0)\\ &= \int_{-\infty}^{\infty}\int_{-\infty}^{\infty}K^{\mathrm{SHO}}(x,x_0,y,y_0;t)\psi(x_0,y_0,0)\,\mathrm{d}x_0\,\mathrm{d}y_0,\end{aligned} \tag{28}$$

where $K^{\mathrm{SHO}}(x,x_0,y,y_0;t)$ is the propagator for the simple harmonic oscillator [17]

$$\begin{aligned}K^{\mathrm{SHO}}(x,x_0,y,y_0;t) = \frac{m\eta}{2\pi\mathrm{i}\hbar\sin\eta t}\exp\Bigg(\frac{\mathrm{i}m\eta}{2\hbar\sin\eta t}\big(&(x^2+x_0^2+y^2+y_0^2)\cos\eta t\\ &-2xx_0-2yy_0\big)\Bigg).\end{aligned} \tag{29}$$

By substituting equation (29) into equation (28) and by comparing to equation (27) we obtain

$$\begin{aligned}\psi(x,y,t) &= \exp\left(-\frac{\mathrm{i}t}{\hbar}\sigma_z\gamma(xp_y-yp_x)\right)\exp\left(-\frac{\mathrm{i}t}{\hbar}\left(\frac{\mathbf{p}^2}{2m}+\frac{1}{2}m\eta^2(x^2+y^2)\right)\right)\psi(x,y,0)\\ &= \exp\left(-\frac{\mathrm{i}t}{\hbar}\sigma_z\gamma(xp_y-yp_x)\right)\frac{m\eta}{2\pi\mathrm{i}\hbar\sin\eta t}\int_{-\infty}^{\infty}\int_{-\infty}^{\infty}\exp\Bigg(\frac{\mathrm{i}m\eta}{2\hbar\sin\eta t}\big((x^2+x_0^2\\ &\quad+y^2+y_0^2)\cos\eta t-2xx_0-2yy_0\big)\Bigg)\psi(x_0,y_0,0)\,\mathrm{d}x_0\,\mathrm{d}y_0.\end{aligned} \tag{30}$$

The first factor $\exp\left(-\frac{\mathrm{i}t}{\hbar}\sigma_z\gamma(xp_y-yp_x)\right)$ corresponds to a spin-dependent rotation operator around the z-axis. Comparing with the usual rotation operator $R_z(\phi)=\exp\left(-\frac{\mathrm{i}\phi L_z}{\hbar}\right)$, we extract the rotation angle $\phi=\sigma_z\gamma t$. The effect of the rotation operator on a wavefunction is given by

$$R_z(\phi)f(x,y) = \exp\left(-\frac{\mathrm{i}\phi L_z}{\hbar}\right)f(x,y) = f(x\cos\phi+y\sin\phi,-x\sin\phi+y\cos\phi). \tag{31}$$

Therefore by applying equation (31) to equation (30)

$$\begin{aligned}\psi(x,y,t) &= \exp\left(-\frac{\mathrm{i}t}{\hbar}\sigma_z\gamma(xp_y-yp_x)\right)\frac{m\eta}{2\pi\mathrm{i}\hbar\sin\eta t}\int_{-\infty}^{\infty}\int_{-\infty}^{\infty}\exp\Bigg(\frac{\mathrm{i}m\eta}{2\hbar\sin\eta t}\big((x^2+x_0^2\\ &\quad+y^2+y_0^2)\cos\eta t-2xx_0-2yy_0\big)\Bigg)\psi(x_0,y_0,0)\,\mathrm{d}x_0\,\mathrm{d}y_0\\ &= \frac{m\eta}{2\pi\mathrm{i}\hbar\sin\eta t}\int_{-\infty}^{\infty}\int_{-\infty}^{\infty}\exp\Bigg(\frac{\mathrm{i}m\eta}{2\hbar\sin\eta t}\big(\big((x\cos\phi+y\sin\phi)^2+x_0^2\\ &\quad+(-x\sin\phi+y\cos\phi)^2+y_0^2\big)\cos(\eta t)-2(x\cos\phi+y\sin\phi)x_0\\ &\quad-2(-x\sin\phi+y\cos\phi)y_0\big)\Bigg)\psi(x_0,y_0,0)\,\mathrm{d}x_0\,\mathrm{d}y_0.\end{aligned} \tag{32}$$

By comparing with the propagator integral formula in equation (5), it is straightforward to extract the propagator for the generalized case

$$K(x, x_0, y, y_0; t) = \frac{m\eta}{2\pi i\hbar \sin \eta t} \exp\left(\frac{im\eta}{2\hbar \sin \eta t}\left(\left((x\cos\phi + y\sin\phi)^2 + x_0^2\right.\right.\right.$$
$$\left. + (-x\sin\phi + y\cos\phi)^2 + y_0^2\right)\cos\eta t - 2(x\cos\phi + y\sin\phi)x_0$$
$$\left.\left. - 2(-x\sin\phi + y\cos\phi)y_0\right)\right). \tag{33}$$

Substituting the rotation angle $\phi = \sigma_z \gamma t$ back into equation (33) and using $\cos \sigma_z \gamma t = \cos \gamma t$, and $\sin \sigma_z \gamma t = \sigma_z \sin \gamma t$, we obtain the propagator for arbitrary η and γ

$$K_{\mathrm{SO}}^{(\eta\neq\gamma)}(x, x_0, y, y_0; t) = \frac{m\eta}{2\pi i\hbar \sin \eta t} \exp\left(\frac{im\eta}{2\hbar \sin \eta t}\left(\left(x^2 + y^2 + x_0^2 + y_0^2\right)\cos\eta t\right.\right.$$
$$\left.\left. - 2(xx_0 + yy_0)\cos\gamma t - 2\sigma_z(x_0 y - x y_0)\sin\gamma t\right)\right). \tag{34}$$

This result for the general confined atomic spin–orbit propagator reduces to the expression of the propagator for the unconfined (equation (20)), Larmor (equation (25)), simple harmonic oscillator (equation (29)), and the free particle (equation (22)). Applications to equation (34) are discussed in section 5. Note that it is also straightforward to apply the algebraic method to the unconfined case directly since the kinetic energy itself commutes with the spin–orbit term.

3. ESRD and OSRD spintronics propagators

The confined ESRD and OSRD Hamiltonians are given by

$$H_{\mathrm{ESRD}}^{c} = \frac{\mathbf{p}^2}{2m} + \frac{\alpha}{\hbar}(p_x + p_y)(\sigma_x - \sigma_y) + \frac{1}{2}m\eta^2(x^2 + y^2) \tag{35}$$

$$H_{\mathrm{OSRD}}^{c} = \frac{\mathbf{p}^2}{2m} + \frac{\alpha}{\hbar}(p_x - p_y)(\sigma_x + \sigma_y) + \frac{1}{2}m\eta^2(x^2 + y^2). \tag{36}$$

We start by considering the unconfined case ($\eta = 0$) and later proceed to arbitrary confinement.

3.1. Unconfined case $\eta = 0$

In the ESRD case, we see from equation (35) that the two dimensions are decoupled unlike in the Rashba-only (equation (2)) and Dresselhaus-only (equation (3)) cases. Decoupling means that the total Hamiltonian can be written as a sum of two commuting Hamiltonians corresponding to the motion in two independent dimensions

$$H_{\mathrm{ESRD}} = H_{(x)} + H_{(y)}, \qquad H_{(x)} = \frac{p_x^2}{2m} + \frac{\alpha}{\hbar}p_x(\sigma_x - \sigma_y), \qquad H_{(y)} = \frac{p_y^2}{2m} + \frac{\alpha}{\hbar}p_y(\sigma_x - \sigma_y).$$

We apply the classical action method to the Hamiltonian in the x dimension

$$H = \frac{p_x^2}{2m} + \nu p_x, \tag{37}$$

where ν stands for the factor $\frac{\alpha}{\hbar}(\sigma_x - \sigma_y)$. Applying Hamilton's equation

$$\dot{x} = \frac{\partial H}{\partial p_x} = \frac{p_x}{m} + \nu \tag{38}$$

and using a Legendre transformation, we find

$$L = p_x\dot{x} - H = \frac{m\dot{x}^2}{2} - m\nu\dot{x} + \frac{m\nu^2}{2}. \tag{39}$$

The corresponding equations of motion

$$\frac{\mathrm{d}}{\mathrm{d}t}\frac{\partial L}{\partial \dot{x}} - \frac{\partial L}{\partial x} = \ddot{x} = 0 \tag{40}$$

describe a free particle. The classical action can now be evaluated

$$S = \int_0^t L\,\mathrm{d}t' = \frac{mx\dot{x}}{2}\bigg|_0^t - \int_0^t \left(\frac{mx\ddot{x}}{2} + m\nu\dot{x} - \frac{m\nu^2}{2}\right)\mathrm{d}t'. \tag{41}$$

As opposed to the examples in section 2, the integrand does not equate zero but it can be integrated directly

$$S = \int_0^t L\,\mathrm{d}t' = \frac{mx\dot{x}}{2}\bigg|_0^t - m\nu x|_0^t + \frac{m\nu^2 t}{2}, \tag{42}$$

where the first term corresponds to the usual free-particle component. It is shifted by a second term which is time independent and position dependent. The third term is just a time-dependent phase. Therefore, the propagator for the Hamiltonian in equation (37) is obtained from equation (10)

$$\begin{aligned} K(x, x_0; t) &= \sqrt{\frac{m}{2\pi \mathrm{i}\hbar t}}\exp\left(-\frac{m}{2\mathrm{i}\hbar t}(x - x_0)^2 + \frac{m\nu(x - x_0)}{\mathrm{i}\hbar} - \frac{m\nu^2 t}{2\mathrm{i}\hbar}\right) \\ &= \sqrt{\frac{m}{2\pi \mathrm{i}\hbar t}}\exp\left(-\frac{m}{2\mathrm{i}\hbar t}(x - x_0 - \nu t)^2\right) \end{aligned} \tag{43}$$

or, replacing ν by its value,

$$K(x, x_0; t) = \sqrt{\frac{m}{2\pi \mathrm{i}\hbar t}}\exp\left(-\frac{m}{2\mathrm{i}\hbar t}(x - x_0 - \frac{\alpha}{\hbar}(\sigma_x - \sigma_y)t)^2\right). \tag{44}$$

The propagator in the other dimension $K(y, y_0; t)$ can be obtained in a similar manner. As a result of the decoupling in the Hamiltonian, we find immediately the 2D propagator as a product of two 1D propagators

$$\begin{aligned} K^{(\eta=0)}_{\mathrm{ESRD}}(x, y, x_0, y_0; t) = \frac{m}{2\pi \mathrm{i}\hbar t}\exp\Bigg(-\frac{m}{2\mathrm{i}\hbar t}\Bigg(\left(x - x_0 - \frac{\alpha}{\hbar}(\sigma_x - \sigma_y)t\right)^2 \\ + \left(y - y_0 - \frac{\alpha}{\hbar}(\sigma_x - \sigma_y)t\right)^2\Bigg)\Bigg). \end{aligned} \tag{45}$$

In the OSRD case, the two dimensions are again decoupled but ν takes on a different value. The OSRD propagator is thus obtained similarly

$$\begin{aligned} K^{(\eta=0)}_{\mathrm{OSRD}}(x, y, x_0, y_0; t) = \frac{m}{2\pi \mathrm{i}\hbar t}\exp\Bigg(-\frac{m}{2\mathrm{i}\hbar t}\Bigg(\left(x - x_0 - \frac{\alpha}{\hbar}(\sigma_x + \sigma_y)t\right)^2 \\ + \left(y - y_0 + \frac{\alpha}{\hbar}(\sigma_x + \sigma_y)t\right)^2\Bigg)\Bigg). \end{aligned} \tag{46}$$

For completeness we now derive the K_{ESRD} and K_{OSRD} propagators using the algebraic method. Regarding the ESRD propagator, we first consider each dimension separately and find the effect on the spinorial function $\psi(x)$. Since the kinetic term in $H_{(x)}$ commutes with the potential

term, we use the coordinate representation for the momentum operator $p_x = \frac{\hbar}{i}\partial_x$ to rewrite the ESRD time-evolution operator

$$T(t,0)^{\eta=0}_{\mathrm{ESRD}} = \exp\left(\frac{\left(\frac{-\hbar^2\partial_{xx}}{2m} + \frac{\alpha}{\mathrm{i}}\partial_x(\sigma_x - \sigma_y)\right)t}{\mathrm{i}\hbar}\right)$$
$$= \exp\left(-\frac{\alpha\partial_x(\sigma_x - \sigma_y)t}{\hbar}\right)\exp\left(\frac{\left(\frac{-\hbar^2\partial_{xx}}{2m}\right)t}{\mathrm{i}\hbar}\right). \tag{47}$$

The expression $\exp\left(\frac{\left(\frac{-\hbar^2\partial_{xx}}{2m}\right)t}{\mathrm{i}\hbar}\right)\psi(x,0)$ is known since

$$\psi(x,t) = T^{\mathrm{Free}}(t,0)\psi(x,0) = \exp\left(-\frac{t}{\mathrm{i}\hbar}\left(\frac{\hbar^2\partial_{xx}}{2m}\right)\right)\psi(x,0)$$
$$= \int_{-\infty}^{\infty} K^{\mathrm{Free}}(x,x_0;t)\psi(x_0,0)\,\mathrm{d}x_0, \tag{48}$$

where $K^{\mathrm{Free}}(x,x_0;t)$ is the propagator for the free particle provided in equation (22) in one dimension. After substitution, we obtain

$$\psi(x,t) = T(t,0)\psi(x,0)$$
$$= \exp\left(-\frac{\alpha\partial_x(\sigma_x - \sigma_y)t}{\hbar}\right)\sqrt{\frac{m}{2\pi\mathrm{i}\hbar t}}\int_{-\infty}^{\infty}\exp\left(-\frac{m(x-x_0)^2}{2\mathrm{i}\hbar t}\right)\psi(x_0,0)\,\mathrm{d}x_0. \tag{49}$$

The term $\exp\left(-\frac{\alpha\partial_x(\sigma_x-\sigma_y)t}{\hbar}\right)$ acts as a spin-dependent displacement in the x coordinate. By applying the usual displacement formula

$$\exp(-\xi\partial_x)\psi(x) = \psi(x-\xi) \tag{50}$$

with ξ replaced by a diagonalizable matrix $\alpha(\sigma_x - \sigma_y)t/\hbar$, we immediately obtain

$$\psi(x,t) = T(t,0)\psi(x,0)$$
$$= \sqrt{\frac{m}{2\pi\mathrm{i}\hbar t}}\int_{-\infty}^{\infty}\exp\left(-\frac{m\left(x - x_0 - \frac{\alpha(\sigma_x-\sigma_y)t}{\hbar}\right)^2}{2\mathrm{i}\hbar t}\right)\psi(x_0)\,\mathrm{d}x_0. \tag{51}$$

We then extract the quantum propagator from equations (5) and (51)

$$K(x,x_0,t) = \sqrt{\frac{m}{2\pi\mathrm{i}\hbar t}}\int_{-\infty}^{\infty}\exp\left(-\frac{m\left(x - x_0 - \frac{\alpha(\sigma_x-\sigma_y)t}{\hbar}\right)^2}{2\mathrm{i}\hbar t}\right). \tag{52}$$

Note that we have only obtained the propagator for the motion in x. $K(y, y_0; t)$ is obtained in analogy with $K(x, x_0; t)$. The 2D ESRD propagator is simply the product of $K(x, x_0; t)$ and $K(y, y_0; t)$

$$K^{(\eta=0)}_{\mathrm{ESRD}}(x,y,x_0,y_0;t) = \frac{m}{2\pi\mathrm{i}\hbar t}\exp\left(-\frac{m}{2\mathrm{i}\hbar t}\left(\left(x - x_0 - \frac{\alpha}{\hbar}(\sigma_x - \sigma_y)t\right)^2\right.\right.$$
$$\left.\left. + \left(y - y_0 - \frac{\alpha}{\hbar}(\sigma_x - \sigma_y)t\right)^2\right)\right). \tag{53}$$

The construction of the OSRD propagator is similar

$$K^{(\eta=0)}_{\mathrm{OSRD}}(x,y,x_0,y_0;t) = \frac{m}{2\pi\mathrm{i}\hbar t}\exp\left(-\frac{m}{2\mathrm{i}\hbar t}\left(\left(x - x_0 - \frac{\alpha}{\hbar}(\sigma_x + \sigma_y)t\right)^2\right.\right.$$
$$\left.\left. + \left(y - y_0 + \frac{\alpha}{\hbar}(\sigma_x + \sigma_y)t\right)^2\right)\right). \tag{54}$$

We thus recover the results from equations (45) and (46). By comparing with the usual free-particle propagator in equation (22), it is interesting to note that a shift in the position appears in both dimensions in the exponential. The shift reflects two different inertial frames in relative motion. This effect is caused by the term linear in p in the Hamiltonian.

3.2. Confined case: $\eta \neq 0$

We first consider the classical action method. The two dimensions are again decoupled and it is straightforward to work out the one-dimensional propagator. The Hamiltonian

$$H = \frac{p_x^2}{2m} + \nu p_x + \frac{1}{2}m\eta^2 x^2 \tag{55}$$

corresponds to the Lagrangian

$$L = \frac{m\dot{x}^2}{2} - m\nu\dot{x} + \frac{m\nu^2}{2} - \frac{1}{2}m\eta^2 x^2 \tag{56}$$

after applying a Legendre transformation with $\nu = \frac{\alpha}{\hbar}(\sigma_x - \sigma_y)$ in the constrained ESRD case or $\nu = \frac{\alpha}{\hbar}(\sigma_x + \sigma_y)$ in the constrained OSRD case. It is interesting to note that the Euler–Lagrange equations are identical to those of the usual simple harmonic oscillator potential. The action, however, is different

$$\begin{aligned} S &= \int_0^t L\,\mathrm{d}t' = \int_0^t \left(\frac{m\dot{x}^2}{2} - m\nu\dot{x} + \frac{m\nu^2}{2} - \frac{1}{2}m\eta^2 x^2\right)\mathrm{d}t' \\ &= \frac{1}{2}mx\dot{x}\Big|_0^t - \int_0^t \left(\frac{1}{2}mx\ddot{x} + \frac{1}{2}m\eta^2 x^2 + m\nu\dot{x} - \frac{1}{2}m\nu^2\right)\mathrm{d}t', \end{aligned} \tag{57}$$

where the first two terms inside the integral add up to zero from the equations of motion for the simple harmonic oscillator. Therefore

$$\begin{aligned} S &= \frac{1}{2}mx\dot{x}\Big|_0^t - \int_0^t \left(m\nu\dot{x} - \frac{1}{2}m\nu^2\right)\mathrm{d}t' \\ &= \frac{1}{2}m(x(t)\dot{x}(t) - x(0)\dot{x}(0)) - m\nu(x(t) - x(0)) + \frac{1}{2}m\nu^2 t, \end{aligned} \tag{58}$$

where the first term $\frac{1}{2}m(x(t)\dot{x}(t) - x(0)\dot{x}(0))$ corresponds to the classical action for the usual harmonic oscillator potential. By substituting the harmonic oscillator solution

$$x(t') = \csc\eta t\,(x\sin\eta t' - x_0\sin\eta(t' - t)) \tag{59}$$

into the action S, we obtain

$$S(x, x_0; t) = \frac{m}{2}\left(\left(x_0^2 + x^2\right)\eta\cot\eta t - 2x_0 x\eta\csc\eta t\right) + \frac{m\nu}{2}(2x_0 - 2x + t\nu).$$

Therefore the propagator has the form

$$\begin{aligned} K(x, x_0; t) &= C\exp\left(\frac{\mathrm{i}S}{\hbar}\right) \\ &= C\exp\left(\frac{\mathrm{i}m}{2\hbar}\left(\left(x_0^2 + x^2\right)\eta\cot\eta t - 2x_0 x\eta\csc\eta t + \nu(2x_0 - 2x + t\nu)\right)\right), \end{aligned} \tag{60}$$

where C is again obtained using Feynman's trick

$$K(x, x_0; t) = \sqrt{\frac{m\eta}{2\pi\mathrm{i}\hbar\sin\eta t}}\exp\left(\frac{\mathrm{i}m}{2\hbar}\left(\left(x_0^2 + x^2\right)\eta\cot\eta t - 2x_0 x\eta\csc\eta t + \nu(2x_0 - 2x + t\nu)\right)\right). \tag{61}$$

Note that in the constrained ESRD case, the x and y dimensions have the same sign multiplying ν due to the presence of the term $\nu(p_x + p_y)$, whereas in the constrained OSRD the x and y dimensions have opposite signs multiplying ν due to $\nu(p_x - p_y)$. As a result, the two-dimensional propagators K^c_{ESRD} and K^c_{OSRD} are simply the products of two 1D propagators, and the only difference between the two appears in the terms linear in ν

$$K^c_{\mathrm{ESRD}}(x, y, x_0, y_0; t) = \frac{m\eta}{2\pi \mathrm{i}\hbar \sin \eta t} \exp\left(\frac{\mathrm{i}m}{2\hbar}\left(\left(x_0^2 + x^2 + y_0^2 + y^2\right)\eta \cot \eta t \right.\right.$$
$$\left.\left. - 2(x_0 x + y_0 y)\eta \csc \eta t + \nu(2x_0 - 2x + 2y_0 - 2y + 2t\nu)\right)\right) \tag{62}$$

$$K^c_{\mathrm{OSRD}}(x, y, x_0, y_0; t) = \frac{m\eta}{2\pi \mathrm{i}\hbar \sin \eta t} \exp\left(\frac{\mathrm{i}m}{2\hbar}\left(\left(x_0^2 + x^2 + y_0^2 + y^2\right)\eta \cot \eta t \right.\right.$$
$$\left.\left. - 2(x_0 x + y_0 y)\eta \csc \eta t + \nu(2x_0 - 2x - 2y_0 + 2y + 2t\nu)\right)\right). \tag{63}$$

In equations (62) and (63), ν takes on the values $\nu = \alpha(\sigma_x - \sigma_y)/\hbar$ (ESRD) and $\nu = \alpha(\sigma_x + \sigma_y)/\hbar$ (OSRD). It can be verified that the limits $\eta \to 0$ (unconfined) and $\nu \to 0$ (simple harmonic oscillator) reduce to the corresponding propagators.

We now proceed with the algebraic method for the confined case. When including a harmonic oscillator potential, the algebraic method becomes challenging due to the noncommutativity $\left[p_x, p_x^2 + (1/2)m\omega^2 x^2\right] \neq 0$. As a consequence, the kinetic and potential terms cannot be simply factorized. The usual simple harmonic oscillator propagator has been derived using the algebraic method [18] with the operators

$$L_- = -\tfrac{1}{2}\partial_{xx}, \qquad L_+ = \tfrac{1}{2}x^2, \qquad L_3 = \tfrac{1}{2}x\partial_x + \tfrac{1}{4}, \tag{64}$$

which satisfy the commutation relation of the Lie algebra $su(2)$, namely

$$[L_+, L_-] = 2L_3, \qquad [L_3, L_\pm] = \pm L_\pm. \tag{65}$$

We first consider the Hamiltonian in equation (55) with a shift in the momentum. Therefore we set out to modify the operators to

$$L_- = -\frac{1}{2}\partial_{xx} + \frac{m\nu}{\mathrm{i}\hbar}\partial_x + \frac{m^2\nu^2}{2\hbar^2}, \qquad L_+ = \frac{1}{2}x^2, \qquad L_3 = \frac{1}{2}x\partial_x + \frac{1}{4} - \frac{xm\nu}{2\mathrm{i}\hbar}, \tag{66}$$

which still satisfy equation (65).

By applying a Baker–Campbell–Hausdorff-like relation [23, 24]

$$\exp(\tau L_+ - \overline{\tau} L_-) = \exp\left(\frac{\tau}{|\tau|}\tan(|\tau|)L_+\right)\exp(-2\ln\cos(|\tau|)L_3)\exp\left(-\frac{\overline{\tau}}{|\tau|}\tan(|\tau|)L_-\right) \tag{67}$$

and substituting $\tau = \frac{-\mathrm{i}t m\eta^2}{\hbar}$, $\overline{\tau} = \frac{\mathrm{i}t\hbar}{m}$ and $|\tau| = \eta t$, we rewrite the time-evolution operator as

$$\begin{aligned} T &= \exp\left(-\frac{\mathrm{i}t}{\hbar}\left(\frac{\hbar^2}{m}\left(-\frac{\partial_{xx}}{2} + \frac{m\nu}{\mathrm{i}\hbar}\partial_x + \frac{m^2\nu^2}{2\hbar^2} + \frac{1}{2}m\eta^2 x^2 - \frac{m^2\nu^2}{2\hbar^2}\right)\right)\right) \\ &= \exp\left(\frac{\mathrm{i}tm\nu^2}{2\hbar}\right)\exp\left(-\frac{\mathrm{i}t}{\hbar}\left(\frac{\hbar^2}{m}\left(-\frac{\partial_{xx}}{2} + \frac{m\nu}{\mathrm{i}\hbar}\partial_x + \frac{m^2\nu^2}{2\hbar^2} + \frac{1}{2}m\eta^2 x^2\right)\right)\right) \\ &= \exp\left(\frac{\mathrm{i}tm\nu^2}{2\hbar}\right)\exp\left(\frac{-\mathrm{i}m\eta}{\hbar}\frac{x^2}{2}\tan\eta t\right)\exp\left(-2\left(\frac{1}{2}x\partial_x + \frac{1}{4} - \frac{xm\nu}{2\mathrm{i}\hbar}\right)\ln\cos\eta t\right) \\ &\quad \times \exp\left(\frac{-\mathrm{i}\hbar}{m\eta}\left(-\frac{1}{2}\partial_{xx} + \frac{m\nu}{\mathrm{i}\hbar}\partial_x + \frac{m^2\nu^2}{2\hbar^2}\right)\tan\eta t\right). \end{aligned} \tag{68}$$

By applying the product of exponentials to a wavefunction, the last line in equation (68) corresponds to two commuting operators ∂_{xx} and ∂_x, and it is straightforward to apply them to a wavefunction using equation (48) and the usual displacement formula [17]

$$\exp(a\partial_x) f(x) = f(x+a), \tag{69}$$

which gives

$$\begin{aligned}\psi(x,t) &= T(t,0)\psi(x,0)\\ &= \exp\left(\frac{\mathrm{i}tmv^2}{2\hbar}\right)\exp\left(\frac{-\mathrm{i}m\eta}{\hbar}\frac{x^2}{2}\tan\eta t\right)\exp\left(-\left(x\partial_x+\frac{1}{2}-\frac{xmv}{\mathrm{i}\hbar}\right)\ln\cos\eta t\right)\\ &\quad\times\sqrt{\frac{m\eta}{2\pi\mathrm{i}\hbar\tan\eta t}}\int_{-\infty}^{\infty}\exp\left(-\frac{m\eta}{2\mathrm{i}\hbar\tan\eta t}\left((x-x_0)^2-2\frac{v(x-x_0)}{\eta}\tan\eta t\right)\right)\\ &\quad\times\psi(x_0,0)\,\mathrm{d}x_0.\end{aligned} \tag{70}$$

The term $\exp\left(-\left(x\partial_x+\frac{1}{2}-\frac{xmv}{\mathrm{i}\hbar}\right)\ln\cos\eta t\right)$ cannot be factorized immediately due to the commutator $[x\partial_x, x] = x$. Instead the Zassenhaus formula which relates noncommuting operators in exponentials [25]

$$\begin{aligned}\mathrm{e}^{t(X+Y)} &= \mathrm{e}^{tX}\,\mathrm{e}^{tY}\,\mathrm{e}^{-\frac{t^2}{2!}[X,Y]}\,\mathrm{e}^{\frac{t^3}{3!}(2[Y,[X,Y]]+[X,[X,Y]])}\\ &\quad\times\mathrm{e}^{-\frac{t^4}{4!}(3[Y,[Y,[X,Y]]]+3[X,[Y,[X,Y]]]+[X,[X,[X,Y,]]])}\ldots\end{aligned} \tag{71}$$

is needed. It is interesting to note that $\exp(ax\partial_x + abx)$ can be factorized even in the presence of a non-terminating series in the Zassenhaus formula, namely

$$\begin{aligned}\exp(ax\partial_x+abx) &= \exp(ax\partial_x)\exp(abx)\exp\left(-\frac{a^2bx}{2!}\right)\exp\left(\frac{a^3bx}{3!}\right)\ldots\\ &= \exp(ax\partial_x)\exp\left(\sum_{n=1}^{\infty}\frac{a^n(-1)^{n-1}}{n!}bx\right)\\ &= \exp(ax\partial_x)\exp((1-\exp(-a))bx).\end{aligned} \tag{72}$$

By comparing $\exp\left(-\left(x\partial_x-\frac{xmv}{\mathrm{i}\hbar}\right)\ln\cos\eta t\right)$ with equation (72) we extract $a = -\ln\cos\eta t$, $b = -\frac{mv}{\mathrm{i}\hbar}$. As a result we obtain that

$$\begin{aligned}&\exp\left(-\left(x\partial_x+\frac{1}{2}-\frac{xmv}{\mathrm{i}\hbar}\right)\ln\cos\eta t\right)\\ &\quad=\frac{1}{\sqrt{\cos\eta t}}\exp\left(-\left(x\partial_x-\frac{xmv}{\mathrm{i}\hbar}\right)\ln\cos\eta t\right)\\ &\quad=\frac{1}{\sqrt{\cos\eta t}}\exp(-x\partial_x\ln\cos\eta t)\exp\left(-(1-\exp(\ln\cos\eta t))\frac{mvx}{\mathrm{i}\hbar}\right)\\ &\quad=\frac{1}{\sqrt{\cos\eta t}}\exp(-x\partial_x\ln\cos\eta t)\exp\left(-(1-\cos\eta t)\frac{mvx}{\mathrm{i}\hbar}\right).\end{aligned} \tag{73}$$

Now the term $\exp(-x\partial_x\ln\cos\eta t)$ corresponds to a dilatation operator. The effect of a dilatation operator on a function is given by [18, 22]

$$\exp(ax\partial_x) f(x) = f(\mathrm{e}^a x). \tag{74}$$

Therefore the operator $\exp(-x\partial_x\ln\cos\eta t)$ changes every x to $x/\cos\eta t$.

Combining these results we obtain

$$\begin{aligned}\psi(x,t) &= T(t,0)\psi(x,0)\\ &= \exp\left(\frac{\mathrm{i}tmv^2}{2\hbar}\right)\exp\left(\frac{-\mathrm{i}m\eta}{\hbar}\frac{x^2}{2}\tan\eta t\right)\exp\left(-(1-\cos\eta t)\frac{mvx}{\mathrm{i}\hbar\cos\eta t}\right)\sqrt{\frac{m\eta}{2\pi\mathrm{i}\hbar\sin\eta t}}\\ &\quad\times\int_{-\infty}^{\infty}\exp\left(-\frac{m\eta}{2\mathrm{i}\hbar\tan\eta t}\left(\left(\frac{x}{\cos\eta t}-x_0\right)^2-2\frac{v\left(\frac{x}{\cos\eta t}-x_0\right)}{\eta}\tan\eta t\right)\right)\\ &\quad\times\psi(x_0,0)\,\mathrm{d}x_0\\ &= \sqrt{\frac{m\eta}{2\pi\mathrm{i}\hbar\sin\eta t}}\int_{-\infty}^{\infty}\exp\left(\frac{\mathrm{i}m}{2\hbar}\left(\left(x^2+x_0^2\right)\eta\cot\eta t-2xx_0\eta\csc\eta t\right.\right.\\ &\quad\left.\left.+2v(x_0-x)+v^2t\right)\right)\psi(x_0,0)\,\mathrm{d}x_0. \end{aligned}\tag{75}$$

The propagator for the confined ESRD (OSRD) in one dimension can be extracted

$$\begin{aligned}K(x,x_0;t) = \sqrt{\frac{m\eta}{2\pi\mathrm{i}\hbar\sin\eta t}}\exp\left(\frac{\mathrm{i}m}{2\hbar}\left(\left(x^2+x_0^2\right)\eta\cot\eta t-2xx_0\eta\csc\eta t\right.\right.\\ \left.\left.+2v(x_0-x)+v^2t\right)\right),\end{aligned}\tag{76}$$

which matches equation (61). Again in 2D we obtain the results from equations (62) and (63) as the product of two 1D propagators.

4. Applying the propagator to spin wavepacket evolution

We now apply the propagators for the confined atomic spin–orbit coupled system and for the confined ESRD system to a localized spin wavepacket. The spin wavepacket we consider $\psi(x_0, y_0; t)$ is a Gaussian distribution in space centered at (x', y') with widths w_x and w_y and with spin polarizations determined by constants χ and λ such that $|\chi|^2 + |\lambda|^2 = 1$ and

$$\psi(x_0, y_0; t) = \frac{1}{\pi w_x w_y}\exp\left(-\frac{(x_0-x')^2}{2w_x^2}-\frac{(y_0-y')^2}{2w_y^2}\right)\begin{pmatrix}\chi\\ \lambda\end{pmatrix}.\tag{77}$$

By applying $K_{\mathrm{SO}}^{\eta\neq\gamma}$ (equation (34)) to $\psi(x_0, y_0; t)$ as in equation (5) we obtain

$$\begin{aligned}\psi(x,y;t) = \frac{1}{\pi w_x w_y}\sqrt{\frac{1}{\left(\cos\eta t-\frac{\hbar\sin\eta t}{\mathrm{i}m\eta w_x^2}\right)\left(\cos\eta t-\frac{\hbar\sin\eta t}{\mathrm{i}m\eta w_y^2}\right)}}\exp\left(\frac{\mathrm{i}m\eta(x^2+y^2)\cos\eta t}{2\hbar\sin\eta t}\right.\\ -\frac{x'^2}{2w_x^2}-\frac{y'^2}{2w_y^2}+\frac{m\left(x\cos\gamma t+y\sigma_z\sin\gamma t+\frac{x'\hbar\sin\eta t}{\mathrm{i}m\eta w_x^2}\right)^2}{2\mathrm{i}\hbar\sin\eta t\left(\cos\eta t-\frac{\hbar\sin\eta t}{\mathrm{i}m\eta w_x^2}\right)}\\ \left.+\frac{m\left(y\cos\gamma t-x\sigma_z\sin\gamma t+\frac{y'\hbar\sin\eta t}{\mathrm{i}m\eta w_y^2}\right)^2}{2\mathrm{i}\hbar\sin\eta t\left(\cos\eta t-\frac{\hbar\sin\eta t}{\mathrm{i}m\eta w_y^2}\right)}\right)\begin{pmatrix}\chi\\ \lambda\end{pmatrix}.\end{aligned}\tag{78}$$

Note that we use natural units in generating the plots. We provide an initial spin state with spin-up ($\uparrow$) ($\chi = 1, \lambda = 0$), center the initial wavepacket at $(x', y') = (1, 1)$ for simplicity

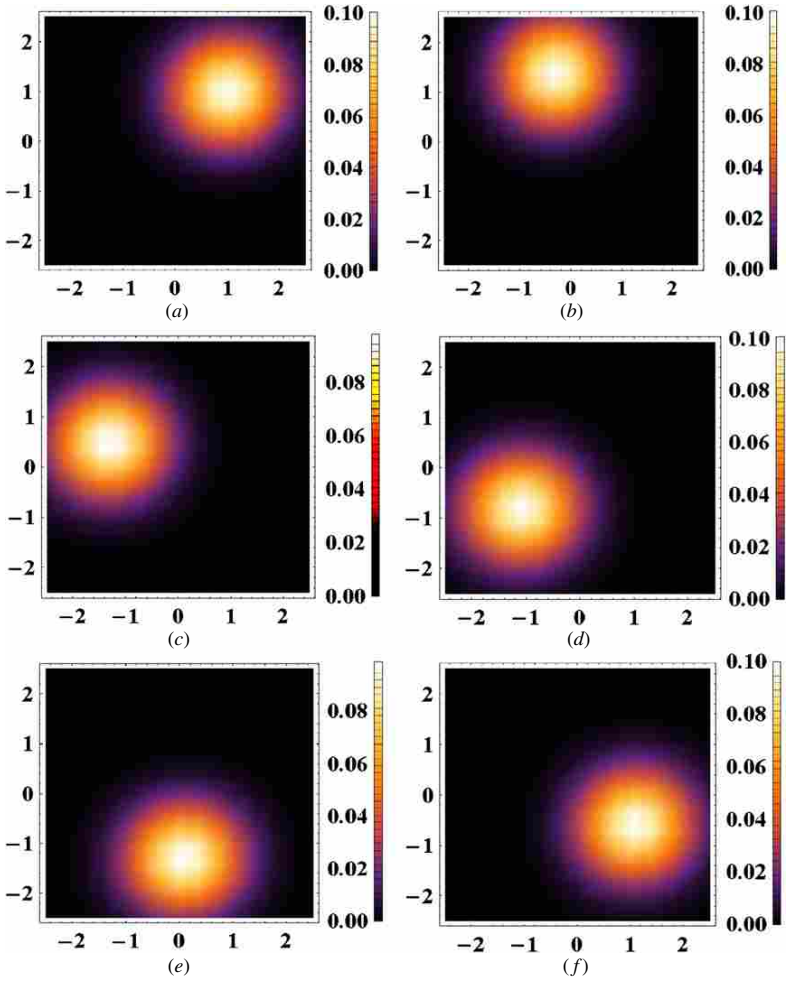

Figure 1. Spin probability density $\rho_\uparrow$ contour plot for a spin state initially up for six successive times from 0 to 0.5 from (a)–(f) with an increment of 0.1 between plots. The parameters are chosen as follows: $m = 1, \hbar = 1, w_x = w_y = 1, \eta = 1, \gamma = 10$.

and display the spin probability density $\rho_\uparrow = |\psi_\uparrow|^2$ at six different times in figures 1(a)–(f). We see that the spin wavepacket performs a counterclockwise rotation.

Next, by applying the propagator for the confined ESRD system (equation (62)) to $\psi(x_0, y_0; t)$ (equation (77)) in equation (5) we obtain

$$\psi(x, y; t) = \frac{1}{\pi w_x w_y}\sqrt{\frac{1}{\left(\cos\eta t - \frac{\hbar \sin\eta t}{\mathrm{i}m\eta w_x^2}\right)\left(\cos\eta t - \frac{\hbar \sin\eta t}{\mathrm{i}m\eta w_y^2}\right)}}\exp\left(\frac{\mathrm{i}m}{2\hbar}\left((x^2+y^2)\eta\cot\eta t + \frac{\alpha}{\hbar}(\sigma_x-\sigma_y)\left(-2x-2y+\frac{2\alpha}{\hbar}(\sigma_x-\sigma_y)t\right)\right)\right)$$

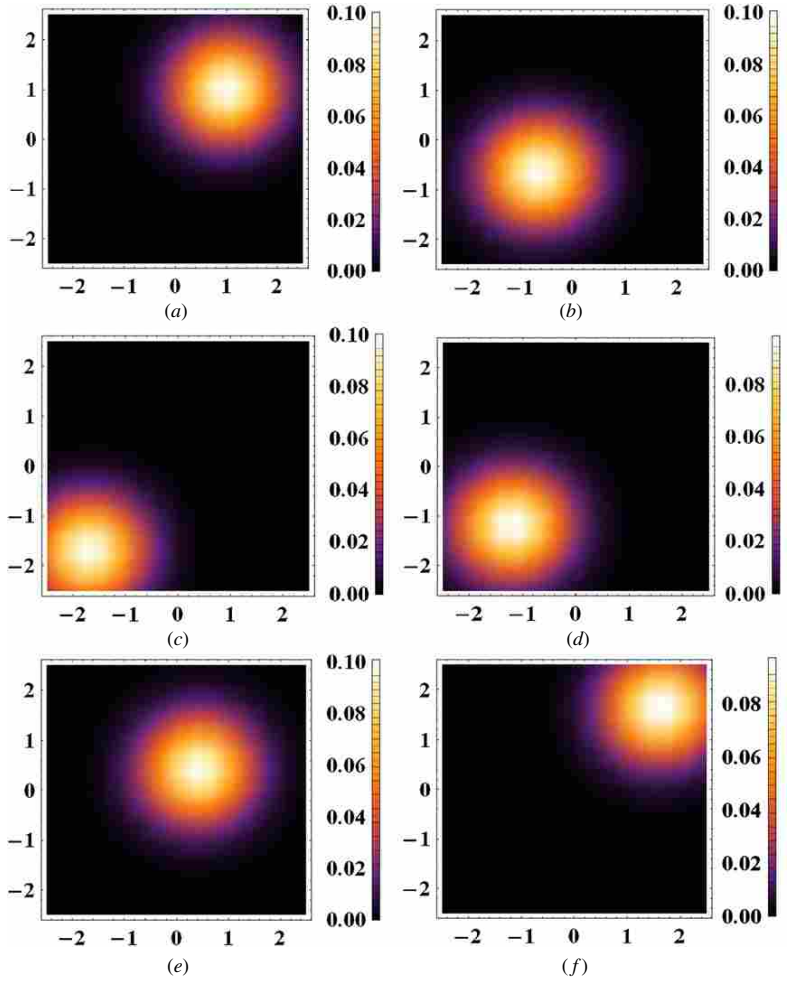

Figure 2. Spin probability density ρ_κ contour plot for a spin state initially $\chi = (-1-i)/2, \lambda = 1$ for six successive times from 0 to 5 from (a)–(f) with an increment of 1 between plots. The parameters are chosen as follows: $m = 1, \hbar = 1, w_x = w_y = 1, \eta = 1, \alpha = 1$.

$$-\frac{x'^2}{2w_x^2} - \frac{y'^2}{2w_y^2} + \frac{m\left(x\eta\csc\eta t - \frac{\alpha}{\hbar}(\sigma_x - \sigma_y) + \frac{i\hbar x'}{mw_x^2}\right)^2}{2i\hbar\left(\eta\cot\eta t + \frac{i\hbar}{mw_x^2}\right)}$$
$$+\frac{m\left(y\eta\csc\eta t - \frac{\alpha}{\hbar}(\sigma_x - \sigma_y) + \frac{i\hbar y'}{mw_y^2}\right)^2}{2i\hbar\left(\eta\cot\eta t + \frac{i\hbar}{mw_y^2}\right)}\Bigg)\begin{pmatrix}\chi\\ \lambda\end{pmatrix}. \tag{79}$$

For simplicity, we choose the initial spin state to be one of the eigenspinors of $\sigma_x - \sigma_y$ such that $\chi = (-1-i)/2, \lambda = 1$ and we denote this spin state as κ. This choice guarantees that spin-flipping does not occur. The initial Gaussian is again chosen to be centered at $(x', y') = (1, 1)$. We plot the spin probability density $\rho_\kappa = |\psi_\kappa|^2$ at six different times in figures 2(a)–(f). We see that the spin wavepacket performs oscillations on the diagonal axis.

In these and other cases the propagator clearly determines the wavepacket evolution. More complex behavior can be observed when the initial wavepacket consists of superpositions of eigenspinors.

5. Discussion

We have obtained propagators for atomic spin–orbit coupled systems and for ESRD and OSRD spintronics systems by using two different methods. The first method is based on the classical action and is familiar from spinless systems [20]. It relies on direct integration, substitution, Legendre transformation and the application of the initial conditions. In reality, the actual integration can often be avoided [19]. However, as the Hamiltonians get more complex, the differential equations to be solved contain more terms and an alternate method becomes preferable. In particular for the most general confined atomic spin–orbit case (section 2.3) we choose to obtain the propagator with the algebraic method. In the algebraic method, we permute noncommutative operators in the exponentials in order to extract factors corresponding to recognizable propagators. This method is not algorithmic but involves the identification of mutually commuting parts. These parts either correspond to systems whose propagators are known or whose action on the wavefunction can be evaluated directly. In the atomic spin–orbit case, the algebraic method involves the propagator of the simple harmonic oscillator and a spin-dependent rotation operator. Both operations can be applied directly to the wavefunctions. The two methods illustrate different approaches and we have used them both to derive the ESRD and ORSRD propagators. Both methods yield the same result with comparable levels of complexity. In the ESRD/OSRD confined case, the confining harmonic oscillator does complicate the algebraic method significantly. This shows that each method has its merits and that the choice of method should be determined carefully by taking into consideration the complexity of the Hamiltonian. This does not exclude the possibility of looking into extending still other methods such as the path-integral method [20] or Schwinger's method [26, 27] to the spin degree of freedom when dealing with spin–orbit coupled Hamiltonians.

The physical systems that we have considered all display the spin–orbit coupling. We have limited our attention to a dependence that is at most quadratic in x and p. Because of the properties of the spin, $\sigma^2 = 1$, quadratic or higher orders of spin do not appear. In general, a linear term in the momentum p can be absorbed in the kinetic energy by shifting the momentum and by adding a constant energy. The equations of motion will be unaffected. This is the momentum equivalent of shifting the equilibrium of an oscillator in the presence of a constant force. However, the action and the propagator of such systems will contain extra terms. This can be compared to the description of motion in inertial frames that are in relative motion. Our systems are also effectively two dimensional only, as momentum in z is frozen out. These effective 2D Hamiltonians find application in real systems. Bernevig *et al* [11] have recently found that the Hamiltonian for strained materials with quantum well parabolic confinement is of the form

$$H = \frac{\mathbf{p}^2}{2m} + \frac{C_3 g}{2\hbar}(yp_x - xp_y)\sigma_z + D(x^2 + y^2), \tag{80}$$

where C_3 is a material-dependent constant and D corresponds to the confinement strength. Landau levels result from such a Hamiltonian without the presence of a magnetic field. Bernevig *et al* [13] also found that ESRD Hamiltonian leads to interesting persistent spin helix phenomena in condensed matter systems. Both Rashba and Dresselhaus interactions can also be replicated in ultracold atoms [4]. ESRD and OSRD apply to systems that have equal amounts of Rashba and Dresselhaus interactions only. Because of the noncommutativities of

the Rashba and Dresselhaus parts, the propagator of the combined interactions differs from the product of the individual propagator.

The construction of propagators in spin–orbit coupled systems remains challenging. Nevertheless for those specific cases treated in this paper, the propagators can be found in closed form and can be applied to predict and display spin evolution.

References

[1] Geim A K and Novoselov K S 2007 *Nature Mat.* **6** 183
[2] Winkler R 2003 *Spin–Orbit Coupling Effects in Two-Dimensional Electron and Hole Systems* 1st edn (Berlin: Springer)
[3] Awschalom D 2002 *Semiconductor Spintronics and Quantum Computation* 1st edn (New York: Springer)
[4] Vaishnav J Y and Clark Charles W 2008 *Phys. Rev. Lett.* **100** 153002
[5] Bandyopadhyay S 2008 *Introduction to Spintronics* 1st edn (Boca Rota, FL: CRC)
[6] Rashba E I 1960 *Fiz. Tverd. Tela* **2** 1224
Rashba E I 1960 *Sov. Phys. Solid State* **2** 1109
[7] Bychkov Yu A and Rashba E I 1984 *J. Phys. C: Solid State Phys.* **17** 6039
[8] Dresselhaus G 1955 *Phys. Rev.* **100** 580
[9] Fu X, Liao W and Zhou G 2008 *Adv. Condens. Matter Phys.* **2008** 152731
[10] Sinova J, Culcer D, Niu Q, Sinitsyn N A, Jungwirth T and MacDonald A H 2004 *Phys. Rev. Lett.* **92** 126603
[11] Bernevig B A and Zhang S-C 2006 *Phys. Rev. Lett.* **96** 106802
[12] Schliemann J, Loss D and Westervelt R M 2005 *Phys. Rev. Lett.* **94** 206801
[13] Bernevig B A, Orenstein J and Zhang S-C 2006 *Phys. Rev. Lett.* **97** 236601
[14] Schliemann J, Egues J C and Loss D 2003 *Phys. Rev. Lett.* **90** 146801
[15] Scully M O, Shea R and McCullen J D 1978 *Phys. Rep.* **43** 485
[16] Scully M O, Lamb W E Jr and Barut A O 1987 *Found. Phys.* **17** 575
[17] Merzbacher E 1998 *Quantum Mechanics* 3rd edn (New York: Wiley)
[18] Wang Q 1987 *J. Phys. A: Math. Gen* **20** 5041
[19] Poon K M and Munoz G 1999 *Am. J. Phys.* **67** 547
[20] Feynman R 1965 *Quantum Mechanics and Path Integrals* 1st edn (New York: McGraw-Hill)
[21] Gottfried K 2004 *Quantum Mechanics: Fundamentals* 2nd edn (New York: Springer)
[22] Suzuki M 1983 *Physica* A **117** 103
[23] Truax D R 1985 *Phys. Rev.* D **31** 1988
[24] Fisher R A, Nieto N M and Sandberg V D 1984 *Phys. Rev.* D **29** 1107
[25] Zassenhaus H 1939 *Abh. Math. Sem. Univ. Hamburg* **13** 1
[26] Schwinger J 2001 *Quantum Mechanics* (Berlin: Springer)
[27] Barone F A, Boschi-Filho H and Farina C 2003 *Am. J. Phys.* **71** 483

Appendix D

Spin Dynamics for Wave Packets in Rashba Systems

This paper is published in Physical Review B **80** 235309 (2009).

Spin dynamics for wave packets in Rashba systems

Bailey C. Hsu* and Jean-François S. Van Huele†
Department of Physics and Astronomy, Brigham Young University, Provo, Utah 84602, USA
(Received 24 June 2009; revised manuscript received 2 November 2009; published 8 December 2009)

We explore spin dynamics for localized wave packets in Rashba systems using spin quantum propagators. We derive exact (one-dimensional) and approximate (two-dimensional) analytic expressions for the propagators and apply them to Gaussian wave packets to obtain localized solutions of systems manifesting Rashba interactions. We observe and describe the evolution of the wave packets. We identify characteristic structures in the wave-packet evolution and look for features with specific spintronics applications such as spin separation and spin accumulation. We discuss the relative importance of those features as a function of the Rashba coupling strength α and the width of the wave packet w. In particular, we find a trade off between spatial oscillation and global separation of the spin when varying α and w.

DOI: 10.1103/PhysRevB.80.235309 PACS number(s): 71.70.Ej, 73.21.Hb, 85.75.−d

I. INTRODUCTION

Spintronics is a promising technology where the focus is on manipulating the spin degree of freedom of electrons in addition to their charge.[1–4] Efficient spin injection, spin transport, and spin detection need to be achieved to insure the functionality of spintronics devices. Among the many areas of interest in spintronics, spin-orbit coupling (SOC) is an important mechanism to control spin dynamics without introducing an external magnetic field.[5] All spin-orbit coupled systems that have been proposed share one common characteristic: their Hamiltonians couple momentum and/or position operators to spin operators. These systems have been studied to exhibit various spin-dependent phenomena including spin-Hall effect,[6–8] quantum spin-Hall effect,[9] spin accumulation at the edge,[10] persistent spin-helix,[11,12] and *Zitterbewegung-like* motion for wave packets.[13,14] The presence of two or more incompatible (noncommuting) spin operators in the Hamiltonian adds a layer of dynamical complexity for electrons carrying specific spin components. Two widely discussed SOC contributions are the Rashba and the Dresselhaus effects.[15–17] The Rashba effect is the signature of structure inversion asymmetry present in quantum wells while the Dresselhaus effect is the signature of bulk inversion asymmetry present in zinc-blende structures lacking inversion symmetry. The spin degree of freedom in the Rashba system has also been proposed to construct a Rashba adder and more general functions of a spin logic circuits.[18–20]

Several treatments have been applied to analyze the spin dynamics inside Rashba systems: Heisenberg picture method,[13] linear-response theory,[21] fixed energy Green function,[22–24] direct numerical integration,[25,26] and density-matrix approach.[27] In this contribution we develop the quantum-mechanical spin propagator method from the Schrödinger equation for Rashba SOC interaction in one-dimensional (1D) and two-dimensional (2D) condensed-matter systems. The advantage of calculating the propagator separately is that it can be applied to any initial state. Rather than dealing with plane waves we choose to study localized solutions, in particular, spin-polarized Gaussian wave packets, which are interesting in their own right. For example, phenomena such as Zitterbewegung are known to be transient for wave packets[28] including in condensed-matter systems.[29,30] Results from Gaussian wave-packet dynamics have been obtained previously[13,26] and we mention how our results obtained using the propagator in closed forms compare with them. We also study the dependence of the results on the Rashba coupling strength (in the Hamiltonian) and on the localization (width of the wave packet). We display plots of the polarization at specific times while controlling these two parameters.

The paper is organized as follows: in Sec. II, we briefly introduce two analytic propagator construction methods. We give the exact analytic quantum propagators which we derived for the 1D Rashba system with harmonic confining potential. We also give approximate analytic quantum propagators based on the Trotter formula for the 2D Rashba system. In Sec. III, we first construct the spin densities in the 1D Rashba system by applying the specific analytic propagator to an initial Gaussian wave packet in space and polarized along specific directions and we identify four characteristic features. We then generate wave-packet evolutions numerically and highlight four new features of the spin densities in the 2D Rashba system. In the 2D case, in addition to changing the overall width of the wave packet, we also consider the effect of uneven widths in two dimensions on the result. In Sec. IV we discuss our results and make a qualitative comparison between different cases and by connecting to current spintronics research.

II. PROPAGATOR CONSTRUCTION

The propagator $K(x,x_0;t-t')$ gives the conditional transition amplitude between two position eigenstate vectors $|x\rangle$ and $|x_0\rangle$ over a time interval $t-t'$ such that $K(x,x_0;t-t')=\langle x|U(t-t')|x_0\rangle$, where $U(t-t')$ is the time-evolution operator.[31] Without loss of generality we set $t'=0$ in this paper. Because the Hamiltonians we consider involve spin operators, the propagators have a 2×2 matrix representation for spin-1/2 particles. We now proceed to construct analytic expressions of propagators using two different analytic methods applied to the 1D and 2D Rashba systems, respectively.

The Hamiltonian for the confined 1D Rashba system is

$$\mathcal{H} = \frac{p_x^2}{2m} - \frac{\alpha}{\hbar}\sigma_y p_x + \frac{1}{2}m\omega^2 x^2, \tag{1}$$

where α is the experimentally controlled Rashba coupling strength, σ_y is the Pauli spin operator, and ω is the confinement strength. We have obtained exact analytic expressions for the propagator for the confined ($\omega \neq 0$) and the unconfined ($\omega=0$) case using an analytic method based on the manipulation of noncommuting operators in exponentials.[32,33] After lengthy but straightforward calculations one obtains the 1D confined Rashba propagator $K_{1D}^c(x,x_0;t)$

$$K_{1D}^c = \sqrt{\frac{m\omega}{2\pi i\hbar \sin \omega t}}\exp\left\{\frac{im}{2\hbar}\left[(x^2+x_0^2)\omega\cot\omega t - 2xx_0\omega\csc\omega t - \frac{2\alpha\sigma_y}{\hbar}(x-x_0) + \frac{\alpha^2}{\hbar^2}t\right]\right\}. \tag{2}$$

By setting $\omega=0$ in the Hamiltonian in Eq. (1), we also derive the 1D unconfined Rashba propagator $K_{1D}^u(x,x_0;t)$

$$K_{1D}^u = \sqrt{\frac{m}{2\pi i\hbar t}}\exp\left[-\frac{m\left(x-x_0+\frac{\alpha\sigma_y t}{\hbar}\right)^2}{2i\hbar t}\right]. \tag{3}$$

We note that the expression for K_{1D}^u is also recovered in the unconfined limit $\omega\to 0$ in the propagator in Eq. (2). It can be checked that the corresponding propagators for vanishing Rashba term ($\alpha=0$) K_{1D}^c in Eq. (2) and K_{1D}^u in Eq. (3) reduce to the 1D simple harmonic-oscillator propagator and the 1D free-particle propagator, respectively.[31]

The Hamiltonian for the 2D Rashba system with parabolic confinement in x and unconfined in y is

$$\mathcal{H} = \frac{p_x^2+p_y^2}{2m} + \frac{\alpha}{\hbar}(p_y\sigma_x - p_x\sigma_y) + \frac{1}{2}m\omega^2 x^2. \tag{4}$$

The presence of two noncommuting Pauli matrices in the Hamiltonian makes it more challenging to obtain the propagator in closed form.[27] Therefore we construct approximate analytic expressions for the propagator in the confined ($\omega \neq 0$) and the unconfined ($\omega=0$) case using an analytic method based on the Trotter formula generalized to spin systems.[34] The Trotter formula for two noncommuting operators a and b, exact to $\mathcal{O}(\tau^3)$, gives

$$e^{-\tau(a+b)} = e^{-\tau a/2}e^{-\tau b}e^{-\tau a/2} + \mathcal{O}(\tau^3). \tag{5}$$

By replacing a and b with the potential term V and the kinetic term T, respectively, in the time-evolution operator $U(t)=e^{-it(T+V)/\hbar}$ and by setting $\tau=it/\hbar$, the propagator K is obtained by projecting the time-evolution operator $U(t)$ on position eigenvectors

$$K = \langle x|U(t)|x_0\rangle \approx \langle x|e^{-itV/2\hbar}e^{-itT/\hbar}e^{-itV/2\hbar}|x_0\rangle. \tag{6}$$

A Trotter formula exact to $\mathcal{O}(\tau^5)$ can be used to give exact analytical result for the free particle and the linear potential problem. For the confined Rashba potential in Eq. (4), we evaluate the propagator correctly to order τ^3. In Eq. (4), noncommutativities appear both between position and momentum operators and between Pauli matrices. Instead of setting a and b equal to the potential and kinetic terms, respectively, we extract from Eq. (4) the parts for which the propagator can be found analytically [in analogy to Eq. (2) in the x direction and to Eq. (3) in the y direction] and set them equal to b, such that $b=\frac{\mathbf{p}^2}{2m}+\frac{\alpha}{\hbar}(p_y-p_x)\sigma_x+\frac{m\omega^2x^2}{2}$ and $\mathbf{p}^2=p_x^2+p_y^2$. The Trotter formula can now be applied with the remaining terms set equal to a, namely, $a=\frac{\alpha}{\hbar}p_x(\sigma_x-\sigma_y)$.

After some algebraic manipulations, the propagator $K_{2D}^c(x,x_0,y,y_0;t)$ is obtained for the 2D (semi)confined Rashba system

$$K_{2D}^c \approx \sqrt{\frac{\omega}{t\sin\omega t}}\frac{m}{2\pi i\hbar}\exp\left\{\frac{im}{2\hbar}\left[\left(x^2+x_0^2+\frac{\alpha^2t^2}{\hbar^2}\right)\times\omega\cot\omega t - \left(2xx_0+\frac{\alpha^2t^2}{\hbar^2}\right)\omega\csc\omega + \frac{\alpha^2t}{\hbar^2} + \omega(\cot\omega t+\csc\omega t)\frac{\alpha t}{\hbar}(\sigma_x-\sigma_y)(x-x_0) - \frac{2\alpha\sigma_x}{\hbar}(x-x_0) + \frac{\left(y-y_0+\frac{\alpha\sigma_x t}{\hbar}\right)^2}{t}\right]\right\}. \tag{7}$$

By setting $\omega=0$ in the Hamiltonian in Eq. (4), we derive the 2D unconfined Rashba propagator $K_{2D}^u(x,x_0;t)$

$$K_{2D}^u \approx \frac{m}{2\pi i\hbar t}\exp\left\{-\frac{m}{2i\hbar t}\left[\left(x-x_0+\frac{\alpha\sigma_y t}{\hbar}\right)^2 + \left(y-y_0-\frac{\alpha\sigma_x t}{\hbar}\right)^2\right]\right\}. \tag{8}$$

We can also recover the expression K_{2D}^u in the unconfined limit $\omega\to 0$ of the propagator in Eq. (7). The corresponding propagators for vanishing Rashba terms ($\alpha=0$) can be checked: K_{2D}^c in Eq. (7) and K_{2D}^u in Eq. (8) reduce to the 2D simple harmonic oscillator and 2D free-particle propagator, respectively.[31]

Once the propagator is obtained, we can obtain the wave-packet evolution $\psi(x,t)$ by applying it to an initial wave packet $\psi(x_0,0)$

$$\psi(x,t) = \int_{-\infty}^{\infty} K(x,x_0;t)\psi(x_0,0)dx_0. \tag{9}$$

In this work we choose $\psi(x_0,0)$ to be a spinor with Gaussian distribution in space centered at $x_0=0$ and with width w, such that $\psi(x_0,0)=\frac{1}{\sqrt{\pi w}}\exp(-x_0^2/2w^2)(\chi|\uparrow\rangle+\xi|\downarrow\rangle)$, where $|\uparrow\rangle$ and $|\downarrow\rangle$ are up-in-z and down-in-z spin states with constant coefficients χ and ξ chosen to satisfy $|\chi|^2+|\psi|^2=1$. Because of the linearity of the Schrödinger equation and of the propagator, the method can be applied to spinors with different spatial localizations for spin-up and spin-down particles. In particular, it can be applied repeatedly for arbitrary times in spin separating dynamics without further modifications.

We choose the wave packets to have a zero net momentum in x and in y. The effect of adding an initial momentum to the wave packet adds an overall velocity to the individual spin components. Since S_y is a constant of the motion in the

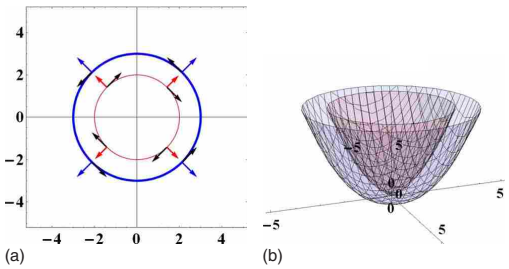

FIG. 1. (Color online) (a) The 2D electronic eigenstates for a Rashba SOC system in a momentum representation. The horizontal and the vertical axes are p_x and p_y, respectively. We label the net momentum with (radial) blue and red arrows and the eigenspinors with (azimuthal) black arrows. (b) The dispersion relation in the Rashba system. The colors of two parabola (blue and red) match the ones of two concentric circle in (a).

1D case, the dynamics is otherwise unaffected when plotting the y polarization. On the other hand, for the x and z polarizations, there will be additional features on top of a global translation in x, as is to be expected for a Rashba interaction defined in the rest frame of the material. These can be obtained following exactly the same procedure and we do not discuss them systematically in this paper. The absence of position dependence in the unconfined Rashba system implies that p_x and p_y are constants of the motion.

III. RESULTS

In this section we apply the propagator to localized wave packets in two situations: the 1D and the 2D Rashba systems. In each situation we consider both unconfined and confined cases. The eigenstates and eigenvalues for the Rashba system are provided in Fig. 1. In Fig. 1(a) two concentric circles correspond to two dispersion relations arising from the Rashba SOC for a fixed energy. Eigenspinors and momentum eigenvalues are given by azimuthal and radial arrows. In all cases, we consider the effect on the spin dynamics of changing two parameters: the Rashba coupling strength α and the width w of the initial wave packet. We provide plots with natural units $\hbar=1$, $m=1$. Note also that since we are interested in the influence of the width on the dynamics, we select an absolute length unit d such that the width w and the positions x and y are all expressed in terms of d rather than being correlated as a result of the choice of units. We also provide the units for the following variables: α in units of $\hbar^2/md$ and t in units of $md^2/\hbar$. This allows us to recover experimentally accessible values of the Rashba strength α by substituting realistic value of $\hbar$ and m and by choosing an appropriate length unit d. This also determines a unit width and a unit time and therefore realistic orders of magnitude for time and for wave packet width. In Sec. IV, we check this explicitly for an absolute length unit of 200 nm in 1D and verify that the corresponding Rashba strength is experimentally accessible. We then give an explicit quantitative description of how to find an appropriate value for d to match minimum and maximum experimentally accessible values of the Rashba strength in 2D.

We label spin states using the following convention: the up-in-x ($|\uparrow\rangle_x$) and down-in-x ($|\downarrow\rangle_x$) spin states correspond to a balanced superpositions of up-in-z ($|\uparrow\rangle$) and down-in-z ($|\downarrow\rangle$) spin states

$$|\uparrow\rangle_x = \frac{|\uparrow\rangle + |\downarrow\rangle}{\sqrt{2}}, \quad |\downarrow\rangle_x = \frac{|\uparrow\rangle - |\downarrow\rangle}{\sqrt{2}} \tag{10}$$

and similarly for up-in-y ($|\uparrow\rangle_y$) or down-in-y ($|\downarrow\rangle_y$) spin states

$$|\uparrow\rangle_y = \frac{|\uparrow\rangle + i|\downarrow\rangle}{\sqrt{2}}, \quad |\downarrow\rangle_y = \frac{|\uparrow\rangle - i|\downarrow\rangle}{\sqrt{2}}. \tag{11}$$

We plot the spin density $\langle \mathbf{S}\rangle(x,y)$ corresponding to the local expectation values of the spin operator.

A. One-dimensional Rashba system

Here we consider successively the unconfined and parabolically confined 1D Rashba system. For these 1D Rashba systems we select the x direction, corresponding to a horizontal line in Fig. 1(a), to make our analysis. The propagators used in this section are obtained in closed form as explained in Sec. II. An initial up-in-z spin state is chosen for all cases in the 1D Rashba system. We have observed four interesting features which we refer to as: spin separation (SS), bamboo-shooting structure (BSS), persistent spin helix structure (PSHS), and spin accumulation (SA). Note that SS, BSS, and PSHS are observed in the unconfined case and SA is observed in the confined case. We now discuss each of these features separately.

1. Spin separation

The Hamiltonian in Eq. (1) in the unconfined limit $\omega \to 0$ leads directly to two eigenspinors of S_y that travel with opposite velocities. On Fig. 1(a) this would correspond to red and blue arrows lying on the horizontal axis and pointing away from the center. When we add the opposite but unequal momentum contributions for a given spin in the inner and outer circles we see that spin up dominates on the right and spin down likewise on the left of the figure. This leads, for a localized wave packet, to a separation in x of two distinct y component of the spin as can be seen from the plot of $\langle S_y\rangle(x)$ in Fig. 2. We checked numerically that we can increase the rate of separation by increasing α.

Indeed, by increasing α we enlarge the difference between the two eigenenergies (the difference in radius of the circles). This in turn leads to a larger overall net momentum for each spin component and thus to a more rapid separation between the two spin components. The spreading of the wave packets depends both on α and w. The effect of w on the spreading is similar to that for the usual quantum spreading of free-particle wave packets: a small w leads to faster spreading. We notice that a smaller w also leads to faster spin separation as a result of the faster spreading. However the price to be paid is that the amplitude decreases as $\sqrt{1/(1+t^2/w^4)}$. As for α, we see slightly more spreading of the wave packet for

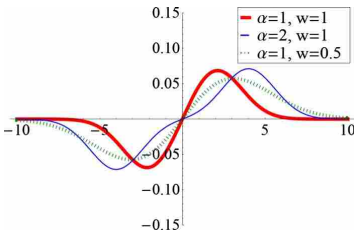

FIG. 2. (Color online) Spin density $\langle S_y\rangle(x)$ as a function of position x (in units of d) at $t=2$ (in units of $md^2/\hbar$) with different sets of α (in units of $\hbar^2/md$) and w (in units of d).

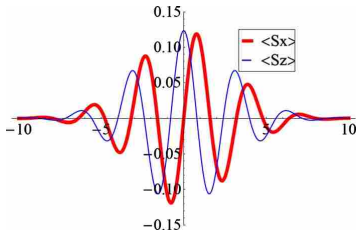

FIG. 4. (Color online) Spin densities $\langle S_x\rangle(x)$ and $\langle S_z\rangle(x)$ as a function of position x (in units of d) at $t=2$ (in units of $md^2/\hbar$), $w=0.5$ (in units of d), and $\alpha=1$ (in units of $\hbar^2/md$).

larger α. Related spin separation can be seen, for example, in the total densities ρ in 1D wave-packet dynamics study (See Ref. 26).

2. Bamboo-shooting structure

The BSS is observed in Fig. 3 for initial spins that are not eigenspinors of the Hamiltonian in Eq. (1) with $\omega\to 0$, such as the z component of the spin. Noneigenspinors can be expressed as superpositions of eigenspinors. Therefore an oscillation between the two eigenmodes arises. This has been referred to as a *Zitterbewegunglike* motion, an oscillatory motion between positive and negative energies as derived from Dirac's equation for relativistic electrons. Such intrinsic oscillations have been related to the occurrence of intersubband mixings[35] in contrast to the extrinsic oscillation which is caused by spin-dependent scattering.[36] The packet is extending in both directions at a constant velocity and oscillations extend (without moving) further at the same time. In this way a BSS, a successive "rise" of polarization at specific locations, is formed as the packet evolves.

As we increase α, we see fewer intrinsic oscillations: they occur only close to the original location of the wave packet. Indeed, a large α significantly decreases the overall amplitude of the oscillation. These oscillations can be related to the eigenspinors of the Hamiltonian traveling with opposite velocities. By measuring the noneigenspinors which are superpositions of eigenspinors, we find out that these eigenspinors tend to travel with opposite velocities. For relatively small α, the eigenspinors travel slower. Interference effects are more prominent for noneigenspinors due to the decreased propagation speed in opposite directions. As for the effect of w on intrinsic oscillations, we observe more intense oscillations for more localized packets.

We also observe an attenuation in time of the BSS feature. To quantify the transient nature of the feature that we observe, we calculate the exponential decay of the center of the wave packet ($x=0$) and find

$$\langle S_z\rangle(0) = \frac{1}{\pi w^2}\sqrt{\frac{1}{1+\left(\frac{\hbar t}{mw^2}\right)^2}}\exp\left(-\frac{m^2t^2\alpha^2w^2}{m^2w^4\hbar^2+t^2\hbar^4}\right). \tag{12}$$

The contribution of the Rashba interaction (i.e., α-dependent factor) can be separated from the ordinary free-particle spreading. At short times we get a Rashba exponential attenuation proportional to $\exp(-\Gamma^2t^2)$, where $\Gamma=\frac{\alpha}{w\hbar}$. The value of the attenuation time Γ^{-1} is on the order of the picosecond, which is similar to the value found in the literature.[29] The attenuation times in Rashba systems are significantly longer than the Zitterbewegung decay times found in graphene and carbon nanotube work, as expected from the characteristic length scales involved.[30]

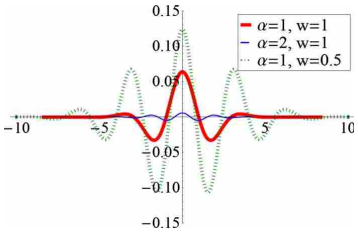

FIG. 3. (Color online) Spin density $\langle S_z\rangle(x)$ as a function of position x (in units of d) at $t=2$ (in units of $md^2/\hbar$) with different sets of α (in units of $\hbar^2/md$) and w (in units of d).

3. Persistent spin helix structure

By representing $\langle S_x\rangle(x)$ and $\langle S_z\rangle(x)$ on the same plot in Fig. 4, we see that the spin polarization correlates with the x position in what constitutes a spin helix. Since the packet is extending with a constant velocity in the x direction, its spin takes on the value given by $\langle S_x\rangle(x)$ and $\langle S_z\rangle(x)$ and therefore performs helicoidal motion as the packet spreads out. It is interesting to note that $\langle S_x\rangle(x)$ and $\langle S_z\rangle(x)$ are shifted in space with respect to each other. S_y corresponds to a conserved quantity leading to persistent behavior of the spin. This phenomenon has been predicted by Bernevig *et al.*[11] and has been recently observed by Koralek *et al.*[37] The period of the helix can be controlled by α: for bigger α the spatial period decreases. As in the case of the BSS, the PSHS disappears as a result of vanishing oscillations for increasing α. The persistent helix structure can be seen in other cases, such as the systems with combined Rashba and Dresselhaus effects balanced in strength. It has been shown that the combined system corresponds to a global spin rotation of a one-dimensional Rashba system.[11] We notice that having started

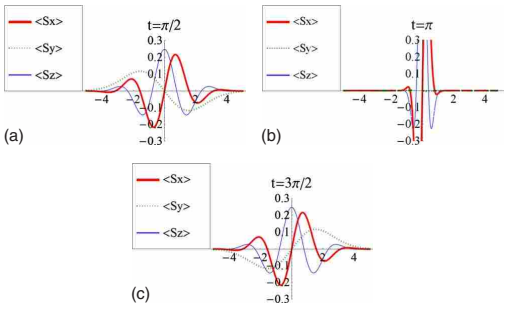

FIG. 5. (Color online) Spin densities $\langle S_x\rangle(x)$, $\langle S_y\rangle(x)$, and $\langle S_z\rangle(x)$ as a function of position x (in units of d) with $\alpha=1$ (in units of $\hbar^2/md$), $w=0.5$ (in units of d), and $\omega=1$ (in units of $\hbar/md^2$) evaluated at three different times (in units of $md^2/\hbar$).

from a localized Gaussian wave packet with finite width, the packet spreads as it moves and accordingly $\langle S_x\rangle(x)$ and $\langle S_z\rangle(x)$ decrease away from $x=0$. This feature is not to be attributed to a lack of persistence of the correlation between the spin orientation and the x position but to a decrease in the wave packet for larger distances. The spin helix is effectively transformed into a double Gaussian-shaped conical surface. In order to enhance the PSHS arising from the noneigenspinors, we have to reduce the spin-separation feature from the eigenspinors. This means that we can choose either a smaller α or a more localized wave packet, i.e., a smaller width w, to achieve the desired effect. The shift between the x and z polarizations has also been observed in time evolution of spin expectation values (See Ref. 13).

4. Spin accumulation

Confinement can cause specific spin components to accumulate at edges with either a hard wall potential or a harmonic-oscillator potential.[10] When we apply the confined propagator K_{1D}^c on the wave packet, we observe accumulations of specific spin components at the boundary in addition to the three features discussed above. Accumulation means that a given spin component appears at the boundary without oscillating from left to right.

We find two kinds of spin accumulation mechanisms: same spin components and opposite spin components at the boundary. Figure 5 exhibits the spin dynamics under the influence of a confining potential with an initial up-in-z spin state. We observe that for the eigenspinors, $\langle S_y\rangle(x)$ oscillates from left to right like a simple harmonic oscillator. For the noneigenspinors, we see that the z component oscillates with a reflection symmetry (even symmetry) around the $x=0$ and the same z component accumulating at the edge. In contrast, the x component oscillates without a reflection symmetry (odd symmetry) along the center line, leading to opposite spin components accumulating at the boundary. Note that the spin accumulation is only obtained for relatively small w. A possible reason is found in the faster spreading that follows from higher localization for fixed confining strength. The effect is also enhanced for small α due to the increase in the oscillations.

B. Two-dimensional Rashba system

We now proceed to analyze the wave-packet dynamics in the two-dimensional Rashba system. We consider both confined and unconfined systems. We use Trotter's formula from Sec. II to find the propagators. We obtain the evolution using Monte Carlo integration in Eq. (9).

Note that none of the three operators S_x, S_y, and S_z have global eigenspinors in momentum space in the 2D Rashba system. It is straightforward to show that the eigenspinors are momentum dependent, a fact which can also be seen in Fig. 1(a). In 1D Rashba systems, we confined the momentum distribution to be on either the x or the y axis leading to specific joint global eigenspinors of either the Hamiltonian and S_y or the Hamiltonian and S_x. In two-dimensional cases, such global eigenspinors do not exist. If the initial spin comes with a fixed momentum corresponding to a plane wave in a free-particle approximation, the eigenspinors can be identified from Fig. 1. Our task is to provide the Rashba dynamics of a Gaussian wave packet in coordinate space. The coordinate wave packet covers different sets of momentum-dependent eigenspinors as seen in Fig. 1(a) and therefore, the 2D oscillation originating from the superpositions in 2D Rashba systems has a more intricate structure. We observe four interesting features for four sets of initial spin states and measurements of the specific spin densities: ripple formation structure (RFS), triangular oscillations (TO), asymmetric spin rotations (ASR), and diagonal symmetry structure (DSS). We consider successively the effect of varying the Rashba coupling strength α, and the widths w_x and w_y of the initial Gaussian wave packet as we discuss these features.

1. Ripple formation structure

RFS is observed when the initial spin state is up-in z and the spin density $\langle S_z\rangle(x,y)$ is measured after a time t. As can be seen in Fig. 6, the wave packet exhibits peaks and troughs corresponding to regions of up-in-z and down-in-z spins.

We observe the effect of increasing the Rashba strength by comparing Figs. 6(a) and 6(b). The density of ripples increases with α and the up-in-z spin travels radially out. By increasing the width equally in two dimensions, we see fewer ripples for a fixed region of space when comparing Figs. 6(a) and 6(e). This is similar to the 1D case where multiple oscillations occur for highly localized wave packets. By changing the ratio of w_x and w_y we see that we can make the ripples less prominent in one direction or the other, as seen in Figs. 6(c) and 6(d).

We observe symmetry patterns in Fig. 6 which we now proceed to discuss. Within our numerical accuracy, we obtain azimuthal symmetry for the symmetric initial wave packets in Figs. 6(a) and 6(b). For unequal initial wave-packet localization in Figs. 6(c) and 6(d), we observe that the two figures are connected by a $\pi/2$ rotation relating the direction of enhanced fringes.

We notice that the direction along which the successive fringes appear are not purely horizontal [Fig. 6(c)] or vertical [Fig. 6(d)]. This effect can be understood from a semiclassical argument which indicates that a spin and momentum-dependent force induces a distortion. By working out the

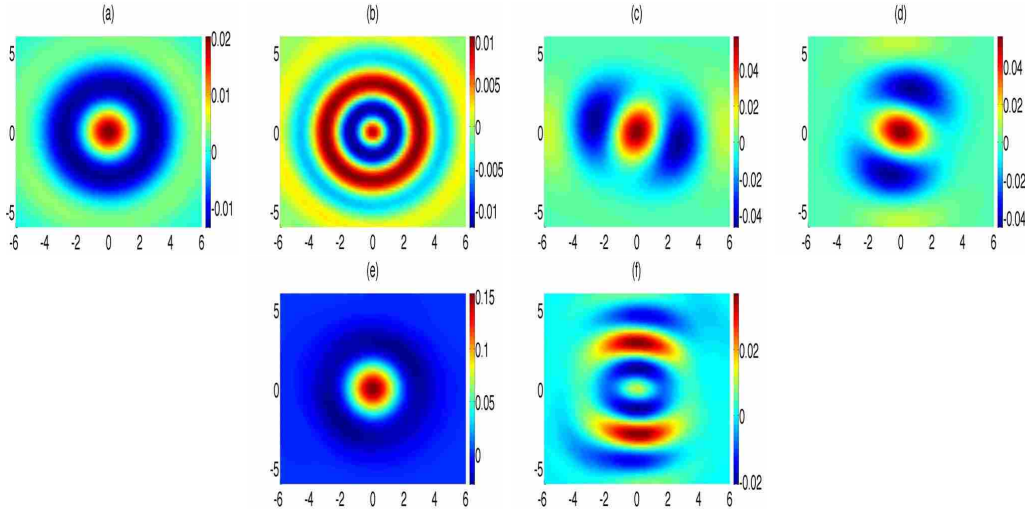

FIG. 6. (Color online) Spin-density $\langle S_z\rangle(x,y)$ contour plots for an initial up-in-z spin state evaluated at $t=3$ (in units of $md^2/\hbar$) with different α (in units of $\hbar^2/md$), w_x, and w_y (in units of d). (a) $\alpha=0.5$, $w_x=w_y=1.0$, (b) $\alpha=1.0$, $w_x=w_y=1.0$, (c) $\alpha=0.5$, $w_x=1.0$, $w_y=2.0$, (d) $\alpha=0.5$, $w_x=2.0$, $w_y=1.0$, (e) $\alpha=0.5$, $w_x=2.0$, $w_y=2.0$, and (f) $\alpha=1.0$, $w_x=2.0$, $w_y=1.0$.

Heisenberg equations of motion for the unconfined Rashba Hamiltonian, we obtain

$$\dot{p}_x = 0, \quad \dot{p}_y = 0, \quad \dot{x} = \frac{p_x}{m} - \frac{\alpha\sigma_y}{\hbar}, \quad \dot{y} = \frac{p_y}{m} + \frac{\alpha\sigma_x}{\hbar},$$

$$\dot{\sigma}_x = -\frac{2\alpha p_x \sigma_z}{\hbar^2}, \quad \dot{\sigma}_y = -\frac{2\alpha p_y \sigma_z}{\hbar^2},$$

$$\dot{\sigma}_z = \frac{2\alpha p_x \sigma_x}{\hbar^2} + \frac{2\alpha p_y \sigma_y}{\hbar^2}. \tag{13}$$

By considering the semiclassical force in the x direction, one shows that

$$F_x = m\ddot{x} = -\frac{m\alpha\dot{\sigma}_y}{\hbar} = \frac{2m\alpha^2 p_y \sigma_z}{\hbar^3} \tag{14}$$

and thus the force is both p_y and σ_z dependent, corresponding to the result of Fig. 6(d). This resembles a spin-dependent Coriolis force. As we observe from the figure, the upper and the lower half planes feel equal and opposite forces which leads to the distortion (since the wave packet itself is dispersing in two opposite y direction). A similar argument can be made using the vertical force F_y for Fig. 6(c). We note that the spin σ_z in Eq. (14) can be found for initial spin polarization along z to be $\sigma_z(t) = \sigma_z(0)\cos(2\alpha t\sqrt{p_x^2+p_y^2}/\hbar^2)$ so that the α dependence of the Coriolis force is not simply proportional to the strength of the Rashba coupling strength.

By comparing Figs. 6(d) and 6(f), we see again that a larger α causes the number of fringes to increase. The larger α value leads to the up-in-z spin traveling further from its initial central location in analogy to what we described in Fig. 6(b).

Recall that in the 1D Rashba system, the superposition of the two eigenstates represents an oscillation in space. Similarly in the 2D case, S_z does not have a global eigenspinor of the system, therefore it exhibits BSS in two dimensions with equal weights from x and y leading to circular ripple formation. The ripples appear for both large and small α, however, the crest of the ripple changes. For small α, the crest of the $\langle S_z\rangle(x,y)$ stays at the center with the wave propagating out similar to the BSS structure in 1D. As for large α, similarly to the case in 1D where noneigenspinors travel in opposite directions, $\langle S_z\rangle(x,y)$ travels out as a circular wave with a decreased amplitude. This can also be seen in the 1D BSS where smaller oscillations occur for larger α. Both eigenspinors of S_z travel with two larger group velocities. It should also be noted that more ripples appear in a fixed region of space for a larger α. This is consistent with the BSS discussed in Sec. III A 2. Circular ripples in 2D have been predicted for Gaussian wave-packet evolution.[26]

2. Triangular oscillations

Starting with an initial up-in-x spin state and measuring the spin density $\langle S_x\rangle(x,y)$, we observe TO from the contour plots in Fig. 7. By analogy with our discussion in 1D we know that the up-in-x spin state has a downward momentum when a y-localized wave packet is considered. The inclusion of x localization complicates the dynamics. There are two effects governing the dynamics: fringe formation in the x

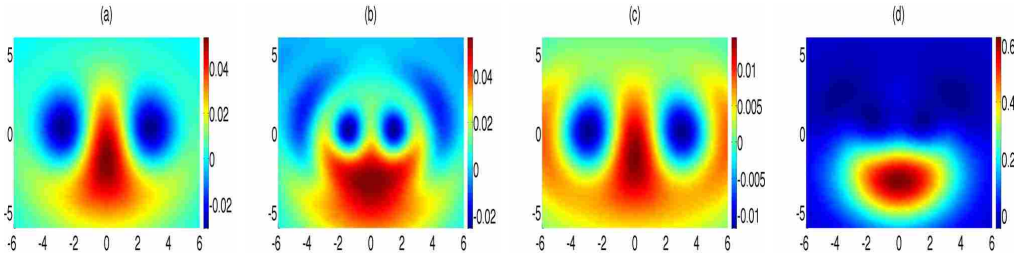

FIG. 7. (Color online) Spin-density $\langle S_x\rangle(x,y)$ contour plots for a initial up-in-x spin state evaluated at $t=3$ (in units of $md^2/\hbar$) with different α (in units of $\hbar^2/md$), w_x, and w_y (in units of d). (a) $\alpha=0.5$, $w_x=w_y=1.0$, (b) $\alpha=1.0$, $w_x=w_y=1.0$, (c) $\alpha=0.5$, $w_x=0.5$, $w_y=1.0$, and (d) $\alpha=1.0$, $w_x=2.0$, $w_y=2.0$.

direction and uniform downward (toward negative y) motion of the up-in-x wave packet.

In Fig. 7(a), it is clear that the spin is flipped on the horizontal axis on either side of the original location. This is a result of fringe formation as in the BSS in the 1D Rashba system. In Fig. 7(b), we see more fringes forming when we enlarge α. A larger α also leads to more downward momentum for the up-in-x spin. It is interesting to note that it is the part of the wave packet localized closest to the y axis that is moving downward. We observe the effect of even widths in Fig. 7(c), where we have a wave packet highly localized in x. By comparing Fig. 7(a) with Fig. 7(c) (α fixed), we see more fringes forming in the x direction. Figure 7(d) illustrates the fact that when we have a larger α and overall less-localized wave packets, again we see fewer fringes than in Fig. 7(b). In Fig. 7(d) the wave packet has moved further downward than in Fig. 7(c) due to a larger α which is consistent with previous observations and a faster downward momentum for the up-in-x component, which is consistent with all the observations in this feature.

The interplay between fringe formation and uniform downward motion leads to various dynamics. The larger α is, the more fringes (shorter wavelength) will form in the x direction, which is consistent with 1D BSS. At the same time, a larger α will lead to more momentum for the eigenspinors, which allows up-in x to move faster downward along the y axis. With a fixed α, the fringes can be enhanced (or suppressed) by selecting appropriate widths for the wave packet. In the case considered, where the fringes are formed only in the x direction, we need more (less) localization in x (y). The same applies in the y direction. This feature can also be observed if starting with a down-in-x spin. This choice leads to the vertical flipping of the result shown in Fig. 7. It should also be noted that this feature can be extended to the case where we have an initial spin state up-in y and we measure the $\langle S_y\rangle(x,y)$. The result would correspond to a $\pi/2$ rotation of the graphs shown in Fig. 7.

3. Asymmetric spin rotation

Starting with an initial up-in-z spin state and measuring the in-plane spin density $\langle S_x\rangle(x,y)$ or $\langle S_y\rangle(x,y)$, we observe an ASR in the contour plots of Fig. 8. Since an up-in-z spin state can be written as a superposition of either in x or y in spin space, measuring the dynamics of either x or y creates an interesting phenomenon. ASR is a rotation that should not be associated with the usual rotation in the x-y plane. By measuring the x component, we first immediately observe the two components separating in y. This separation is similar to the 1D localization case. The presence of the other dimension pulls the spin toward the other direction. As a result, the two opposite spin components start to perform ASR. ASR is a manifestation of the existence of a spin torque.[38]

It is straightforward to show that the rotation operator L_z is not a conserved quantity in the 2D unconfined Rashba system described by the Hamiltonian in Eq. (4) with $\omega=0$. Instead L_z+S_z is a conserved quantity in the system. It is also interesting to note that by providing an initial up-in-z spin state, we see a counterclockwise ASR while a clockwise ASR is observed for an initial down-in-z spin state. Again, there are two competing dynamical effects in this case: one is the fringe formation and the other is the motion of the eigenspinors. The fringe formation for the eigenspinors of S_x appears on the horizontal axis. The motion of the two eigenspinors is upward and downward, respectively, as can be seen in Fig. 1(a).

In Figs. 8(a) and 8(b), we see the effect of increasing α for a highly localized wave packet. Again, a larger α leads to a larger momentum for the two eigenspinors of S_x. A larger α also leads to more fringes as discussed in the previous two features. Therefore with the combination of these two effects for a larger α, we see a "banana cluster" forming up and down in Fig. 8(b). We show the effect of uneven widths in Fig. 8(c), where the high localization in x leads to more fringes in the x direction. By comparing Figs. 8(c) and 8(d), we see that the effect of increasing α leads to even higher fringe concentration. In Fig. 8(e), the fringes become less prominent as the wave packet is less localized. By comparing Figs. 8(e) and 8(f) we see that stronger upward and downward motion inhibits ASR. Finally we note that this feature of the spin density $\langle S_x\rangle(x,y)$ can also be observed for the spin density $\langle S_y\rangle(x,y)$ as a result of the symmetry of the Hamiltonian in Eq. (4) when $\omega=0$.

4. Diagonal symmetry structure

DSS is observed with an initial (x or y) in-plane spin state and a measurement of the other (y or x) in-plane components.

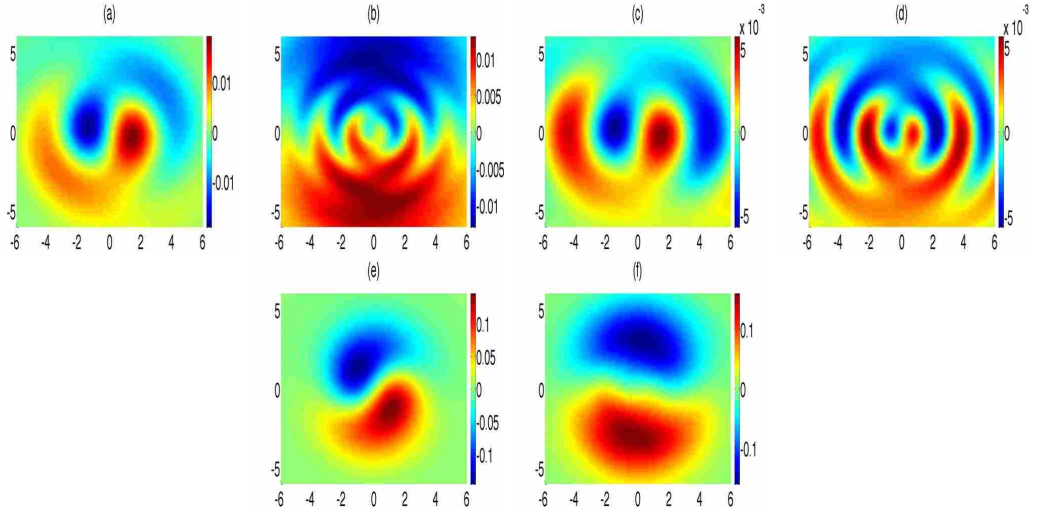

FIG. 8. (Color online) Spin-density $\langle S_x \rangle(x,y)$ contour plot for an initial up-in-z spin state evaluated at $t=3$ (in units of $md^2/\hbar$) with different α (in units of $\hbar^2/md$), w_x, and w_y (in units of d). (a) $\alpha=0.5$, $w_x=w_y=1.0$, (b) $\alpha=1.5$, $w_x=w_y=1.0$, (c) $\alpha=0.5$, $w_x=0.5$, $w_y=1.0$, (d) $\alpha=1.0$, $w_x=0.5$, $w_y=1.0$, (e) $\alpha=0.5$, $w_x=w_y=2.0$, and (f) $\alpha=1.0$, $w_x=w_y=2.0$.

For small α, we see two opposite y components of the spin moving downward and separating in the x direction. In the upper half of Fig. 9(a) the spin projection is reversed but less pronounced. This resembles a "four-leaf clover" structure. The up-in-y domain is along the main diagonal ($x=-y$) and the down-in-y domain is along the other diagonal ($x=y$). Although not perfect, the symmetry in Fig. 9 is based on the diagonals. The reflection symmetry does not exist about the x axis but about the two diagonal $x=y$ and $x=-y$ axes instead, corresponding to the traveling direction of two opposite spin components for larger α in Fig. 9(d).

As for the effect of localization, we see fewer fringes along the two diagonal lines for larger overall width of the wave packet. When changing the ratio of the horizontal and vertical widths, the effect is less significant than what we observed in other cases. This follows from the fact that the width does not correspond to the orientation of the fringes. By comparing Figs. 9(c) and 9(d), we see that the up-in-y and down-in-y components travel on the diagonal axes due to the combined effects of downward motion contributed from initial spin (up-in x) and of horizontal motion contributed from the measurement for the eigenspinors of S_y as can be checked in Fig. 1(a).

Lastly, we consider a 2D Rashba system with inclusion of a confining harmonic-oscillator potential in the x direction, as an illustration of the use of propagators in 2D confined systems. We see that the x confinement distorts the initially symmetric wave packets in Fig. 10(a) compared to the unconfined packet in Fig. 6(a). The unequal width in x and y still leads to additional ripples in Fig. 10(b) in analogy to Fig. 6(d) but now the confinement limits the spread of the wave packet in the x direction.

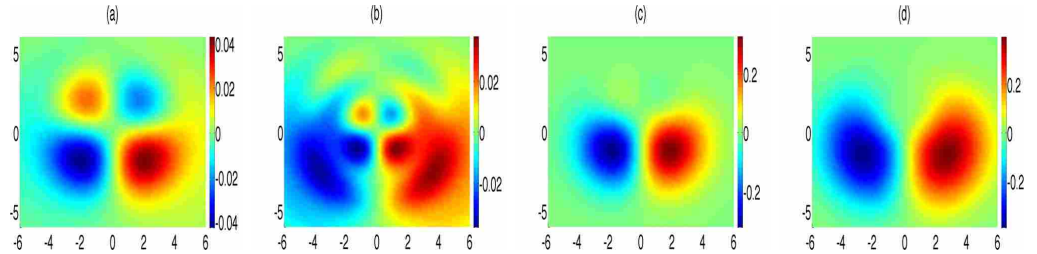

FIG. 9. (Color online) Spin-density $\langle S_y \rangle(x,y)$ contour plot for an initial up-in-x spin state evaluated at $t=3$ (in units of $md^2/\hbar$) with different α (in units of $\hbar^2/md$), w_x, and w_y (in units of d). (a) $\alpha=0.5$, $w_x=w_y=1.0$, (b) $\alpha=1.0$, $w_x=w_y=1.0$, (c) $\alpha=0.5$, $w_x=2.0$, $w_y=2.0$, and (d) $\alpha=1.0$, $w_x=2.0$, $w_y=2.0$.

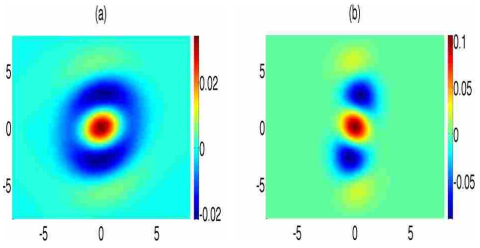

FIG. 10. (Color online) Spin-density $\langle S_z\rangle(x,y)$ contour plot for a initial up-in-z spin state evaluated at $t=3.0$. (a) $\alpha=0.5$, $\omega=0.5$, $w_x=w_y=1.0$ and (b) $\alpha=0.5$, $\omega=0.5$, $w_x=2.0$, $w_y=1.0$.

IV. DISCUSSION

We have plotted the spin densities $\langle S_x\rangle$, $\langle S_y\rangle$, and $\langle S_z\rangle$ for evolved Gaussian wave packets with different widths and initial spin states using the Rashba propagators with or without harmonic confinement and with different values of Rashba coupling strength α. In general, the plots show localized wave packets which have undergone spin-dependent separation, deformation, and spreading. They indicate where in space specific values of the spin operator components can be expected. The plots thus give a direct picture of polarization density.

All figures in this work are presented in scaled units which can be converted to realistic values that can be used to compare with experimental data. This can be achieved either by selecting an appropriate unit length d in the 1D case or by fitting d to recover specific values of α in the 2D case, with particular interest in recovering experimentally accessible values.

For example, in the 1D case, if we take the effective mass $m=0.05m_e$ (Ref. 26) and an absolute length unit $d=200$ nm, we can obtain a unit value of $\alpha=7.645\times10^{-12}$ eV m (bold and dotted lines in Figs. 2–5) two units of α, 1.529×10^{-11} eV m (thin line in Figs. 2 and 3) and a unit of time equal to $t=17.2$ ps. These values of α lie in the range of experimentally accessible Rashba strengths.[1] This choice also corresponds to wave packet widths $w=200$ nm (bold and thin lines in Figs. 2 and 3) or $w=100$ nm (dotted lines in Figs. 2–5), which are also in agreement with values found in the literature.[29] Using these values we obtain identical plots to those presented in Figs. 2–5 but now with realistic position values and expectation values on the axes.

The scaling in the 2D figures proceeds as follows. For example, in order to fit the minimum experimentally accessible α which is currently about 6×10^{-12} eV m to the scaled choice of $\alpha=0.5$ (low end), one selects the absolute length unit $d=127.43$ nm and the unit time $t=7$ ps. Similarly, one can fit $\alpha=1$ (high end) to the maximum experimentally accessible α which is currently about 4×10^{-11} eV m and again one can calculate the absolute unit length $d=38.23$ nm and the time unit $t=0.63$ ps.

All these results illustrate how the propagator allows us to track wave packets analytically, numerically, and pictorially for the study of Rashba systems. As might be expected, the Rashba interaction causes a spatial separation of the spin states: the twofold separation achieved in Fig. 2 is reminiscent of the Stern-Gerlach separation in an inhomogeneous magnetic field. More complex spatial patterns of polarization develop as a result of spreading, precession, geometry (2D), and confinement. As the wave packet spreads from its initial location as a result of the Rashba effect and as the electron precesses, the polarization will display an oscillation in space. Because the rates of spreading and precession are determined by the parameters, the maxima and the minima of the oscillation are fixed in space as in the PSHS seen in Fig. 4. When α increases, the velocity of separation increases also. However, if α is too large, the BSS feature is suppressed. On the other hand when α is too small, the Rashba effect is negligible and we recover free-particle behavior. Therefore, α should be carefully chosen depending on the specific purpose. For example, in the 1D case, for fixed width, spin separation will be enhanced by increasing the Rashba strength to $\alpha=1.529\times10^{-11}$ eV m, or beyond, using the maximum experimentally accessible value of $\alpha=4\times10^{-11}$ eV m.

When we increase the overall width w of the initial wave packet and therefore decrease localization, the wave packet spreads more slowly in analogy to free-particle spreading and we observe fewer fringes from the oscillations. Similarly, faster spreading occurs for smaller w. For example, for the experimentally accessible values of α, spin separation in Fig. 2 will be maximized by choosing a minimal width such as 100 nm in the 1D case and likewise for the 2D case. We also observe that the effect of the relative widths w_x/w_y on the fringe pattern depends on the particular spin components considered. For cases where initial polarization and measurement axis are given by, respectively (z and z), (x and x), and (z and x) in Figs. 6–8, the relative width plays an important role in the formation of fringes. This effect is suppressed when the initial and measured axes refer to orthogonal in-plane components (x and y) or (y and x). Again the optimal value of w_x and w_y should be selected for maximal effect.

We observe spatial separation and oscillations of the spin states in the 1D and 2D Rashba systems. The spatial separation of the spin states generates a *spin* current. This mechanism is enhanced by selecting a larger α, a smaller w, or both. On the other hand, the oscillations of the spin states is enhanced by selecting a smaller α, a smaller w, or preferably both. The system we considered is sufficiently complex that several of the features we identify occur simultaneously and are thus not necessarily mutually exclusive. Also the features we discuss arise in plots of different physical quantities. For example, the spin separation in Sec. III A 1 is observed in the y component in spin space whereas the BSS in Sec. III A 2 is observed at the same time and with comparable parameters but in the z component in spin space. The spin field-effect transistor proposed by Datta and Das[2] is an example of the use of an oscillation mechanism to control the spin. Some of the features described in this paper do appear in other work, although descriptions may vary. In particular SS, the components of BSS, the geometry of RFS, and the shifted components in PSH have previously been identified.[13,26]

We have presented a straightforward and flexible method to evaluate the spin dynamics in Rashba systems that can be extended to other SOC systems, such as Dresselhaus systems or a combination of the Rashba and Dresselhaus interactions. We have focused on the study of initial wave packets localized in position in 1D and 2D, unconfined and confined Rashba systems. The plots presented here are just a few selected examples of wave-packet evolution from which the main features were identified. These features do occur for values of the Rashba strength, wave-packet widths, and times which lie within the range of currently accessible values. The strength of the method can be shown effectively with the use of real-time animations. In conclusion this nonexhaustive study of wave-packet spin dynamics illustrates how propagator methods make it possible to retrieve complex information in SOC systems involving incompatible observables.

*bhsu@byu.net
†vanhuele@byu.edu

[1] D. Awschalom, *Semiconductor Spintronics and Quantum Computation*, 1st ed. (Springer, Berlin, 2002).
[2] S. Datta and B. Das, Appl. Phys. Lett. **56**, 665 (1990).
[3] I. Žutić, J. Fabian, and S. D. Sarma, Rev. Mod. Phys. **76**, 323 (2004).
[4] Supriyo Bandyopadhyay and Marc Cahay, *Introduction to Spintronics*, 1st ed. (CRC, Boca Raton, 2008).
[5] R. Winkler, *Spin-Orbit Coupling Effects in Two-Dimensional Electron and Hole Systems* (Springer, Berlin, 2003).
[6] J. Sinova, D. Culcer, Q. Niu, N. A. Sinitsyn, T. Jungwirth, and A. H. MacDonald, Phys. Rev. Lett. **92**, 126603 (2004).
[7] S-Q Shen, Phys. Rev. B, **70**, 081311(R) (2004).
[8] Y. K. Kato, R. C. Myers, A. C. Gossard, and D. D. Awschalom, Science **306**, 1910 (2004).
[9] B. A. Bernevig and S.-C. Zhang, Phys. Rev. Lett. **96**, 106802 (2006).
[10] X. Fu, W. Liao, and G. Zhou, Adv. Condens. Matter Phys. **2008**, 152731.
[11] B. A. Bernevig, J. Orenstein, and S. C. Zhang, Phys. Rev. Lett. **97**, 236601 (2006).
[12] M. H. Liu, K. W. Chen, S. H. Chen, and C. R. Chang, Phys. Rev. B **74**, 235322 (2006).
[13] J. Schliemann, D. Loss, and R. M. Westervelt, Phys. Rev. B **73**, 085323 (2006).
[14] P. Brusheim and H. Q. Xu, Phys. Rev. B **74**, 205307 (2006).
[15] E. I. Rashba, Fiz. Tverd. Tela (Leningrad) **2**, 1224 (1960) [Sov. Phys. Solid State **2**, 1109 (1960)].
[16] Yu. A. Bychkov and E. I. Rashba, J. Phys. C **17**, 6039 (1984).
[17] G. Dresselhaus, Phys. Rev. **100**, 580 (1955).
[18] A. Sarkar and T. K. Bhattacharyya, J. Appl. Phys. **101**, 036108 (2007).
[19] A. Sarkar and T. K. Bhattacharyya, Appl. Phys. Lett. **90**, 173101 (2007).
[20] J. Chen, W. Chao, and Q. W. Shi, Proceedings of the 2004 11th IEEE International Conference on Electronics, Circuits, and Systems, 2004, pp. 195–198.
[21] M. Pletyukhov and A. Shnirman, Phys. Rev. B **79**, 033303 (2009).
[22] A. Csordás, J. Cserti, A. Pályi, and U. Zülicke, Eur. Phys. J. B **54**, 189 (2006).
[23] Y.-Y. Chin, J.-Y. Chiu, M.-C. Chang, and C.-Y. Mou, J. Magn. Magn. Mater. **310**, e702 (2007).
[24] J. Brüning, V. Geyler, and K. Pankrashkin, J. Phys. A **40**, F697 (2007).
[25] J. Wang and C. Q. Wu, Chin. Phys. Lett. **25**, 3001 (2008).
[26] V. Ya. Demikhovskii, G. M. Maksimova, and E. V. Frolova, Phys. Rev. B **78**, 115401 (2008).
[27] K. Bencheikh and G. Vignale, Phys. Rev. B **77**, 155315 (2008).
[28] J. A. Lock, Am. J. Phys. **47**, 797 (1979).
[29] J. Schliemann, Phys. Rev. B **75**, 045304 (2007).
[30] W. Zawadzki and T. M. Rusin, arXiv:0909.0463 (unpublished).
[31] E. Merzbacher, *Quantum Mechanics*, 3rd ed. (Wiley, New York, 1998).
[32] Q. Wang, J. Phys. A **20**, 5041 (1987).
[33] B. C. Hsu and J.-F. S. Van Huele, J. Phys. A: Math. Theor. **42**, 475304 (2009).
[34] H. De Raedt and B. De Raedt, Phys. Rev. A **28**, 3575 (1983).
[35] J. Wang, K. S. Chan, and D. Y. Xing, Phys. Rev. B **73**, 033316 (2006).
[36] J. E. Hirsch, Phys. Rev. Lett. **83**, 1834 (1999).
[37] J. D. Koralek, C. P. Weber, J. Orenstein, B. A. Bernevig, S.-C. Zhang, S. Mack, and D. D. Awschalom, Nature (London) **458**, 610 (2009).
[38] A. Manchon and S. Zhang, Phys. Rev. B **79**, 094422 (2009).

Appendix E

Econophysics: a Propagator Approach

The two papers provided are published in Journal of Utah Academy of Science, Arts, and Letters and Journal of Idaho Academy of Science.

Quantum Finance and the Relationship Between Quantum Mechanics and Financial Markets

Bailey C. Hsu
Department of Physics and Astronomy, Brigham Young University

I highlight similarities and differences between quantum and financial systems and explore how results in one field may inform us about the other.

Introduction

Econophysics, an interdisciplinary study between economics and physics, has gained in popularity in the past few years. It applies existing methods from physics to financial systems. One particular branch of econophysics, quantum finance, sheds some light on the similarity between quantum mechanics and the financial market [1] unlike the traditional partnership between statistical mechanics and finance. As a physicist, I am interested in studying the contributions of physics to different fields of study. In this paper, I explore the applicability of quantum concepts to market analysis. The paper is organized as follows: after focusing on the time-line of econophysics,

I introduce concepts from quantum mechanics and finance. Then I compare the two seemingly very different systems, and finally I explore the possibilities of cross-fertilization.

Time-line of Econophysics

Quantitative methods in finance have a history dating at least back to Gauss in 1845 [2]. In 1895, the Italian economist and philosopher, Vilfredo Pareto first pointed out that wealth distribution and population size obey a power law, the Pareto distribution. There are numerous applications of the Pareto distribution in the occurrence of events such as earthquakes, stock market crashes, war size, avalanches, storms, and other natural phenomena.

In 1900, the French mathematician Louis Bachelier created a model for the stock options in Paris. He wrote down and solved the parabolic equation known to physicists as the diffusion equation [3]. In 1905, Albert Einstein actually approached and solved the same parabolic diffusion equation in his study of Brownian motion, a crucial development in random walk theory [4]. In the 1960s, the question as to whether the financial distribution can really be described by normal (Gaussian) distributions came up and was answered negatively. Eugene Fama pointed out in his PhD thesis that the frequency distribution of the changes in the logarithm of the price has the characteristic of high peaks and fat tails (a.k.a leptokurtic) [5]. The mathematician Benoit Mandelbrot pioneered the use of additional non-Gaussian distributions known as the Levy laws [6]. Recently, Chris Anderson coined the term "the Long Tail" [7] exemplifed in people buying hard-to-find items. Companies such as Amazon.com or Netflix.com which both serve as online entertainment providers apply Long-Tail strategies to their business, thereby illustrating the importance of choosing the correct quantitative tools in econophysics.

Long-Tail also has been mentioned as manifestations of rare events which can be related to the recent crash of the market [8].

Concepts in Quantum Mechanics and Finance

Quantum Mechanics

Physics deals with the evolution and the trajectories of particles. Newto-

nian mechanics which enable us to predict the position and the velocity of objects at a specific time has a microscopic counterpart: quantum mechanics. Instead of predicting exact locations and velocities, quantum mechanics describes the world in a probabilistic manner using a wavepacket (leading to a probability distribution) to depict the particle location. Therefore quantum mechanics is also referred to as wave mechanics. This distribution can also be interpreted through the Heisenberg Uncertainty Relation which states the impossibility of measuring the position and the momentum simultaneously with unlimited accuracy. A famous macroscopic example of the appearance of randomness in quantum mechanics is Schrodinger's cat [9]. Until we open the box in which the cat, the poison, and the radioactive poison trigger are located, we don't know if the cat is alive or dead. The cat in the unopened box is therefore in a superposition of two possible states: alive and dead. This counterintuitive situation has many physical realizations in the laboratory.

Finance

In finance, we are interested in the dynamics of our stock shares and in the future earnings of the companies we invest in. For the financial managers, one goal is to maximize the wealth of the company and another to maximize the earnings per share. However it is an impossible task for the financial manager to make perfect decisions concerning stock prices due to numerous microeconomic (firm-related) and macroeconomic (external) factors. In finance, the future value of an investment is given by its present value and by the interest rate. However, the interest rate varies in time and the spot (instantaneous) interest rate varies stochastically. This is why the stock price can be described using a probability distribution function in analogy with the wavepacket used in quantum mechanics. In finance, the portfolio is a sum total of all the assets owned by a firm or an individual. It makes sense to consider a specific portfolio with a specialized probability density function. In order to maximize the profits, an investor has to make investment decisions using different strategies and thus avoiding the risk of the market by hedging.

Connecting the Quantum World and the Financial Market

The quantum world and the financial market display common characteristics.

Both fields deal with randomness and uncertainties. Randomness in the

quantum world originates in the measurement process as seen in the Schrodinger cat example. In the financial world, the randomness comes from many degrees of freedom, namely the many buyers and sellers in the market. This resembles many-body systems in physics and can therefore be characterized as a stochastic process. This effect is becoming more prominent as online trading becomes easier and more popular with increased simultaneous transactions.

The uncertainties in the quantum world have been defined in the previous section as the incompatibility of two conjugate variables: position and momentum. It has also been shown that there exist such two variables in the stock market: the stock price and the stock velocity [1]. Other than randomness and uncertainties, the quantum and financial world share some common mathematical structure. The Schrodinger equation is the Rosetta Stone for determining the dynamics of a wave if enough information such as the potential and the initial positions are given. The Schrodinger equation itself is a purely deterministic differential equation without any randomness. In finance, a mathematical model for European option trading was developed by Fischer Black and Myron Scholes in 1973. It can be transformed into a differential equation form [10]. It is interesting to recall that Louis Bachelier and Albert Einstein's parabolic diffusion equation looks quite similar to Black-Scholes' after some algebraic manipulation. However, there is additional information in Black-Scholes, namely the spot interest rate, which doesn't appear in the diffusion equation. Also the diffusion coefficient for Black-Scholes is a negative quantity while it is a positive quantity in physics.

This can be interpreted as the fact that Black-Scholes provides the dynamics for the option values backwards in time. The Black-Scholes differential equation can also be transformed into a Schrodinger-like formula without the complex unit $i = -1$ (since portfolios are real) and $\hbar$ (an intrinsic variable in the quantum world). Comparing the Schrodinger equation with the transformed Black-Scholes (TBS) equation, we find an interesting correlation. By matching the coefficients of the two equations, we find that σ, the volatility of the market defined as the fluctuation of the prices over a specified time horizon in the TBS, is equivalent to $\frac{\hbar}{\sqrt{m}}$ where m is the inertial mass of the electron in the Schrodinger equation. By setting $m = 1$, we find $\sigma = \hbar$ where σ is intrinsic in the financial world while $\hbar$ is intrinsic in the quantum world. The case $\sigma = 0$ which corresponds to no fluctuations at all (like the future value with fixed deposit and fixed interest rate) while $\hbar = 0$ means that we are working with classical dynamics which has a precise knowledge of the particle's position and momentum. Since the TBS is very similar in math-

ematical structure to quantum mechanics, it makes sense we use the methods from quantum physics for TBS.

Example 1: Applying the Quantum Propagator to the Black-Scholes Model

The quantum propagator, a useful tool in quantum mechanics, expresses the conditional probability for a particle starting from location x_0 at time 0 to end up at location at x1 at time t. It is denoted as K(x, x_0; t, 0) [11]. Propagator K(x, x_0; t, 0) propagates the whole wavefunction from location x0 at time 0 to location x at time t like propagating ripples on a water surface when throwing stones Fig. 1. Therefore if we know the initial wavepacket ψ_{ini}, we can calculate the final wavepacket ψ_{fin} by using the propagator formalism. Once the final wavepacket is found, we can plot the probability density to see the dynamics in real space. Similarly, a financial propagator exists which propagates the portfolio distribution. Fig. 1 illustrates both types of propagations.

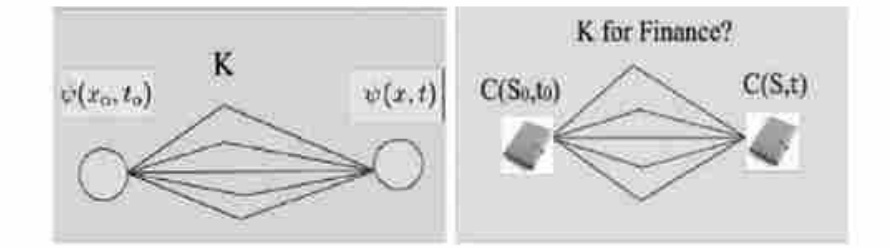

Figure 1: A financial propagator evolves the initial portfolio distribution to a final portfolio distribution.

Several methods to construct the propagators are given in the literature [11, 12]. The corresponding TBS Hamiltonian looks like a 1D Rashba quantum wire Hamiltonian [13] which plays an important role in spintronics, an emerging alternative to traditional electronics using the spin of an electron instead of its charge [14]. The propagator can be solved analytically using specific methods [15]. However, there still are some differences between the Rashba model and the TBS Hamiltonian as discussed in the following section.

Example 2: Searching for an Equivalent Financial Spin

The TBS Hamiltonian has the same mathematical structure as the Rashba quantum wire Hamiltonian, including a so-called drift (linear) term. How-

ever, there is one significant difference between Rashba and TBS, namely the spin of the electron. It is therefore appropriate to raise the question, "Is there a financial spin?". By comparing the coefficients of the drift terms, we see that the potential financial spin might be the spot interest rate [16].

Nevertheless, similarity in mathematical structure doesn't guarantee the existence of physical variables in both systems. As mentioned previously, the Black-Scholes model is different from the parabolic diffusion equation which Einstein and Bachelier used. The difference also contains a spot interest rate term. In physics, spin is intrinsic, discrete, and usually two-valued (up and down). It is apparent that spot interest rate is not two-valued, but takes on discrete values if we discretize the time. Spin in the physical world could also be 3-valued, 5-valued or n-valued. It is mentioned in the literature that the spot interest rate is related to different cycles of the market, 6 to be exact [17]. According to this work, the spot interest rate can be used as an indicator to extract hidden information about the market. In physics, the Stern-Gerlach experiment comes into light as the discovery of the hidden information of an electron, namely spin [18]. In the Stern-Gerlach experiment, a beam passes through an inhomogeneous magnetic field, and we see a clear separation of two different spins which is an intrinsic property of the electron in the quantum world. Is there a similar financial magnetic field too? And what is the financial experiment that plays the same role as Stern-Gerlach?

Conclusion

In his 1933 Nobel Prize acceptance speech [19], Paul Dirac said: "The methods of theoretical physics should be applicable to all those branches of thought in which the essential features are expressible with numbers," subscribing to the importance of cross-disciplinary study. The quantum world and the financial market indeed share some common characteristics and there are probably still more to be discovered. I showed here how the appearance of randomness and mathematical similarity can function as a reservoir of ideas and creativity for both the quantum and financial world.

References

[1] Belal E. Baaquie, *Quantum Finance: Path Integrals and Hamiltonians for Options and Interest Rates*, 1st ed. (Cambridge University Press, 2007).

[2] M. B. W. Tent, *Prince of Mathematics: Carl Friedrich Gauss,* 1st ed. (A K Peters Ltd, 2006).

[3] L. Bachelier, "Theorie de la Speculation", Annales Scientifiques del'Ecole Normale Superieure, 3e Series, 17, 21-86 (1900).

[4] A. Einstein, "Uber die von der molekularkinetischen Theorie derWarme geforderte Bewegung von in ruhenden Flussigkeiten suspendiertenTeilchen", Annalen der Physik (4. Folge) **17**, 549-560 (1905).

[5] Eugene Fama, "The Behavior of Stock-Market Prices", J. Bus. January 1965, **38**(1), 34-105 (1965).

[6] B. B. Mandelbrot, "The Variation of Certain Speculative Prices", J.Business **36**, 394-419 (1963).

[7] Anderson, Chris, "The Long Tail", *Wired* (URL:http://www.wired.com), Oct. 2004. (Accessed May 2008).

[8] Stanley, Eugene, "Econophysics and the Current Economic Turmoil", http://polymer.bu.edu/hes/articles/s08a.pdf. (Accessed Jan 2009).

[9] John A. Wheeler and Wojciech H. Zurek, *Quantum Theory and Measurement*, 2nd ed. (Princeton, 1983).

[10] Fischer Black; Myron Scholes, "The Pricing of Options and Corporate Liabilities", Journal of Political Economy **81**(3), 637-654 (1973).

[11] E. Merzbacher, *Quantum Mechanics*, 3rd ed. (Wiley, 1997).

[12] R. A. Feynman and A. R. Hibbs, *Quantum Mechanics and Path Integrals, 1st ed.* (McGraw Hill, 1965).

[13] Yu. A. Bychkov and E. I. Rashba, "Oscillatory effects and the magnetic susceptibility of carriers in inversion layers", J. Phys. C **17**, 6039-6045 (1984).

[14] R. Winkler, *Spin-orbit Coupling Effects in Two-Dimensional Electron and Hole Systems*, 1st ed. (Springer, 2003).

[15] B. C. Hsu and J-F. S. Van Huele, "Propagator in Spintronics", Journal of the Utah Academy of Sciences, Arts, and Letters, 141-153 (2007).

[16] B. C. Hsu and J-F. S. Van Huele, "Propagators in random systems: the Black-Scholes examples and beyond", Journal of the Idaho Academy of Science, **44**, (2), 008-07, 1-121 (2008).

[17] T-K Siu et al, "Extracting Information from Spot Interest Rates and Credit Ratings using Double Higher-Order Hidden Markov Models", Computational Econ., **26**(3-4), 69-102 (2006).

[18] W. Gerlach and O. Stern, Z. Phys. **8**, 110 (1922).

[19] http://nobelprize.org. (Accessed May 2008).

Propagator in Random Systems: the Black-Scholes Example and Beyond

Bailey Hsu* and Jean-François Van Huele†
Department of Physics and Astronomy, Brigham Young University

April 11, 2008

*britchap@gmail.com
†vanhuele@byu.edu

Propagator in Random Systems: the Black-Scholes Example and Beyond

Abstract

We highlight some similarities and some differences between financial and quantum systems. The comparison provides inspiration for the introduction of new degrees of freedom in the description of the evolution of the systems.

Introduction

Both the microworld and the financial world are infused with randomness and uncertainty. Still, rigorous methods using mathematical tools such as differential equations have been developed to study quantum physics and

the market quantitatively . We look at two such equations: the Schrödinger equation and the Black-Scholes equation for option trading. They exhibit interesting similarities. In this paper we use the propagator, a useful tool in the study of the evolution of a system to compare the quantum and the financial domains in the hope of detecting cross-fertilizing elements.

Randomness and Uncertainty

In financial markets, randomness originates in the extremely large number of degrees of freedom, with many buyers and sellers of stocks exposed to economic, political, and other factors. Whether or not individual traders act rationally, the system behaves stochastically. In the Black-Scholes financial model for European options [1] the traders of the option can only exercise their right to buy or sell at the time of maturity. The resulting Black-Scholes equation provides the individual investor with a deterministic tool to hedge financial risk by getting information on portfolio composition. In the quantum world randomness enters in the description of individual particles. The wavefunction of an electron represents its probability amplitude in space. The Schrödinger equation is a fully deterministic

process to study the evolution of this probability distribution. Usually the randomness enters in the measurement process [2] independently of the Schrödinger equation, except for the fact that the wavefunction contains information on measurement outcomes. Simultaneous knowledge of complementary variables such as position x and momentum p is limited by the Heisenberg Uncertainty Relation $\Delta x \Delta p \geq \frac{\hbar}{2}$, where $\hbar$ is Planck's constant. Interestingly a similar incompatibility between financial variables, such as stock price x and stock velocity $\dot{x}$ can be derived $\Delta x \Delta \dot{x} \geq \frac{\sigma^2}{2}$, where σ is the volatility or the standard deviation of price fluctuations over a specified time horizon [3]. Clearly, the origins of the randomness in microphysics and finance are quite different.

Correspondence between the Equations

The Schrödinger equation for an electron of mass *m* in a potential *V* is

$$i\hbar \frac{\partial \psi}{\partial t} = (-\frac{\hbar^2}{2m}\frac{\partial^2}{\partial_x^2} + V(x, \frac{\partial}{\partial_x}))\psi \equiv H_S \psi, \tag{1}$$

where ψ is the wavefunction and H_S is the Hamiltonian operator. The Black-Scholes equation for European options is

$$\frac{\partial C}{\partial t} + rS\frac{\partial C}{\partial S} + \frac{\sigma^2 S^2}{2}\frac{\partial^2 C}{\partial^2 S} = rC, \tag{2}$$

where $C(S,t)$ is the portfolio of an investor, $S(t)$ is the stock price, and r is the spot (instantaneous) interest rate. To enhance the similarity between Eq. (1) and Eq. (2) we introduce a new variable $x = lnS$ and obtain

$$\frac{\partial C}{\partial t} = (-\frac{\sigma^2}{2}\frac{\partial^2}{\partial x^2} + (\frac{\sigma^2}{2} - r)\frac{\partial}{\partial x} + r)C. \tag{3}$$

By formally associating ψ with C and σ^2 with $\frac{\hbar^2}{m}$, we can now define a Black-Scholes Hamiltonian

$$H_{BS} = -\frac{\sigma^2}{2}\frac{\partial^2}{\partial x^2} + (\frac{\sigma^2}{2} - r)\frac{\partial}{\partial x} + r. \tag{4}$$

A cautionary remark is in order. Eq. (1) has an additional factor of i compared to Eq. (3) and H_{BS} is not hermitian. In quantum physics hermiticity is required for measurable variables because it guarantees real outcomes, in particular real energies.

Construction of Propagator

The quantum propagator, $K(x, x_0; t, 0)$ represents the conditional probability of finding a particle at location x and time t if located at position x_0 at time 0. For time-independent Hamiltonians, we use a time-development operator $T(t,0) = \exp(\frac{Ht}{i\hbar})$ to describe the evolution of the states representing the system. By projecting $T(t,0)$ into position eigenstates (states with precise location x), we can follow the dynamics in position space $K(x, x_0; t, 0) =< x|T(t,0)|x_0 >$. There are several methods to construct propagators [4, 5, 6]. Here we focus on the eigenfunction expansion [4]. Since eigenstates $|E_n >$ form a complete set $I = \sum_n |E_n >< E_n|$ and obey the property $H|E_n >= E_n|E_n >$, we get

$$\begin{aligned} K(x, x_0; t, 0) &= \sum_n < x|exp(-\frac{i}{\hbar}Ht)|E_n >< E_n|x_0 > \\ &= \sum_n {\psi_n}^*(x)\psi_n(x_0)exp(-\frac{i}{\hbar}E_n(t)) \end{aligned} \tag{5}$$

where $\psi(x) =< x|E_n >$ and $\psi^*(x) =< E_n|x >$. We apply this method to the quantum free-particle Hamiltonian $H_{FP} = -\frac{\hbar^2}{2m}\frac{\partial^2}{\partial x^2}$ and to H_{BS} in Eq. (4).

Rewriting both Hamiltonians in terms of p, where $p \equiv i\frac{\partial}{\partial x}$, we obtain

$$\begin{aligned} H_{FP} &= \frac{p^2}{2m} && (6) \\ H_{BS} &= \frac{\sigma^2 p^2}{2\hbar^2} + (\frac{1}{2}\sigma^2 - r)\frac{i}{\hbar}p + r \\ &= \frac{\sigma^2}{2\hbar^2}(p + \frac{i\hbar}{\sigma^2}(\frac{\sigma^2}{2} - r))^2 + r + \frac{\hbar^2}{2\sigma^2}(\frac{\sigma^2}{2} - r)^2 && (7) \end{aligned}$$

We see that, except for a constant term, H_{BS} looks very much like H_{FP} which has a continuous set of eigenstates and thus

$$\begin{aligned} K(x, x_0; t, 0)_{FP} &= \int_{-\infty}^{\infty} e^{-\frac{i}{\hbar}(\frac{p^2 t}{2m})} e^{-\frac{i}{\hbar}p(x-x_0)} dp \\ &= \sqrt{\frac{m}{2\pi i\hbar t}} e^{-\frac{m(x-x_0)^2}{2i\hbar t}} \\ K(x, x_0; t, 0)_{BS} &= \int_{-\infty}^{\infty} e^{-\frac{i}{\hbar}(\frac{\sigma^2 p^2}{2\hbar^2} - (\frac{\sigma^2}{2} - r)\frac{i}{\hbar}p + r)t} e^{-\frac{i}{\hbar}p(x-x_0)} dp \\ &= e^{-rt}\frac{1}{\sqrt{2\pi t\sigma^2}} e^{-\frac{1}{2t\sigma^2}(x - x_0 + \tau(r - \frac{\sigma^2}{2}))^2}. && (8) \end{aligned}$$

We have verified that the same result for K_{BS} can be derived using Feynman's path-integral method [3].

Spin Systems

The quantum systems that we considered so far did not include spin. In reality spin plays an important role in many atomic systems and solids. Therefore it becomes important to extend the propagator technique to spin systems [7]. In atomic physics, an electron in the electric field of the nucleus experiences a magnetic field in its own rest frame. This spin-orbit coupling effect has a counterpart in spintronics [8] originating in the asymmetry of the potential (Rashba effect) [9, 10] or the asymmetry of the crystal structure (Dresselhaus effect) [11]. The Rashba and Dresselhaus Hamiltonians are

$$H_R = \frac{\mathbf{p}^2}{2m} + \frac{\alpha}{\hbar}(p_x\sigma_y - p_y\sigma_x), \quad H_D = \frac{\mathbf{p}^2}{2m} + \frac{\beta}{\hbar}(p_x\sigma_y - p_y\sigma_x), \tag{9}$$

where α and β correspond to the spin-orbit strength for the Rashba and Dresselhaus couplings and $\sigma_x, \sigma_y, \sigma_z$ are the spin Pauli matrices. By comparing Eq. (9) with Eq. (7), we make the following observations: **1**. Both systems contain a (drift) term linear in p. Rashba and Dresselhaus propagators can therefore be constructed in analogy with K_{BS} in Eq. (8). **2**.

Rashba and Dresselhaus are 2D systems while Black-Scholes is 1D, but 1D quantum wires with spin or 2D extensions of Black-Scholes model can be considered. **3**. Pauli matrices appear in the drift term in Eq. (9) which leads to spin-dependent phenomena while no such matrices appear explicitly in Eq. (7). Instead the coefficient of the linear term is the spot interest rate, r. This raises the question as to whether a degree of freedom similar to spin can be found for Black-Scholes systems and by extension in the physics of financial markets.

Conclusion

We have seen that random systems can be studied using propagators. Stocks and quantum particles obey differential equations that exhibit some striking similarities and are both amenable to the propagator method. The differences between them point to possible extensions such as the existence of a financial spin. Is there an intrinsic, discrete, two-valued degree of freedom in the financial world, and can it be observed like physical spin? Vice versa can the presence of interest rate terms in the Black-Scholes model inform us about existing "drift" terms in physical equations? It is hard

to see how the interest rate r could play the role of spin since r is neither discrete nor two-valued. Indeed mathematical similarities need not imply a correspondence between the variables of physics and finance. Still, the joint appearance of randomness and common formal methods can be a source of creativity as illustrated in the study of propagators.

References

[1] Fischer Black; Myron Scholes, "The Pricing of Options and Corporate Liabilities", Journal of Political Economy **81**(3): 637-654 (1973).

[2] J. A. Wheeler and W. H. Zurek, *Quantum Theory and Measurement*, 2nd ed. (Princeton, 1983).

[3] Belal E. Baaquie, *Quantum Finance: Path Integrals and Hamiltonians for Options and Interest Rates*, 1st ed. (Cambridge University Press, 2007).

[4] E. Merzbacher, *Quantum Mechanics*, 3rd ed. (Wiley, 1997).

[5] R. A. Feynman and A. R. Hibbs, *Quantum Mechanics and Path Integrals*, 1st ed. (McGraw Hill, 1965).

[6] F. A. Barone, H. Boschi-Filho, and C. Farina, "Three methods for calculating the Feynman propagator". Am. J. Phys., **71**(5): 483-491(2003).

[7] B. C. Hsu and J-F. S. Van Huele, "Propagator in Spintronics", Journal of the Utah Academy of Sciences, Arts, and Letters, 141-153 (2007).

[8] R. Winkler, *Spin-orbit Coupling Effects in Two-Dimensional Electron and Hole Systems*, 1st ed. (Springer, 2003).

[9] Yu. A. Bychkov and E. I. Rashba, "Oscillatory effects and the magnetic susceptibility of carriers in inversion layers", J. Phys. C **17**, 6039-6045 (1984).

[10] E. I. Rashba, Fiz. Tverd. Tela (Leningrad) **2**, 1224 (1960) (Sov. Phys. Solid State **2**, 1109 (1960)).

[11] G. Dresselhaus, "Spin-Orbit Coupling Effects in Zinc Blende Structures", Phys. Rev. **100**, 580-586 (1955).

Appendix F

Code

F.1 1D Rashba Mathematica Code

This code was written in Mathematica 6.0 for 1D Rashba systems in Appendix D. It should be noted that the analytic integration of wave packets is done with pencil and paper. The result of the integration is reflected in ψtotal in the code.

$$\psi\text{total} = \left(\begin{array}{l} \dfrac{e^{-\frac{i m^2 \sigma^2 \left(x^2+\frac{t^2 \alpha^2}{\hbar^2}\right)}{2 t \hbar \left(m \sigma^2+i t \hbar\right)}} \sqrt{\frac{m \sigma^2}{m \sigma^2+i t \hbar}} \left(a \text{Cos}\left[\frac{m t x \alpha}{\hbar \left(i m \sigma^2-t \hbar\right)}\right]+b \text{Sin}\left[\frac{m t x \alpha}{\hbar \left(i m \sigma^2-t \hbar\right)}\right]\right)}{\sqrt{\sqrt{\pi} \sqrt{\sigma^2}}} \\ \\ \dfrac{e^{-\frac{i m^2 \sigma^2 \left(x^2+\frac{t^2 \alpha^2}{\hbar^2}\right)}{2 t \hbar \left(m \sigma^2+i t \hbar\right)}} \sqrt{\frac{m \sigma^2}{m \sigma^2+i t \hbar}} \left(b \text{Cos}\left[\frac{m t x \alpha}{\hbar \left(i m \sigma^2-t \hbar\right)}\right]-a \text{Sin}\left[\frac{m t x \alpha}{\hbar \left(i m \sigma^2-t \hbar\right)}\right]\right)}{\sqrt{\sqrt{\pi} \sqrt{\sigma^2}}} \end{array} \right);$$

```
ψup1 = ψtotal[[1, 1]];
ψdn1 = ψtotal[[2, 1]];


Plot[{-I * (Conjugate[ψup1] * ψdn1 - Conjugate[ψdn1] * ψup1) /. {a → 1, b → 0,
    m → 0.05 * 9.1 * 10^(-31), σ → 5 * 10^(-7), α → 5 * 10^(-31),
    ħ → 1.054 * 10^(-34), t → 2 * 10^(-10)}, -I * (Conjugate[ψup1] * ψdn1 -
      Conjugate[ψdn1] * ψup1) /. {a → 1, b → 0,
    m → 0.05 * 9.1 * 10^(-31), σ → 5 * 10^(-7), α → 10 * 10^(-31),
    ħ → 1.054 * 10^(-34), t → 2 * 10^(-10)},
  -I * (Conjugate[ψup1] * ψdn1 - Conjugate[ψdn1] * ψup1) /. {a → 1, b → 0, m → 0.05 * 9.1 * 10^(-31), σ → 2.5 * 10^(-7), α → 5 * 10^(-31),
    ħ → 1.054 * 10^(-34), t → 2 * 10^(-10)}}, {x, -5 * 10^(-6), 5 * 10^(-6)},
 PlotRange → {-4 * 10^11, 4 * 10^11}, BaseStyle → Large, ImageSize → Large,
 PlotStyle → {{Thickness[0.01], Red}, {Thickness[0.003], Blue},
   {Thickness[0.003], Dotted, Green}}, AxesLabel → {x, "<Sy>"}]
```

F.2 2D Rashba Matlab Code

This code was written in Matlab for 2D Rashba systems in Appendix D.

```
function rashba2d

global x c X Y waveiniup waveinidn Rho x0 y0 alpha Psiup Psidn r

dt= 3.0;          Lt =3.0;         Nt = Lt/dt; dx =0.2; Lx =12.0;
Nx = Lx/dx; dy =0.2; Ly =12.0;        Ny = Lx/dy; alpha=1; m=1;
hbar=1;

nr=50000; ampup=1/sqrt(2); ampdn=1/sqrt(2);



wx=2; wy=2; x=(-Nx/2:(Nx/2))*dx; y=(-Ny/2:(Ny/2))*dy;

[X, Y] = meshgrid(x,y);

Psiup = exp(-(X.^2+Y.^2)); Rho=(abs(Psiup).^2); plotrho pause(0.1)

for j=1:Nt x0=-6.0+12.0*rand(nr,1); y0=-6.0+12.0*rand(nr,1);
    c=[];
    d=[];
for k=1:Nx+1 for m=1:Ny+1 r=sqrt((X(k,m)-x0).^2+(Y(k,m)-y0).^2);
```

```
waveiniup=1/sqrt(pi*wx*wy)*ampup*exp(-((x0.^2/wx^2)+(y0.^2/wy^2)));
waveinidn=1/sqrt(pi*wx*wy)*ampdn*exp(-((x0.^2/wx^2)+(y0.^2/wy^2)));
c=[c,(144/nr)*sum(1/(2*pi*1i*dt*j).*exp(-((X(k,m)-x0).^2.
  +(Y(k,m)-y0).^2-alpha^2*(dt)^2*j)/(2*1i*dt*j)).*(cos(alpha*r)
  .*waveiniup+1i*sin(alpha*r).*waveinidn.*(1i*(X(k,m)-x0)
  +(Y(k,m)-y0))./r))];
d=[d,(144/nr)*sum(1/(2*pi*1i*dt*j).*exp(-((X(k,m)-x0).^2.
  +(Y(k,m)-y0).^2-alpha^2*(dt)^2*j)/(2*1i*dt*j)).*(cos(alpha*r)
  .*waveinidn+1i*sin(alpha*r).*waveiniup.*(-1i*(X(k,m)-x0)
  +(Y(k,m)-y0))./r))];
end end Psiup=transpose(reshape(transpose(c),Nx+1,Nx+1));
Psidn=transpose(reshape(transpose(d),Nx+1,Nx+1));

Rho= 1i*(-conj(Psiup).*Psidn+conj(Psidn).*Psiup); plotrho
pause(0.1) end


function plotrho global X Y Rho surf(X,Y,Rho) shading interp;
colormap jet; set(gca,'FontSize',40)




colorbar('FontSize',28)
```

```
xlabel(''); ylabel('');

topline =sprintf('(d)'); title(topline);
```

F.3 2D Stern-Gerlach Matlab Code

This code was written in Matlab for 2D Stern-Gerlach systems in section 4.3.

```
function SGE2d

global X Z Rho

dt = 0.1; Lt = 2.0; Nt = Lt/dt; dx =1/16; Lx = 32;   Nx = Lx/dx;
dz = dx; Lz = 32; Nz = Lz/dx; B = 1.0;B0 = 0.0;
Amplup=1.0/sqrt(2); Ampldn=0.0/sqrt(2); wx=1;wz=1;

x = (-Nx/2:(Nx/2-1))*dx; x0 =0.0; z = (-Nz/2:(Nz/2-1))*dz; z0
=2.0; [X, Z] = meshgrid(x, z);
%Magnetic field and plot:
Bx = -B*X; By =0; Bz = B0 + B*Z; figure(1); plotB(Nx, Nz, Bx, Bz);
%pause
Babs = sqrt(Bx.^2 + By.^2 + Bz.^2);
%gaussian w pkt
Wpktup = (Amplup/sqrt(pi*wx*wz))*exp(-1*((X - x0).^2/wx^2 + (Z -
z0).^2/wz^2));
```

```
Wpktdn = (Ampldn/sqrt(pi*wx*wz))*exp(-1*((X - x0).^2/wx^2 + (Z -
z0).^2/wz^2)); Rho = (abs(Wpktup)).^2 - (abs(Wpktdn)).^2;
figure(2);

plotrho pause(0.05)

Cs = cos(dt*Babs); Sn = sin(dt*Babs); ExPot11 = (Cs +
1i*Sn.*Bz./Babs); ExPot12 = 1i*Sn.*(Bx - 1i*By)./Babs; ExPot21 =
1i*Sn.*(Bx + 1i*By)./Babs; ExPot22 = (Cs - 1i*Sn.*Bz./Babs);

Psiup = Wpktup; Psidn = Wpktdn; ExKinFT = ExpKE(dt, Lx, Nx, Lz,
Nz); for k = 1:Nt


    WpupFT = fft2(ExPot11.*Psiup+ExPot12.*Psidn); %Trotter
    WpdnFT = fft2(ExPot21.*Psiup+ExPot22.*Psidn);
    %WpupFT = fft2(Psiup);
    %WpdnFT = fft2(Psidn);
    Wpup = ifft2(ExKinFT.*WpupFT);
    Wpdn = ifft2(ExKinFT.*WpdnFT);
    Psiup = ExPot11.*Wpup+ExPot12.*Wpdn;
    Psidn = ExPot21.*Wpup+ExPot22.*Wpdn;

    Rho =conj(Psiup).*Psiup-conj(Psidn).*Psidn;
```

```
    plotrho
    pause(0.01)

function plotrho global X Z Rho

surf(X, Z, Rho); shading interp; colormap jet;
set(gca,'FontSize',28) colorbar('FontSize',28) axis ([-8 8 -8 8]);

xlabel('');  ylabel(''); topline = sprintf(''); title(topline);
%
function plotB(Nx, Nz, Bx, Bz) global X Z

indx = 1:30:Nx; indz = 1:30:Nz;

xx = X(indx, indx); zz = Z(indz, indz);

Bxx = Bx(indx, indx); Bzz = Bz(indz, indz);

quiver(xx, zz, Bxx, Bzz, 5.0,'LineWidth',5.0); axis ([-8 8 -8 8]);

xlabel('x');  ylabel('z'); topline = sprintf('(a)');
set(gca,'FontSize',40) title(topline);
%
function Res = ExpKE(dt, Lx, Nx, Lz, Nz)
Kx = (2*pi/Lx)*[0:Nx/2-1 -Nx/2:-1];     %kx grid
Kz = (2*pi/Lz)*[0:Nz/2-1 -Nz/2:-1];     %kx grid
```

```
[KX, KZ] = meshgrid(Kx, Kz);

Kin = 0.5*(KX.*KX + KZ.*KZ);            %kinetic energy

Res = exp(-i*dt*Kin);

%
```